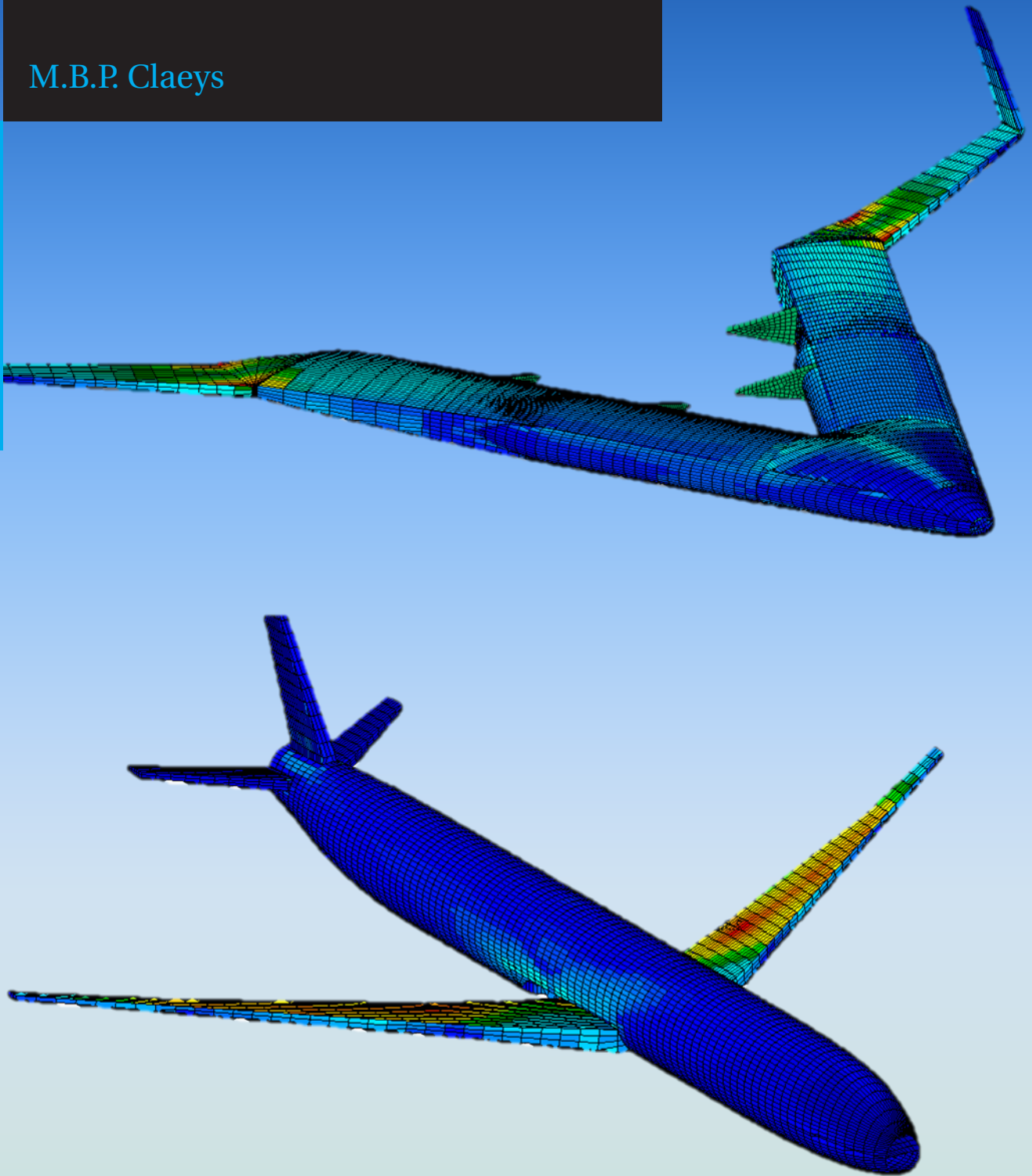


Flying V and Reference Aircraft Structural Analysis and Mass Comparison

Master Thesis Research

M.B.P. Claeys

Technische Universiteit Delft



FLYING V AND REFERENCE AIRCRAFT STRUCTURAL ANALYSIS AND MASS COMPARISON

MASTER THESIS RESEARCH

by

M.B.P. Claeys

in partial fulfillment of the requirements for the degree of

Master of Science
in Aerospace Engineering

at the Delft University of Technology,
to be defended publicly on Wednesday August 22, 2018 at 9:00 AM.

Student number:	4101944	
Project duration:	February 1, 2018 – August 22, 2018	
Supervisor:	Dr. ir. R. Vos	TU Delft
	J. Clausen	Airbus Operations GmbH Future Projects Hamburg
Thesis committee:	Prof. Dr. ir. L.L.M. Veldhuis	Delft University of Technology FPP Chair
	Dr. ir. R. Vos	Delft University of Technology FPP
	Dr. C. Kassapoglou	Delft University of Technology ASM/ASCM
	K. Bender	Airbus Operations GmbH Future Projects Hamburg

This thesis is confidential and cannot be made public until February 2023.

An electronic version of this thesis is available at <http://repository.tudelft.nl/>.
Number of equivalent words; 29 994

ABSTRACT

This paper is a representation of the research that has been performed with regards of the weight estimation of the Flying V and its conventional reference aircraft. The goal is to establish the feasibility of the Flying V as a structural concept. In order to do this a structural model of the Flying V has been created, as well as the design and structural model of a conventional reference aircraft. This paper will cover every step required to design and analyze both models, while at the same time making sure that both models can be compared to each other. By implementing a chain of 6 software packages both models started at parametric conceptual design and were developed to the point where they have been analyzed using the finite element method to obtain the (FEM) structural mass.

The introduction can be found in Chapter 1. Chapter 2 gives an overview of the entire process. Both the set-up of the thesis and its process flow are discussed here, as well as a detailed goal statement. In Chapter 3 the design mission was established. In addition the design requirements are mentioned as well. Both the requirements and mission are the same for both aircraft. Chapter 4 describes conceptual design of the reference aircraft. Herein the used assumptions were stated and explained, and the resulting graphical and parametric model was shared. Chapter 5 does the same for the Flying V. Chapter 6 explains how the graphical models were appended in order to obtain a full three dimensional model, ready for the analysis. It was explained how ZORRO-X was applied to do this, and manual corrections were discussed as well. The loading of the models is described in Chapter 7, it describes how ODILILA was implemented to obtain the different aerodynamic loads. Ground loads and mass distributions were obtained in this chapter as well. From this, the initial C.G. ranges were established. Load cases were build up by combining aero, mass and ground loads. In total 22 load cases were used during the sizing optimization. The FEM optimization was initiated in Chapter 8. This was done by mapping the aforementioned loads and setting the design criteria and constraints. Finally the results are summarized in Chapter 9. The results include the analysis of critical load cases, critical design constraint, thicknesses and displacements of both the Flying V and the reference aircraft. It was found that while the Flying V still has some structural problems at the kink and nose-fuselage intersection, the overall FEM mass of the Flying V is still lighter than that of the conventional reference aircraft. It is expected that the proposed solutions for the structural problems will not influence the mass to such an extent that this is no longer the case. Therefore the conclusion, stated in Chapter 10, is that the Flying V is indeed a viable structural concept. Based on current results it is expected that after further research, optimization and implementation of the proposed solutions summarized in Chapter 11, the Flying V might even prove not only viable but even desirable compared to conventional aircraft.

PREFACE

This thesis research is done as part of my curriculum for the master degree of aerospace engineering. As it is the final deliverable its completion also marks the end of my studies at the Technical University of Delft.

The subject of this thesis lies close to my heart. After all, when studying Aerospace, what would be greater than designing a new aircraft. Not only was I able to work on a conceptual design of a new aircraft, but I actually had the opportunity to do this at Airbus. So after many years I managed to complete a goal set so long ago in my fourth year of secondary education in a manner even I could not dream of at that time. I truly consider myself lucky for the opportunities I had during my studies.

Of course none of this could have happened without the help and support from my loving parents, who stood by me even in the hard times. I shall be forever indebted and grateful to you both.

As for the work during the thesis itself I simply must mention Klaus Bender. He helped me during this entire process and was always willing to answer any questions I had, being related to this thesis or aircraft in general. You have taught me a lot and helped creating this once in a lifetime opportunity for me. Thank you.

My gratitude too, goes to my supervisor at Airbus, who assisted and guided me; Jörn Clausen. He helped me with the implementation of his automation tool ZORRO. Thank you as well to all the other colleagues at Airbus who helped me in some way or another.

Last, but definitely not least, the support I received from people at the university. My supervisor Roelof Vos, who guided me in the right direction. And Max Baan and Luuk van der Schaft, who helped on the implementation of ParaPy. You all provided valued guiding, input and support. Without it I would not have been able to complete this thesis.

AUTHOR'S NOTE

Prior to this research a literature study was performed on the topic in order to determine the best way to obtain the structural mass of a non conventional aircraft. It was found that topology optimization has some desirable properties with respect to flexibility towards geometry. However, a proof of concept showed that, while feasible, such a project far exceeds the available resources for a 7 month thesis project. In this master thesis research the other feasible solution method was applied; Finite Element Method (FEM) analysis.

CONTENTS

Abstract	iii
Preface	v
Author's Note	vii
List of Figures	xiii
List of Tables	xvii
List of Symbols and Abbreviations	xix
Abbreviations	xix
Symbols	xx
1 Introduction	1
I Thesis Outline	3
2 Thesis Goal and Method	5
2.1 Goal	5
2.2 Method	5
II Aircraft Models	7
3 Aircraft Design Mission and Requirements	9
3.1 Design Mission	9
3.2 Design Requirements	10
4 Reference Aircraft	11
4.1 Method	11
4.2 Assumptions	12
4.2.1 Wing Sizing: Constant Span VS. Constant Aspect Ratio	12
4.2.2 Empennage Sizing: Volume Coefficient VS. Area Coefficient	14
4.2.3 Passenger Density and Payload Weight.	15
4.3 Reference Model	16
4.3.1 Numerical Parameters	16
4.3.2 Graphical Model	17
5 Flying V	21
5.1 Flying V Model	22
5.1.1 Numerical Parameters	22
5.1.2 Graphical Model	23
III FEM Analysis	27
6 Structural Modeling	29
6.1 Method	29
6.1.1 PATRAN and NASTRAN	29
6.1.2 ZORRO-X Tool	30
6.2 Flying V Structural Model	31
6.2.1 Parts Subdivision.	31
6.2.2 Graphical Model Adjustments	33
6.2.3 Initial Structural Model and Mesh	35
6.2.4 Manual Adjustments.	37

6.2.5	Final Structural Model and Mesh.	37
6.3	Reference Aircraft Structural Model.	38
6.3.1	Parts Subdivision.	38
6.3.2	Initial Structural Model and Mesh	38
6.3.3	Manual Adjustments.	39
6.3.4	Final Structural Model and Mesh.	41
6.4	Material Selection.	42
7	Load Modeling	43
7.1	Method	43
7.2	Structural and Operational Loads.	43
7.2.1	Payload Range Diagram and Sizing Points	43
7.2.2	Fuel Location	44
7.2.3	Mass and Center of Gravity Analysis	45
7.3	Aerodynamic Loads.	49
7.3.1	General Information	49
7.3.2	Procedure	50
7.4	Ground Loads.	52
7.5	Load Cases	52
8	FEM Implementation	55
8.1	Aero Mapping.	55
8.2	Inertia Mapping.	56
8.3	Boundary Conditions	56
8.4	ZORRO-M.	56
8.4.1	Sizing Criteria	56
8.4.2	Sizing Constraints	58
8.4.3	Smoothing.	58
8.4.4	Convergence.	59
8.4.5	Test Run	59
9	Results	61
9.1	Thickness	61
9.1.1	Initial Results	61
9.1.2	Kink Analysis.	61
9.1.3	Updated Results	62
9.2	Frame Size	64
9.2.1	Nose-cabin Intersection Frame	64
9.2.2	Central Nose Frame	66
9.2.3	Central Cabin Frame.	66
9.3	Critical Load Cases	67
9.4	Critical Design Criteria	69
9.5	Deformations	70
9.5.1	Tip Deflection	70
9.5.2	Center Deflection	71
9.6	Weight	72
9.6.1	Convergence.	72
9.6.2	Final Mass Distribution	72
9.7	Center of Gravity	74
IV	Conclusion and Recommendations	75
10	Conclusion	77
11	Recommendations and Proposals for the Future	79
11.1	Project Recommendations	79
11.2	Software Recommendations	80

A	Conceptual design	81
A.1	Used Equations	81
A.1.1	Wing Planform	81
A.1.2	Weights	82
A.1.3	Fuselage Planform	82
A.1.4	HTP Planform	82
A.1.5	VTP Planform	82
A.1.6	Used Constants	83
A.2	Properties Flow Diagrams	84
A.2.1	A350	84
A.2.2	Flying V	86
A.2.3	Reference AC	86
B	Flying V Structural Model Parts Assembly	87
B.1	Nose and Cabin Connection	87
B.2	Cabin and Wing Connection	87
C	Mass Breakdown and CG Range Numerical Properties	89
C.1	CG Locations	89
C.2	Mass Distribution Variation of Sizing Points	90
C.3	CG Diagrams	91
C.4	Fuel Distribution	92
D	ODILILA Documentation	93
D.1	Working Principles	93
D.1.1	Aero Data for Performance	93
D.1.2	Aero Data for Handling Qualities and Loads	93
D.1.3	Geometry	93
D.2	Implementation	93
D.2.1	Induced Drag and Lift	93
D.2.2	Compressibility	93
D.2.3	Optimization	94
D.3	Verification	94
E	Summary of Important ODILILA Results	97
F	Additional Flying V Results	99
F.1	Thickness	99
F.2	Critical Load Cases	100
F.3	Critical Design Criteria	101
G	Full Reference Aircraft Results	103
G.1	Thickness	103
G.2	Critical Load Cases	104
G.3	Critical Design Criteria	105
	Bibliography	107

LIST OF FIGURES

2.1	Set-up of a Structural Analysis	6
2.1a	Thesis Set-up	6
2.1b	Sizing vs. Optimization	6
2.2	Structural Design Process Flow	6
3.1	Design Mission	9
4.1	Wing Span in Function of MTOW	13
4.2	Stability Safety Margin	14
4.3	Reference Aircraft Structure	18
4.3a	Left View	18
4.3b	Top View	18
4.3c	Isometric View	18
4.4	Wing-Fuselage Intersection	19
4.4a	Left View	19
4.4b	Isometric View	19
4.5	Empennage-Fuselage Intersection	19
4.5a	Left View	19
4.5b	Top View	19
4.5c	Isometric View	19
5.1	Flying V Structure	24
5.1a	Left View	24
5.1b	Top View	24
5.1c	Isometric View	24
5.2	Flying V Stringers	25
5.2a	Top View	25
5.2b	Isometric View	25
5.2c	Internal View	25
6.1	Flying V Exported Elements from ParaPy	31
6.1a	Left View	31
6.1b	Isometric View	31
6.1c	Top View	31
6.2	Flying V Parts Subdivision	33
6.3	Adjusted Nose Part Flying V	34
6.3a	Front View	34
6.3b	Left View	34
6.3c	Top View	34
6.3d	Isometric View	34
6.4	Adjusted Wing Part Flying V	35
6.4a	Front View	35
6.4b	Left View	35
6.4c	Top View	35
6.4d	Isometric View	35
6.5	Stringer Pitch Variation	36
6.5a	Different Center	36
6.5b	Different Curvature	36
6.6	Flying V Wing Kink Structure	37

6.7	Flying V Structural Model	38
6.7a	Top View	38
6.7b	Front View	38
6.7c	Isometric View	38
6.8	Center Fuselage Manual Adjustments	40
6.8a	Side View	40
6.8b	Front ISO View	40
6.8c	Rear ISO View	40
6.9	Reference Aircraft Structural Model	41
6.9a	Front View	41
6.9b	Left View	41
6.9c	Top View	41
6.9d	Isometric View	41
7.1	Payload Range Diagram of the Flying V	44
7.2	Mass Breakdown and Resulting CG Ranges	48
7.2a	Flying V Mass Breakdown & CG Range	48
7.2b	Reference Aircraft Mass Breakdown	48
7.2c	Reference Aircraft CG Range	48
8.1	Flying V Center Deformation and Implemented Solution	59
8.1a	Initial Deformation	59
8.1b	Structural Modification	59
9.1	Flying V Thickness Distribution	61
9.2	Thickness	62
9.2a	Flying V Top	62
9.2b	Reference AC Top	62
9.2c	Flying V Bottom	62
9.2d	Reference AC Bottom	62
9.3	Flying V Kink Thickness Distribution	63
9.3a	Front View	63
9.3b	Back View	63
9.4	Flying V Center Frame and Ribs	64
9.4a	Front View	64
9.4b	Isometric View	64
9.5	Nose Frame	66
9.6	Cabin Frame	66
9.7	Critical Load Case	68
9.7a	Flying V Top (range 1)	68
9.7b	Reference AC Top (range 1)	68
9.7c	Flying V Bottom (range 1)	68
9.7d	Reference AC Bottom (range 1)	68
9.7e	Flying V Top (range 2)	68
9.7f	Reference AC Top (range 2)	68
9.7g	Flying V Bottom (range 2)	68
9.7h	Reference AC Bottom (range 2)	68
9.8	Critical Design Criteria	69
9.8a	Flying V Top	69
9.8b	Reference AC Top	69
9.8c	Flying V Bottom	69
9.8d	Reference AC Bottom	69
9.9	Maximum Tip Deflection	70
9.9a	Flying V	70
9.9b	Reference Aircraft	70
9.10	Maximum Frame and Beam Deflection [mm]	71

9.11 Group Mass Iterations	73
9.11a Flying V Mass Iterations	73
9.11b Reference AC Mass Iterations	73
A.1 Process Flow of Conceptual Design of the A350 Model - Part 1	84
A.2 Process Flow of Conceptual Design of the A350 Model - Part 2	85
A.3 Process Flow of Conceptual Design of the Flying V Model	86
B.1 Flying V Nose-Cabin Connection	87
B.1a Top View	87
B.1b Internal Isometric View	87
B.2 Flying V Cabin-Wing Transition	88
B.2a Transition Rib Adjustments	88
B.2b Transition with Wing Skin Elements	88
B.2c Transition Front View	88
C.1 Flying V CG Diagram	91
C.2 Reference Aircraft CG Diagram	91
D.1 Lift Gradient Vs. Aspect Ratio	94
D.2 Lift Gradient Vs. Sweep Angle	95
D.3 Induced Drag Vs. Number of Span-wise Panels	95
D.4 Discritization Effect on Lift Gradient	96
D.4a Chord Discritization	96
D.4b Span Discritization	96
E.1 Flying V Additional Thicknesses	99
E.1a Ribs	99
E.1b Spars	99
E.2 Critical Load Conditions	100
E.2a Ribs, Range 1	100
E.2b Spars, Range 1	100
E.2c Ribs, Range 1	100
E.2d Spars, Range 2	100
E.3 Critical Design Criteria	101
E.3a Ribs	101
E.3b Spars	101
G.1 Reference Aircraft Thickness	103
G.1a Isometric Top View	103
G.1b Isometric Bottom View	103
G.2 Critical Load Conditions	104
G.2a Isometric Top View, Range 1	104
G.2b Isometric Bottom View, Range 1	104
G.2c Isometric Top View, Range 1	104
G.2d Isometric Bottom View, Range 2	104
G.3 Critical Design Criteria	105
G.3a Isometric Top View	105
G.3b Isometric Bottom View	105

LIST OF TABLES

3.1 Aircraft Requirements	10
4.1 Comparison of Keeping Span or keeping Aspect Ratio Constant	12
4.2 Reference Aircraft Design Data	16
4.3 Reference Aircraft Real Wing Design Data	17
5.1 Flying V Design Data	22
5.2 Flying V Compensated Design Data	23
5.3 Flying V Real Wing Design Data	23
6.1 Flying V Structural Modeling Parts	33
6.2 Used Composites	42
7.1 Flying V Mass Breakdown	46
7.2 Reference Aircraft Mass Breakdown	46
7.3 CG Locations for Sizing Points of the Flying V	47
7.4 CG Locations for Sizing Points of the Reference Aircraft	47
7.5 Trim Drag Penalty	51
7.6 Ground Loading Definitions	52
7.7 Compiled Load Cases	53
8.1 Geometric Sizing Constraints	58
9.1 Wing Tip Deflection [m]	71
9.2 Group Convergence	72
9.3 FEM Design Group Mass Distribution [kg]	73
9.4 CG Locations of the Flying V	74
9.5 CG Locations of the Reference Aircraft	74
A.1 Used Constants in Conceptual Design Equations	83
C.1 Flying V CG locations	89
C.2 Reference Aircraft CG Locations	89
C.3 Flying V Mass Variation of Sizing Points	90
C.4 Reference Aircraft Mass Variation of Sizing Points	90
C.5 Flying V Available Tank Volume	92
C.6 Reference Aircraft Available Tank Volume	92
E.1 Flying V Aerodynamic Results	97
E.2 Reference Aircraft Aerodynamic Results	97

LIST OF SYMBOLS AND ABBREVIATIONS

Abbreviations

Abbreviation	Description
AC	aircraft
AC_{ref}	Reference Aircraft
AoA	Angle of Attack
BC	Boundary Condition
CG	Center of Gravity
CoP	Center of Pressure
FEM	Finite Element Method
HTP	Horizontal Tail Plane
LE	Leading Edge
LH	Left Hand (Side)
MPC	Multiple Point Connector
MTOW	Maximum Take-Off Weight
RH	Right Hand (Side)
TE	Trailing Edge
VTP	Vertical Tail Plane

Symbols

Symbol	Description	Unit
ϵ	Strain	$\mu\epsilon$
η	Relative Semi-span Location	[-]
η_k	Kink Relative Semi-span Location	[-]
λ	Wing Taper Ratio	[-]
$\Lambda_{.25}$	Wing Quarter-chord Sweep Angle	deg
λ_{HTP}	HTP Taper Ratio	[-]
λ_{VTP}	VTP Taper Ratio	[-]
L/D	Lift to Drag ratio	[-]
l/d	Fineness Ratio	[-]
L/D_c	Cruise Lift to Drag Ratio	[-]
L/D_{max}	Maximum Lift to Drag Ratio	[-]
w/s	Wing Loading	kg/m^2
A	Aspect ratio	[-]
a	Speed of Sound (at flight level)	m/s
A_{HTP}	HTP Aspect Ratio	[-]
A_{VTP}	VTP Aspect Ratio	[-]
b	Wing Span	m
b_{HTP}	HTP Span	m
b_{VTP}	VTP Span	m
c_k	Kink Chord	m
c_L	Lift Coefficient	[-]
c_r	Wing Root Chord	m
c_t	Wing Tip Chord	m
$c_{r,HTP}$	HTP Root Chord	m
$c_{r,VTP}$	VTP Root Chord	m
$c_{t,HTP}$	HTP Tip Chord	m
$c_{t,VTP}$	VTP Tip Chord	m
CoP_x	x-Coordinate of the Center of Pressure	m
CoP_y	y-Coordinate of the Center of Pressure	m
d	Fuselage Diameter	m
dP	Pressure Differential	Pa
g	Gravitational Acceleration	m/s^2

l	Fuselage Length	m
M	Mach Number	[-]
M_0	Desired Maximum Take-off Mass	kg
M_1	End Mission Mass	kg
M_2	End Extra Mission Mass	kg
M_e	Empty Mass	kg
M_f	Total Fuel Mass	kg
M_P	Payload Mass	kg
M_{f1}	Mission Fuel Mass	kg
M_{f2}	Additional Fuel Mass	kg
MAC	Mean Aerodynamic Chord	m
MAC_y	y-Coordinate of the Mean Aerodynamic Chord	m
$MAC_{x,25}$	x-Coordinate of the Quarter-chord Mean Aerodynamic Chord	m
$MTOM$	Maximum Take-off Mass (weight)	kg (N)
S	Wing Area	m^2
S_w	Wetted Area	m^2
S_w/S_{ref}	wetted to reference area ratio	[-]
S_{HTP}	HTP Surface Area	m^2
S_{VTP}	VTP Surface Area	m^2
SFC	Specific Fuel Consumption	$g/KN * s$
MFUW (MFUM)	Maximum Fuel Weight (Mass)	N (kg)
MPLW (MPLM)	Maximum Payload Weight (Mass)	N (kg)
MZFW (MZFM)	Maximum Zero Fuel Weight (Mass)	N (kg)
MZPW (MZPM)	Maximum Zero Payload Weight (Mass)	N (kg)

1

INTRODUCTION

The Flying V is a conceptual aircraft design that has been designed over the past years by Airbus and the Delft University of Technology. Previous studies were performed establishing the aerodynamic feasibility of the proposal by F. Faggiano [1], and a model was created featuring the oval cabin design [2]. The next step and goal of this thesis is establishing if the design is structurally feasible. This will be determined by establishing the weight of the structure and comparing it to the weight of a conventional reference aircraft.

How exactly this goal can be obtained is examined in the literature review [3]. Herein a number of strategies are proposed and compared. Literature review learned that topology was the best option, provided that a proof of concept yielded acceptable results. Unfortunately this was not the case, and thus this thesis will apply the next best strategy presented in the literature review: establishing the weight by FEM analysis.

This thesis will make a detailed structural proposal for the Flying V and will optimize said proposal for a set of first load estimates. The same will be done for a newly designed reference aircraft so that the structural feasibility of the Flying V might be addressed. Current state of the art does this by implementing a pre-processing tool such as PATRAN together with NASTRAN to obtain the FEM masses. In this thesis this concept will be used and expanded. For the first time graphical design tools ParaPy and Mares will be connected to PATRAN. Furthermore they will feed data to ODILILA as well, a software package used to optimize aerodynamic performance and analysis. ODILILA in turn will feed data to PATRAN as well. All in all a chain of 6 software packages is used to go from conceptual, parametric design of a new reference aircraft and the Flying V, onto FEM implementation and analysis.

In order to get to the point of doing a FEM analysis, a lot of preparations needed to be made. Chapter 2 will provide the reader with a detailed discription of the goal and an overview of all the required steps required to obtain this goal. Next Chapter 3 provides the reader with the design mission and requirements for both the reference aircraft and the Flying V. Chapter 4 and 5 will discuss the parameteric and geometric models of the reference and Flying V respectively. While in Chapter 6 these models are prepared to a FEM ready model. Chapter 7 will provide the loads to be used in the FEM analysis and will explain how they are implemented to the respective models. After all this has been completed correctly, Chapter 8 will describe how the FEM analysis and optimization was performed. Finally Chapter 9 will discuss the obtained results. This paper ends with the conclusions presented in Chapter 10, and the way forward with recommendations in Chapter 11.

I

THESIS OUTLINE

2

THESIS GOAL AND METHOD

2.1. GOAL

The goal of this thesis is to establish the feasibility of the Flying V as a structural concept, by obtaining its preliminary structural weight and comparing it to a conventional aircraft design for the same mission.

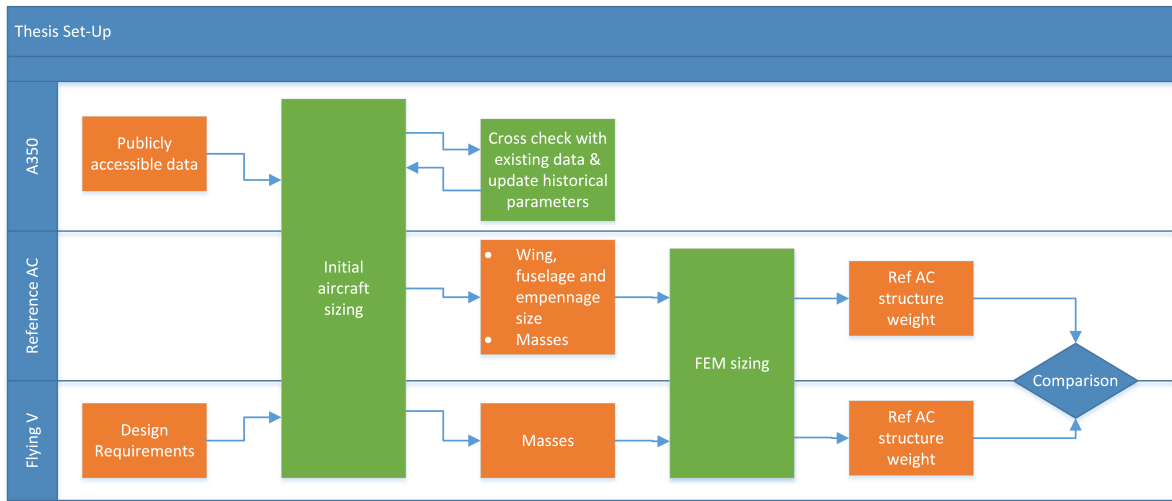
The structural weight will be obtained by Finite Element Method (FEM) analysis. Both aircraft will have the same FEM implementation and optimization, using the same software packages, so that a valid comparison can be made.

2.2. METHOD

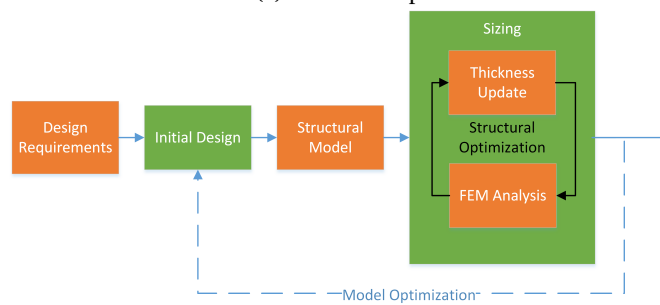
The set-up of this thesis is shown in Figure 2.1a. It shows that a model of the A350 is used to cross check and update historical parameters used during the initial design. Raymar's [4] initial design method has been implemented to obtain the parametric model and top level weights of the reference aircraft, and the top level weights of the Flying V. Both models will be then appended to full structural models and subjected to FEM sizing. This way both models can be compared in terms of structural FEM weight at the end of this thesis.

Note that in this thesis, the models will be sized. No model optimization will be done, but sizing optimization will. The difference between the two is that in model optimization the model is changed, (e.g. by changing the structural lay-out or implementing a new Maximum Take-Off Weight (MTOW) based on the newly obtained structural weight), while sizing optimization will optimize the thickness and stress distributions (and thus the weight) for a single structural concept. This means that the (model) design loop is not being closed during this research, and will be the next big step in the overall design of the Flying V. The difference between model and sizing optimization is visualized in Figure 2.1b. The full arrows show what will be done in this thesis.

Figure 2.2 shows the entire process flow of the structural design and sizing. This image gives an indication about how the different software tools are interconnected. In total six of them are used. ParaPy and MARES for the graphical design, PATRAN [5] and ZORRO-X to create the structural models and mapping the loads, ODILILA [6] to obtain those (aerodynamic) loads and finally NASTRAN and ZORRO-M to size the structural model. Post-processing of the results will be done in PATRAN.



(a) Thesis Set-up



(b) Sizing vs. Optimization

Figure 2.1: Set-up of a Structural Analysis

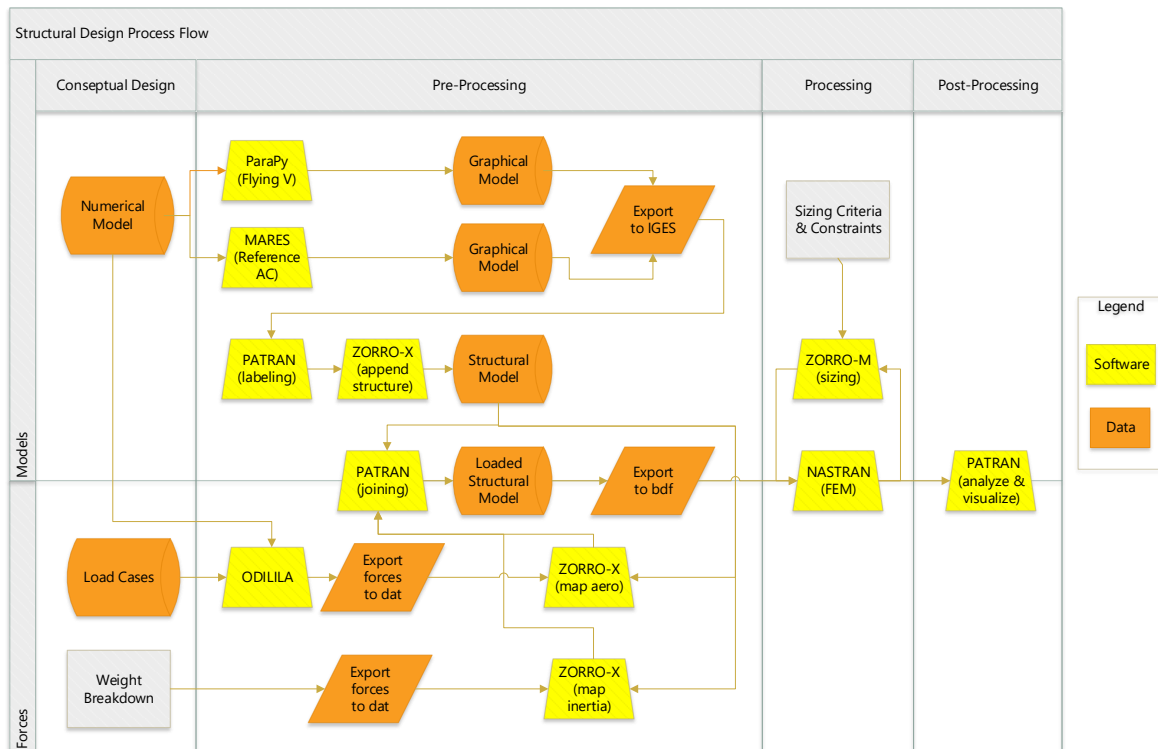


Figure 2.2: Structural Design Process Flow

II

AIRCRAFT MODELS

3

AIRCRAFT DESIGN MISSION AND REQUIREMENTS

This chapter specifies the design mission and requirements of the projected aircraft. Both the Flying V and the reference aircraft will be designed for this mission and applying these requirements.

3.1. DESIGN MISSION

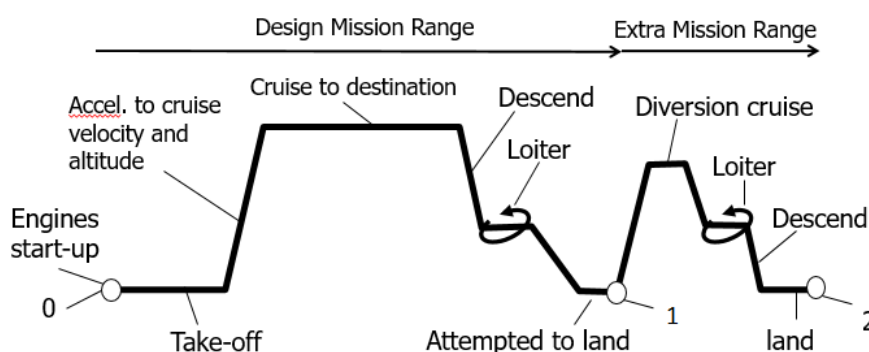


Figure 3.1: Design Mission

As can be seen in Figure 3.1, the entire mission of the aircraft exists out of two major parts. The first is between point 0 and 1, this is the design mission range, the second part is the extra mission range between point 1 and 2. This second part is required by regulations for safety, in case the aircraft needs to divert. Normally each of the segments specified in the figure (i.e. Take-off, Cruise, Descent, etc.) has its own relation between initial and final weight, called weight fraction. In conceptual design all these weight fractions are combined to determine the weight (and thus mass) of the aircraft at point 0 (Maximum Take-off Mass $MTOM = M_0$), point 1 (end mission mass M_1) and point 2 (end extra mission mass M_2).

In this case only one weight fraction is used for the design mission (between point 0 and 1). This has been done because this is sufficient for the purpose of FEM analysis. In addition, making this assumption will simplify the required computations somewhat. So the full design range is subjected to the weight fraction of a cruising aircraft. The extra mission is, in this case, defined as an additional amount of fuel, amounting to 5% of the design mission fuel. This is common practice in conceptual aircraft design.

3.2. DESIGN REQUIREMENTS

Table 3.1: Aircraft Requirements

Name	Variable	Value	Unit
Maximum Wing Span	b	65	m
Minimum Design Range	R	14 850	km
Maximum Take-off Mass	$MTOM$	260 000	kg
Cruise Mach Number	M	0.85	[-]
Cruise Altitude	h_c	11 000	m

Both aircraft should adhere to the same design requirements. These are summarized in Table 3.1. Furthermore the passenger density (pax per m^2 floor) should be the same as the A350. The payload weight is to be derived from this and should be the same for the Flying V and the reference aircraft. How the payload weight can be found is described in Section 4.2.3

4

REFERENCE AIRCRAFT

This chapter will explain how the reference aircraft has been designed. The made assumptions will be explained and the model presented. Once the outer surface model is created, the structural elements such as stringers, frames and ribs will be implemented. Their orientation and spacing will not be optimized, but estimated. Estimations are made to correlate with the structural definitions of the Flying V in order to get the two related as close as possible so they may be compared. The size of the elements will be optimized.

4.1. METHOD

In order to design the reference aircraft the standard process of conceptual design is followed. This method is described in Raymer's book on aircraft design [4]. However, this method uses values based on historical data; among those are the ratio of wetted area to reference area (S_w/S_{ref}), the aspect ratio (A), specific fuel consumption (SFC) and finally the relationship between empty weight (M_e) and the maximum take-off mass ($MTOM(MTOW)$). As the first edition of this book is from 1989 this historical data can no longer be assumed state of the art.

To overcome this issue, a (numeric) model of the A350 has been made. Using this model and comparing the results to actual data, the aforementioned variables can be tweaked to be up to date. It should be noted that some of the data from the A350 used to make this comparison is considered classified and will not be shared in this work. Furthermore, not only data of the A350 is used to establish representative values, but on occasion data-sets of multiple modern aircraft are used to make regression lines. These data-sets and regression lines too are confidential. Nevertheless the tweaked values that are obtained can and will be used as true representative values of today's state of the art.

The numerical model of the A350 has been based on publicly accessible data. Sources were used such as the A350 technical reports by Airbus [7] and numerous sites (i.e. [8–11], the first two being official Airbus site pages). The obtained wing plan-form data has been collected in an Excel sheet and is used together with the Breguet weight equation to tweak the aforementioned historical variables.

In order to visualize the process of the conceptual design of the three models, Appendix A has been included. This appendix contains flow diagrams of all the inputs, relations and outputs. These diagrams can be used to see how the different historical variables were tweaked. In addition to the diagrams, this appendix also includes the equations that have been used.

Now that the historical relations and variables are tweaked to the state of the art, the reference aircraft to the Flying V can be designed. This reference aircraft will have the same design mission and criteria as the Flying V is designed for. These were mentioned in Chapter 3.

4.2. ASSUMPTIONS

As mentioned before the reference aircraft (AC_{ref}) will have the same design criteria as the Flying V. In addition historical data is used that has been derived from the A350 and other modern aircraft. So now the question becomes which design criteria and variables of each reference should be used. These are the design assumptions of the reference aircraft. The next section will describe these different assumptions, stating the advantages and disadvantages of each assumption.

4.2.1. WING SIZING: CONSTANT SPAN VS. CONSTANT ASPECT RATIO

Choosing to adopt the span from the Flying V or keeping the aspect ratio from the historical data, will have different consequences. The influence of this assumption is shown by observing the effects when the wing area (S) is decreased. In order to get a good representation of what is happening a Table 4.1 is used to put the respective values next to each other. Analyzing this table by use of some basic equations [4], (that are also used in the conceptual design) will make the differences become clear.

The same analogy can be made for increasing the wing area. This will eventually lead to the same conclusions.

Table 4.1: Comparison of Keeping Span or keeping Aspect Ratio Constant

For Decreasing S		
Constant Span (b)	Constant Aspect Ratio (A)	Comment
Higher A	Smaller b	From Equation 4.1
Smaller S_w	Smaller S_w	Directly proportional to S (see Equation 4.2)
Higher L/D	Same L/D	From Equation 4.3 and 4.4

$$A = \frac{b^2}{S} \quad (4.1)$$

$$S_w = a * S \quad S_w \equiv S \quad (4.2)$$

Where variable S is the wing area, subscript "w" indicates wetted properties and a is determined by historical data. For now the exact value is not of importance. Only the fact that the wetted area is proportional to the wing area is used at this point. Note that herein only a wing is considered, fuselage and the part of the wing within the fuselage is not taken into account.

$$L/D \equiv \sqrt{A_w} \equiv \sqrt{\frac{b^2}{S_w}} \quad (4.3)$$

Because of Equation 4.2, Equation 4.3 is also equivalent to Equation 4.4

$$L/D \equiv \sqrt{\frac{b^2}{S}} \equiv \sqrt{A} \quad (4.4)$$

As can be seen from Table 4.1, keeping the span constant (when S decreases) will result in a better aerodynamic wing compared to the (historical) state of the art designs. If this optimum aspect ratio is kept, the aerodynamic performance remains the same. Likewise, if the surface area is increased, the wing will not be at the aerodynamic optimum. So this is a clear reason to opt for keeping the same aspect ratio that meets today's standard. Still, there are reasons to choose for the span rather than the aspect ratio. These reasons will be explained next.

Airports around the world are designed to facilitate different sizes of aircraft. To distinguish what aircraft can be served at specific airports, the airports are assigned a category rating. This rating determines factors such as maximum span and (take-off) weight. A lower span will result in being able to serve more airports. (A great example is the A380 which can't land at most airports) In fact this trend goes as far as deliberately keeping the wing span at a lower constant value for a range of MTOW. Naturally these constant values are based on the category ratings of the airports. It can clearly be seen in Figure 4.1 that the wingspan values above 36 up to mid-40 meters are usually not used. The range of MTOW that would ideally require a wingspan between these values will all have a 36 meter span. For a same wing area the aspect ratio will thus decrease, and with it the lift over drag. This penalty is accepted in light of the opportunity to serve more airports. A similar trend can be seen for aircraft that ideally require a span above 65 meter, but here the corresponding range of MTOW is much larger. For higher MTOW the L/D becomes a more important factor and one would like to use the optimum wing. At this point the penalty outweighs the advantages of more airports. Especially since the difference in number of airports being able to serve 65 meter but not 80 meter is less than the difference in airports serving 36 and not 52 meter. This is why only a relatively small MTOW range will receive the reduced span. Note that this figure is indicative only.

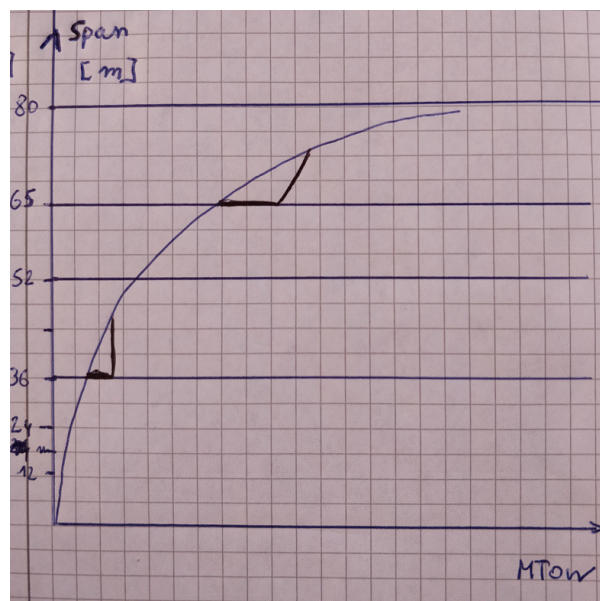


Figure 4.1: Wing Span in Function of MTOW

In addition, landing fees are higher for bigger aircraft as well. In light of these factors a span of e.g. 66 meters will not be used. Following this line of argumentation, the reference aircraft will be designed with the same 65 meter span as the Flying V.

4.2.2. EMPENNAGE SIZING: VOLUME COEFFICIENT VS. AREA COEFFICIENT

Usually volume coefficients are used when designing the empennage of an aircraft. These values aren't published, and they can't be derived from the available data with acceptable level of accuracy. The other option is to use area coefficients instead. To show that these coefficients can be a valid assumption too, the loading diagram is analyzed. In Figure 4.2 only the loads introduced by the passengers are represented. But it will become clear that the same logic can be applied to fuel, crew, baggage and maneuvering loads.

Starting from a generic aircraft, the introduced loads are represented in black. The obtained CG range are indicated in dotted blue. A minimum safety margin needs to be kept, making the minimum handling requirements (displayed in blue) slightly larger than the CG range.

Now, a redesign of this aircraft is performed; the fuselage width is increased while the length is decreased, and the available passenger area (and thus number of passengers) is kept constant. The resulting loading diagram will be narrower because of the shorter fuselage; all the receptive arms to the CG have become smaller. This is true not only for the load introduced by the passengers, but for all the loads on the fuselage, before during and after flight. The loads are represented in red in the figure. According to the volume coefficients, the tail needs to be sized anew to keep the handling limits the same. Because the arm has decreased, these coefficients will increase the tail plane surface areas, to balance out the change in arm length. In reality this redesign of the aircraft does not need the same handling limits as the initial design. The CG range has decreased, so the handling limits can shift as well, and the safety margins remain intact. The new CG range is represented by the dotted green line. As can be seen, the handling limits that are obtained by keeping the same empennage as the initial aircraft design (indicated in green) still satisfies the required safety margin.

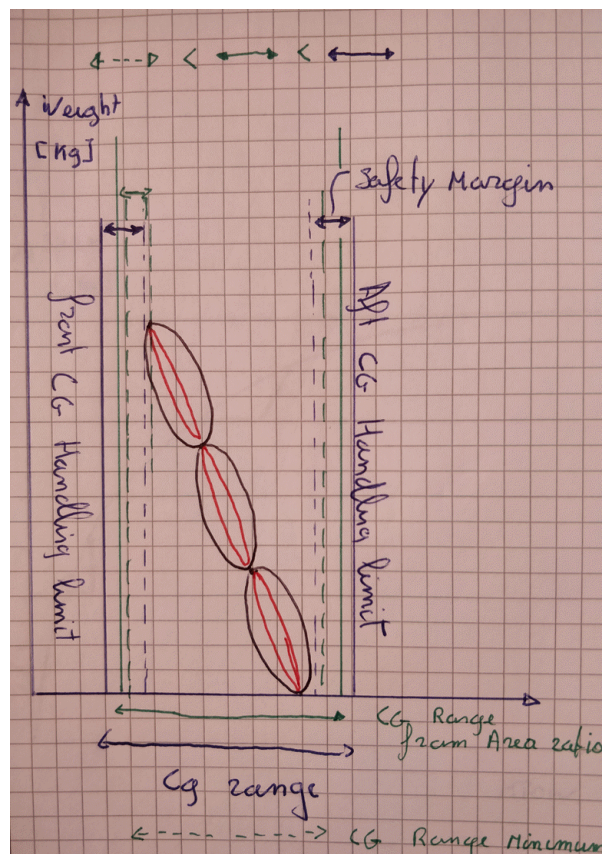


Figure 4.2: Stability Safety Margin

Experience within Airbus has shown that this phenomenon remains true for all conventional passenger aircraft. Therefore the arm length is not a critical factor when designing the empennage for this reference AC and area factors with respect to the wing can be used instead.

Furthermore it should be noted that handling is not the only contributing factor with regards to the aircraft's length (and probably not the main factor either). Other factors, for instance ground handling, contribute as well. So this might also influence the available arm length of the empennage. This is just to show that the arm length should not be considered an influential parameter for initial tail plane sizing.

4.2.3. PASSENGER DENSITY AND PAYLOAD WEIGHT

The final design assumption that has been made is the passenger density. Cabin design is a complex process, many regulations need to be followed; number of passenger per door, per flight attendant, per lavatory to name a few of them. In addition, airliners want to have customized cabins, having more or larger lavatories, different seating arrangements and different class distributions. Because of all these variations it becomes very difficult to take them all in consideration when one wants to design a new aircraft for the same number of passengers. Especially if that new design is non conventional such as the Flying V. A full interior design is not within the scope of this thesis, nor is this in the scope the initial design phase in which the Flying V is in right now. This likely will be performed in a later stage. So for now all these factors are ignored and an overall passenger density is assumed by dividing the total floor area by the total number of passengers. As for class distribution, all passengers are assumed to require the same amount of space, regardless of the class in which they fly. Consequentially, when the cabin interior is designed later on and the same dimensions for the seats specific to a class is used as it was on the reference, the resulting class distribution (percent wise) will not have changed.

So by applying this assumption, the number of passengers can be established. The floor area from the Flying V follows from the model. Using A350 data to determine the passenger density, the number of passengers for the Flying V was found to be 295. Again, by using the A350 data the payload weight per passenger has been found, and the total payload weight of the Flying V can be found as well. The number of passengers and the weight per passenger will be held constant between the Flying V and the reference aircraft. Therefore the payload weight will be the same as well. Consequentially the passenger density between the Flying V, the reference AC and the A350 will be the same.

4.3. REFERENCE MODEL

4.3.1. NUMERICAL PARAMETERS

Table 4.2: Reference Aircraft Design Data

Name	Variable	Value	Unit
Input Values			
Initial Maximum Take-off Mass	M_0	260 000	kg
Wing Loading	w/s	623.41	kg/m^2
Wing Span	b	65	m
Wing Taper Ratio	λ	0.2	[-]
Quarter Chord Sweep Angle	Λ	32	deg
Range	R	14 850	km
Specific Fuel Consumption	sfc	15	$g/kN*s$
Cruise Mach Number	M	0.85	[-]
Speed of sound (at flight level)	a	295.07	m/s
Payload Weight	W_P	56 190	kg
Fineness Ratio	l/d	10.97	[-]
HTP Aspect Ratio	A_{HTP}	4.34	[-]
HTP Taper Ratio	λ_{HTP}	0.4	[-]
VTP Aspect Ratio	A_{VTP}	1.74	[-]
VTP Taper Ratio	λ_{VTP}	0.39	[-]
Computed Values			
Wing Surface Area	S	417.70*	m^2
Wing Aspect Ratio	A	10.12	[-]
Wetted Area	S_{wet}	1 880	m^2
Wing Root Chord	c_r	10.71*	m
Wing Tip Chord	c_t	2.14	m
Mean Aerodynamic Chord	MAC	7.38*	m
MAC y coordinate	MAC_y	12.64	m
Quarter MAC x coordinate	MAC_x	20.64	m
Maximum Lift to Drag Ratio	$(L/D)_{max}$	23.46**	[-]
Cruise Lift to Drag Ratio	$(L/D)_c$	20.31**	[-]
Max to Empty Mass ratio	M_e/M_0	0.41	[-]
Empty Mass	M_e	107 520	kg
End Mission Mass	M_1	167 915	kg
Mission Fuel Mass	M_{f1}	92 085	kg
Additional Fuel Mass	M_{f2}	4 605	kg
Total Fuel Mass	M_f	96 690	kg
Maximum Take-off Mass (iterated)	$MTOM$	260 400	kg
Fuselage Length	l	65.19	m
Fuselage Diameter	d	5.94	m
HTP Area	S_{HTP}	76.89	m^2
HTP Span	b_{HTP}	18.27	m
HTP Root Chord	$c_{r,HTP}$	6.01	m
HTP Tip Chord	$c_{t,HTP}$	2.41	m
VTP Area	S_{VTP}	48.20	m^2
VTP Span	b_{VTP}	9.16	m
VTP Root Chord	$c_{r,VTP}$	7.57	m
VTP Tip Chord	$c_{t,VTP}$	2.95	m
Thickness Ratio ($\eta = 0; 0.3; 1$)	t/c	13; 11.75; 8.5	%

Blue cells refer to historically adjusted data

Gray cells refer to aircraft requirement data

The numerical parameters of the reference aircraft are presented in Table 4.2. They are obtained using Equation A.1 to A.27 given in Appendix A.1. The order of the input variables as represented in this table is the same as the order in which they are required for the equations. The order of the computed values corresponds to the order in which the equations are represented.

The values with an asterisk attached are values with respect to the trapezoidal wing. In reality the wing has a kink in it (at 30% semi-span). Therefore the real values of these variables will be different. These are given in Table 4.3.

The lift to drag ratio's of the reference aircraft are subjected to fuselage-wing interference. This will not be the case in the Flying V. To implement this difference the ratio's (indicated by ** in Table 4.2) have received a small penalty factor.

Table 4.3: Reference Aircraft Real Wing Design Data

Name	Variable	Value	Unit
Wing Surface Area	S	417.61	m^2
Wing Root Chord	c_r	13.92	m
Mean Aerodynamic Chord	MAC	7.97	m
Kink Chord	c_k	7.18	m
Kink Relative Semi-span Location	η_k	0.3	[-]

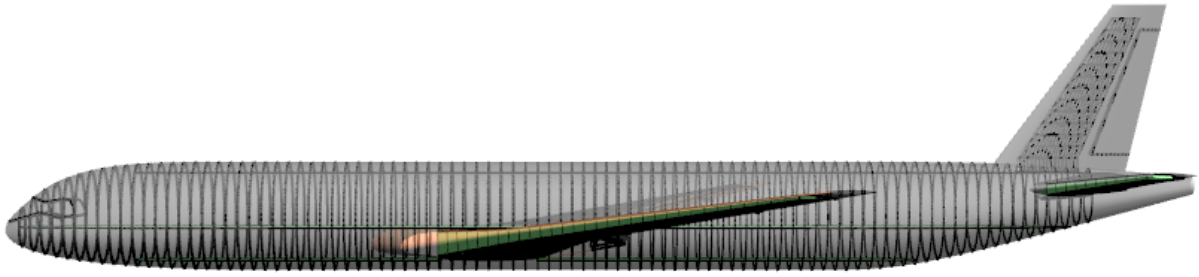
4.3.2. GRAPHICAL MODEL

Using MARES, a software developed by Airbus, this aircraft is modeled from the parametric data given in the previous section. Even though the tool supports interior design as well, together with door and window placement, this will not be done for the reference aircraft. As mentioned before, interior design of an aircraft is an extensive development. Since no interior has been designed for the Flying V, the reference aircraft will not have an interior design either. For the same reason the window and door cut-outs are not considered in these designs. This way the comparison between the aircraft models remains valid.

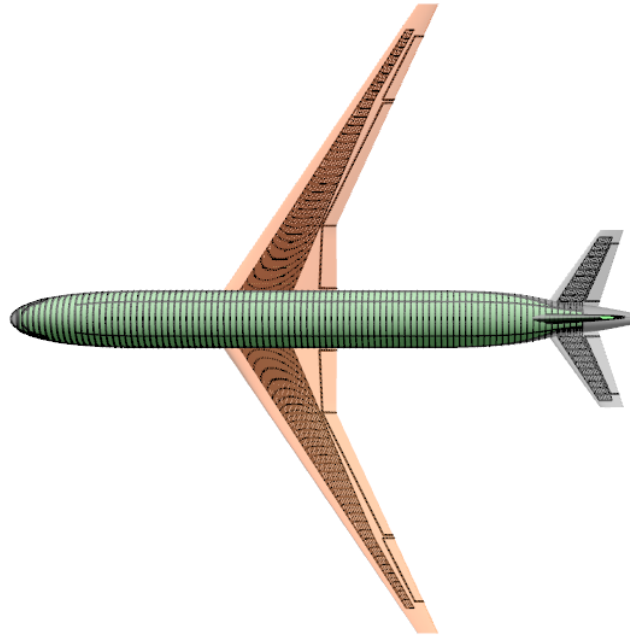
The same software (MARES) is also used to implement the wingbox, control surfaces, floors, frames, ribs and stringers. All of these are required later on for the structural analysis. The internal structure is shown in Figure 4.3.

The frame, rib and stringer spacing are not optimized but they are assumed based on frequent used values by Airbus. These values have always shown to give a good estimate; they result in realistic stress distributions and they are comparable with optimized spacing obtained for multiple aircraft in the past. Again, due to confidentiality this reference data can't be shared. The used pitch values are 25 in (0.635 m), 1 m and 0.2 m for the frame, rib and stringer spacing respectively.

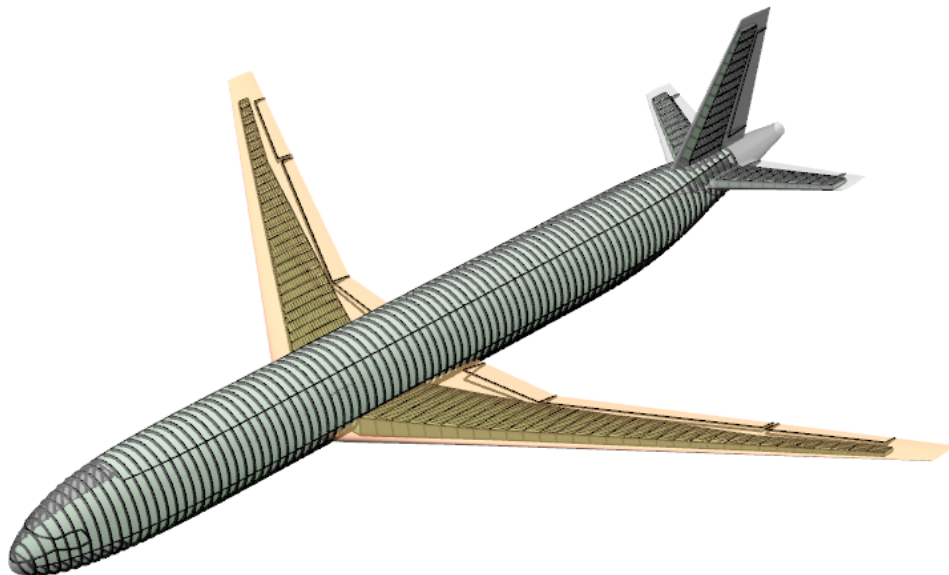
With regards to the rib spacing; in real wings the rib spacing varies over the span. This is because specific rib stations are required because airfoil changes, load introduction etc. This is more detailed design and for now an average, constant rib spacing is assumed. Furthermore a real wing can have 4, 5 or even more airfoils distributed over the wing. For now things are kept more basic and 3 profiles are used. One at the root, another at the kink ($\eta = 0.3$) and the last one at the tip. The airfoils are obtained from Airbus and are confidential. The empennage has just a single NACA 0012 airfoil. This one is used for both HTP and VTP. The orientation of the ribs in real wings is not stream-wise at every point like the ones in the reference frame are. In real wings some are stream wise (i.e. the first rib and kink rib) but other ribs are angled gradually to become perpendicular to the rear spar. In MARES the orientation of the ribs is interpolated between the design ribs/wing sections. In this case these are the ribs at the root, kink and tip. Those are all oriented stream-wise, therefore all the intermediate ribs are stream-wise too. There is no quick option to orient specific ribs to be perpendicular to the rear spar. This is a limitation of the MARES software. The only way to do this would be by defining additional ribs, calculate the required angels and spacing, leading edge point, trailing edge point etc manually. This requires a lot of work and the amount of time spent on this can be applied more effectively in other areas. So for now the automated stream wise orientation of MARES is accepted.



(a) Left View



(b) Top View



(c) Isometric View

Figure 4.3: Reference Aircraft Structure

At the intersection regions the spacing of these elements is slightly altered in order to properly align. For instance, looking closely at Figure 4.3a one can see that the frame spacing at the center wingbox is slightly different to the other frames. To show the intersections the following images are included. As can be seen in Figure 4.4, every third stringer coming from the wing coincides with a frame from the fuselage. Note as well that the center wingbox has no sweep contributed, the stringers too are straight in this section. This is standard practice and is to (among other things) free up sufficient space for the main landing gear storage, air conditioning units etc.

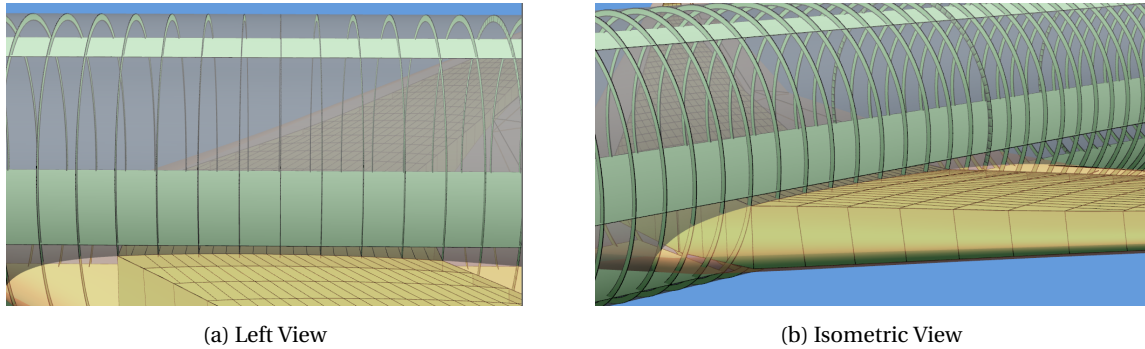


Figure 4.4: Wing-Fuselage Intersection

The intersections of the HTP and VTP to the fuselage are carefully designed. Here the frame spacing in the fuselage is not changed, but rather the respective wingboxes are changed in size. This is possible here because there are less limiting factors to designing the wingboxes. Namely only a single control surface, no landing gear etc. The alignment of the HTP and VTP to the fuselage can be seen in Figure 4.5.

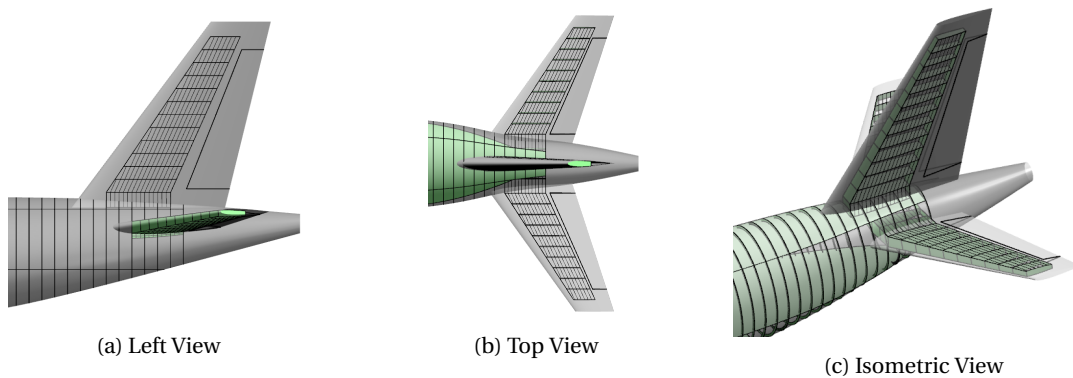


Figure 4.5: Empennage-Fuselage Intersection

5

FLYING V

The model of the Flying V has been developed over the past years. To build the model a software named ParaPy has been used. For more details about how the model was created please refer to the thesis paper of Luuk Van Der Schaft [2]. Most values were obtained directly from this model, but some still needed to be computed. Specifically the aerodynamic forces and weight estimations were computed. To obtain these, the same equations are applied as for the reference aircraft. They can be found in Appendix A.1.

5.1. FLYING V MODEL

5.1.1. NUMERICAL PARAMETERS

Table 5.1: Flying V Design Data

Name	Variable	Value	Unit
Input Values			
Initial Maximum Take-off Mass	M_0	260 000	kg
Range	R	14 850	km
Specific Fuel Consumption	sfc	15	$k/kN*s$
Cruise Mach Number	M	0.85	[-]
Speed of Sound (at flight level)	a	295.07	m/s
Payload Weight	W_P	56 190	kg
Wing Span	b	65	m
Wing Area	S	895	m^2
Root Chord	c_r	24	m
Tip Chord	c_t	3.60	m
Taper Ratio	λ	0.15	[-]
Aspect ratio	A	4.72	[-]
Wetted area	S_w	1983.17	m^2
Thickness Ratio ($\eta = 0; 0.2; 0.38; 0.6; 1$)	t/c	15.5; 15; 16; 9.25; 9	%
Computed Values			
Wing loading	w/s	290.50	kg/m^2
Mean Aerodynamic Chord	MAC	16.28*	m
Quarter MAC x-coordinate	MAC_x	26.64	m
Maximum Lift to Drag Ratio	$(L/D)_{max}$	23.35	[-]
Cruise Lift to Drag Ratio	$(L/D)_c$	20.22	[-]
Max to Empty Mass ratio	M_e/M_0	0.41	[-]
Empty Mass	M_e	106 745	kg
End Mission Mass	M_1	166 305	kg
Mission Fuel Mass	M_{f1}	91 695	kg
Additional Fuel Mass	M_{f2}	4 585	kg
Total Fuel Mass	M_f	96 280	kg
Maximum Take-off Mass (iterated)	$MTOM$	259 215	kg

Blue cells refer to historically adjusted data

Gray cells refer to aircraft requirement data

The wetted area here is obtained by measurements in the ParaPy model. Herein all the surfaces but the nacelles are accounted for. Having a higher wetted area will decrease the L/D somewhat, and thus the MTOM will be a bit higher. To compensate for this the optimized MTOM from Table 5.1 is increased by adding some fuel weight. The updated values are given in Table 5.2. The new MTOM is set to be the same as the desired one by the requirements. This way both aircraft have the same payload, design range, span and MTOM, and a fair comparison can be made.

Same as in the data of the reference aircraft, the values with an asterisk attached are values with respect to the trapezoidal wing, in reality the Flying V has one geometrical kink (not to be confused with the two structural kinks that will be defined later) in it at 60% semi-span. Therefore the real values of these variables will be different. These are given in Table 5.3.

Table 5.2: Flying V Compensated Design Data

Name	Variable	Value	Unit
Maximum Take-off Mass (iterated)	$MTOM$	260 000	kg
Wing Loading	w/s	290.50	kg/m^2
Total Fuel Weight	W_f	97 065	kg

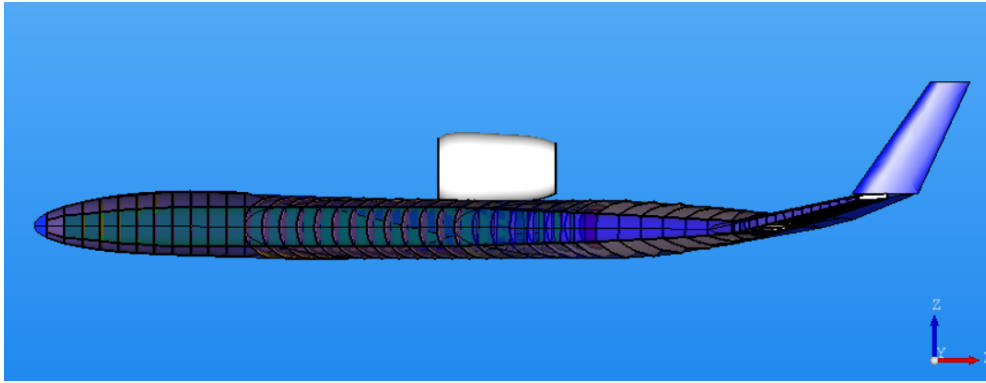
Table 5.3: Flying V Real Wing Design Data

Name	Variable	Value	Unit
Wing Surface Area	S	895	m^2
Wing Root Chord	c_r	24	m
Mean Aerodynamic Chord	MAC	17.82	m
Kink 1 Relative Semi-span Location	η_{k1}	0.38	[-]
Kink 2 Relative Semi-span Location	η_{k2}	0.6	[-]

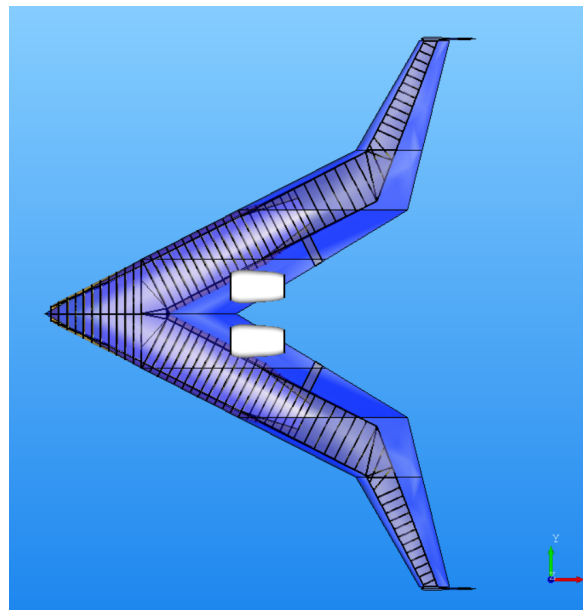
5.1.2. GRAPHICAL MODEL

The graphical model together with an initial structural definition has been established mostly by Luuk's effort during his thesis assignment. This structure includes the ribs, frames, cabin, pressurized oval and spars. Figure 5.1 shows transparent views of the Flying V so that the internal structure may be observed. These pictures are obtained from ParaPy, the software in which the model has been created.

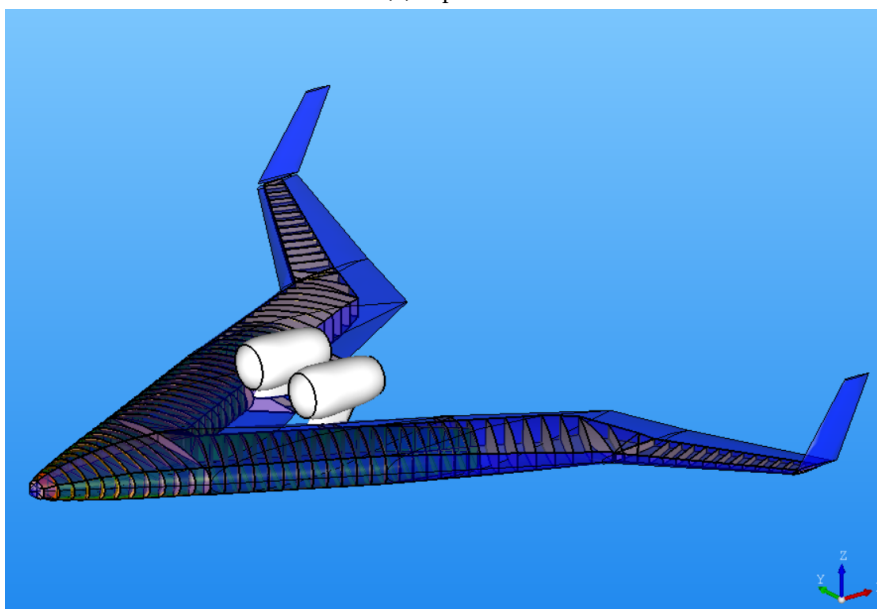
The spacing of the different elements in the Flying V was adopted from the reference aircraft, which got the spacing from Airbus estimates. The rib spacing is 1 meter, the frame spacing is 25 in (or 0.635 meter) and the stringer spacing is approximately 0.2 meter. Note that these values are target values, the actual spacing might be slightly different depending on the location. For instance, in the front where the frames are perpendicular to flight direction, the frame spacing is recalculated in order to keep the frames equidistant in this region. Consequentially the true frame spacing in this region is 0.617 meter. The same method is applied to the frame oriented at an angle up to the end of the pressurized vessel, and the rib spacing starting just behind it, up to the wing kink. Aft of the wing kink the rib spacing up to the tip is made equidistant too. At all times the actual values resulting from this method is kept as close as possible to the target values mentioned before.



(a) Left View



(b) Top View



(c) Isometric View

Figure 5.1: Flying V Structure

At this point the only missing entities compared to the reference model are the stringers. So with the help of Luuk and Max Baan (a ParaPy developer) the stringers were implemented as well. Same as in the reference aircraft the stringers are parallel to the (local) rear spar, and the stringers at the front spar run out at the intersection point. The number of stringers is the input variable and they are distributed equidistant over the curve at which they are defined. The number of stringers is chosen to be as close to the desired pitch of 0.2 meter as possible. This stringer pitch is the same as used in the reference aircraft. In total six curves are used as stringer definitions.

At the first frame of the straight cabin both top and bottom curves of the pressurized vessel are used for stringer definition planes. These curves are on the outer surface. Both of these curves have two stringer definitions on them, one for stringers going inboard to the nose segment, the other for the stringers going outboard to the cabin (and later wing) segment. By doing this, it is ensured that all stringers make a kink at the same frame station, and no intermediate stringer run-outs are required. Furthermore improper alignment of the stringers between these sections is thus avoided.

The frame at which the wing kink is located has stringer definitions on the top and bottom curve of the wingbox. These stringer definitions are only for the wing part after the kink. Before the wing kink the stringer definition of the cabin is used. Because the number of stringers is the same, and up to the kink the length of the curves are (almost) the same no stringer run-outs should occur between the two kinks. Furthermore they should nicely meet up at the kink too. The stringer implementation can be seen in the following figures.

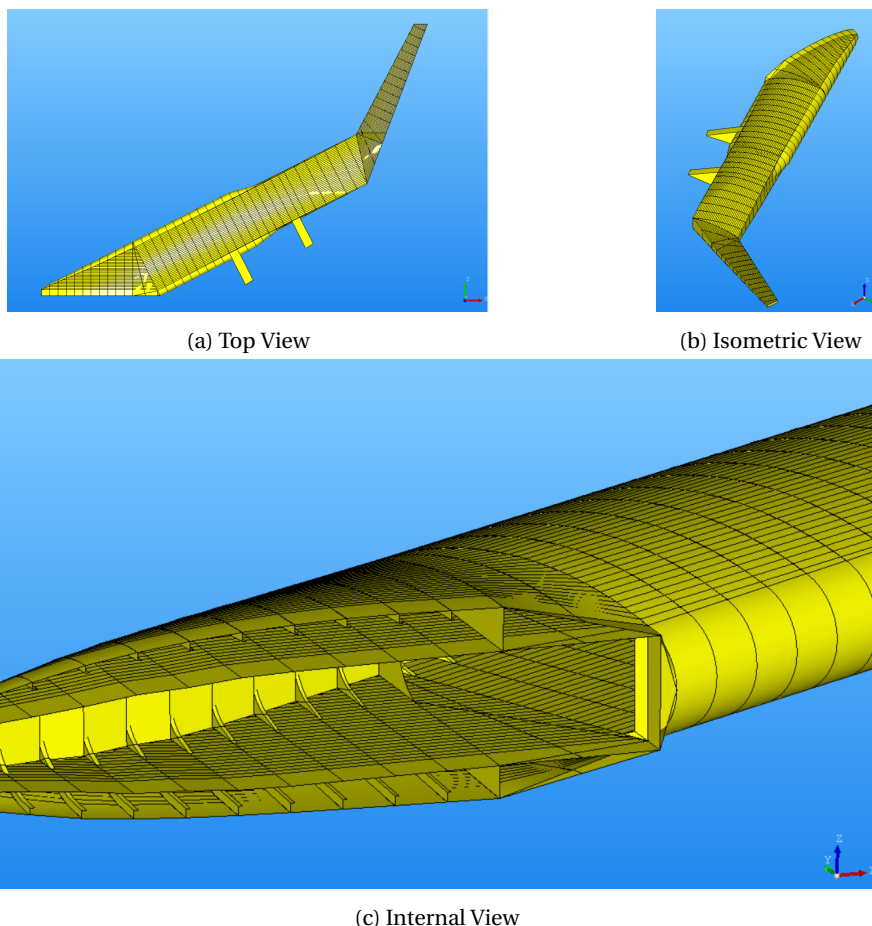


Figure 5.2: Flying V Stringers

Note: in the top view there are some inconsistencies in the stringers. This is an graphical misrepresentation. When changing the angle one will see that there is no problem. Same for some regions of the internal view.

III

FEM ANALYSIS

6

STRUCTURAL MODELING

In this chapter the models are appended to structural models, and the meshes are created. The entire appending process will be laid out in the following pages, explaining how the tool called ZORRO is utilized. Because of limitations some assumptions needed to be made and parts of the mesh required manual adjustments. All of this will be addressed for both the reference aircraft and the Flying V alike.

6.1. METHOD

At this point the models of both aircraft are just parametric and graphical. Furthermore the graphical models are built only using shells. When a FEM analysis will be performed a more detailed model is required i.e. a structural model. The structural model will have different types of elements; not only surfaces but also solid items like beams and struts. The model will be full 3 dimensional, meaning that every stringer, beam and strut will have flanges, webs, volumes and moments of inertia. Frames too will have a 3D profile and the remaining surface items such as skins or floor panels need to have orientations and thicknesses. The floors also require supporting and stiffening structure such as (3D) cross beams, longerons and struts. All the elements will need a material specification with the respective properties attached.

6.1.1. PATRAN AND NASTRAN

The software called PATRAN is used to make and visualize the models before they are fed through to NASTRAN, the software that performs the FEM analysis. Other than the structural model and mesh, the boundary conditions (BC's) and forces are also required by NASTRAN. These too can be created by PATRAN. If all these elements are created PATRAN can write the NASTRAN input deck according to the (NASTRAN) requirements.

NASTRAN itself is just a solver; it has no visualization option at all. It requires an input file of a specific format and lay-out, does the calculations and writes an output file. So in order to visualize or even interpret the outputs from the FEM analysis another software than NASTRAN is required. Again this can (and will) be done by PATRAN.

So to recap; the geometrical models need to be appended and the forces, load cases and boundary conditions need to be added. All this is done in PATRAN, after which it will write the required NASTRAN input deck. NASTRAN is used to perform the FEM analysis and exports the results to data files. These data files can be connected to the model in PATRAN, where they can be visualized and analyzed.

appending the geometrical models to become full 3D structural models manually in PATRAN would be a tremendous task. So a pre-processing tool to automate this entire process has been developed over the years by Jörn Clausen at Airbus. This software will be used to append the existing models to full structural models.

6.1.2. ZORRO-X TOOL

Two different versions exist of ZORRO; the pre-processing tool called ZORRO-X, and the sizing tool ZORRO-M.

For now only the pre-processing ZORRO-X is utilized. ZORRO-X has been made to work in conjunction with PATRAN. It basically writes a PATRAN session file that will make all the adjustments and extensions requested by the user. In essence the user specifies in ZORRO-X what needs to be done to the entities existing in the model. All the repetitive steps of actually modeling (create node by intersection curve and plane, connect nodes by element, specify element properties etc.) is done by ZORRO-X. Naturally ZORRO-X needs to know what steps need to be done to each individual entity. This is why it is important to name all the elements logically, this way ZORRO-X can utilize ranges of elements and the user can easily obtain the location of a specific element by its name.

ZORRO-X is not able to model an entire aircraft structure in one go. There are different modeling methods for different types of structures. As such two major modeling groups are distinguished; the fuselage and the wing. The HTP and VTP are modeled using the same methods as the wing. Each of these two groups has a number of templates that can be used. The most versatile of these templates are the ones that are so called plane based for the input deck. These are the templates that will be used in this thesis research.

Having a plane based template means that the location, orientation of all the elements are defined using planes. The only curves that are still required in the model are the outline of either the wingbox ribs or the fuselage skin frame station (depending on the modeling group that is used at the moment). These curves need to be numbered sequentially in the input model. The stringers and floors are defined by a sequential range of planes.

As mentioned before, the labeling of curves and planes in the input model is crucial. In the wing modeling group the upper and lower edges of the wingbox need to be distinguishable by their label. Therefore the used labels are at least three digits; the later two (tens and unit positions) are sequential from root to tip, while the first digit is specific to the location (i.e. 1 for upper curves, and 2 for lower curves). in the same manner plane ranges for the stringers are distinguished; the later two digits are sequential going from leading edge (LE) to trailing edge (TE), and the first digit is specifying the location (i.e. 1 for the stringers in front of the first structural kink, 2 for between the structural kinks, 3 for behind the second structural kink and 4 for the winglets). In the fuselage modeling group the frame curves are to be labeled sequentially from nose to tail, and if more curves are used to make up 1 half of the fuselage profile, they are distinguished by the first of the three digits in the label. The stringers are labeled sequential from top to bottom.

6.2. FLYING V STRUCTURAL MODEL

As previously explained, ZORRO-X adapts and extends the graphical model in PATRAN to the structural model. Only the curves describing the surfaces at each frame or rib station, together with the planes for the orientation of stringers and floors, are required in this graphical model. Thus these properties are exported from the ParaPy model of the Flying V. This exported model is shown in Figure 6.1.

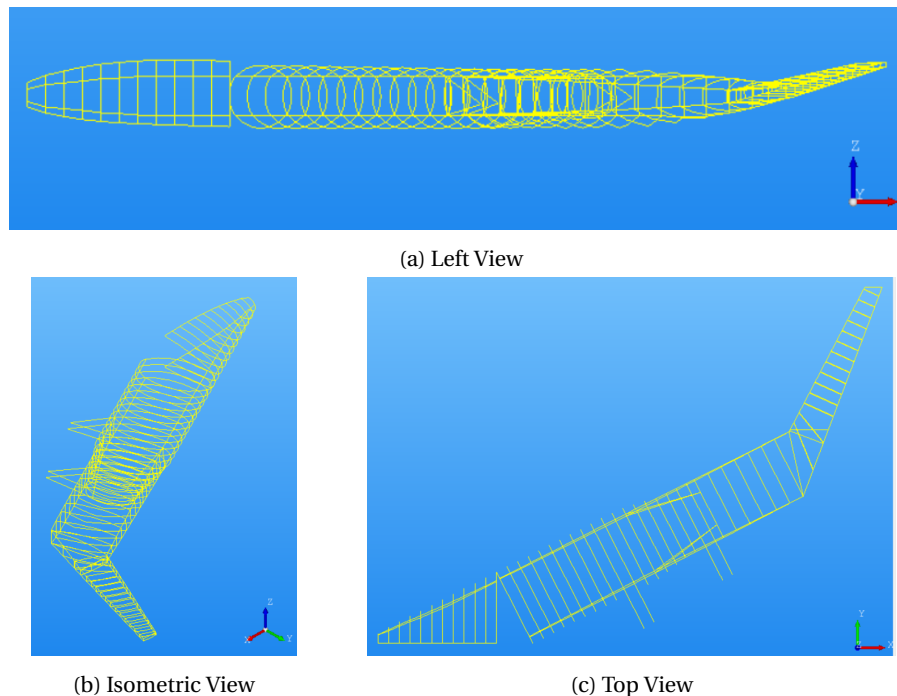


Figure 6.1: Flying V Exported Elements from ParaPy

Notice that the stringer and floor planes are not present in this export. PATRAN was unable to process the exported planes from ParaPy, it did not recognize them as being planes. The definition of a plane (i.e. vector and point, three points, two vectors etc.) is different in both software platforms. Therefore the planes were exported by other means. The normal vectors were exported to txt file, and the points were in the IGES export. The planes were then manually recreated in PATRAN.

In the next couple of sections it will be shown how this model will be appended to the full structural model. First the full model is divided into parts, next some required alterations are made. The following step is to use ZORRO-X to get the initial 3D structure. Meshing errors are resolved manually and the final structural model and mesh are obtained.

6.2.1. PARTS SUBDIVISION

In order to model the Flying V with ZORRO-X, the wing is subdivided into parts. Only half of the Flying V was to be modeled initially, with the purpose of manually mirroring the structure afterwards. This idea has quickly been abandoned though. Manually mirroring the structure would mess up the labeling of all the different elements, nodes etc. While this does not pose a problem for running the model in NASTRAN, it is inconvenient for the user. The labeling as provided to the elements by ZORRO-X is consistent with the location of the elements. Therefore an element's label can be of great help in locating it in the overall structure. Furthermore the mirrored parts of the model might miss some attribute data such as orientation or material properties. This would pose a problem for the FEM analysis of NASTRAN. In order to avoid this the entire model should be checked and complemented for every minor detail. Not an easy thing to do for a model consisting of thousands of elements. For these reasons manual mirroring of the structure is not done.

Furthermore ZORRO-X is made for conventional aircraft. Modeling a non conventional aircraft using a method to model conventional aircraft, requires some ingenuity, assumptions, compromises and alterations in the ZORRO-X program.

So the Flying V needs to be subdivided into parts in order to fit within one of the two categories: fuselage or wing. Three parts are used. They are shown in Figure 6.2.

The first part is the nose section. It is between the light green line and the first red line on the figure. The light green line is located at the most forward point of the nose, the first red line is located at the first frame of the straight fuselage; the first structural kink. Note that this is also the frame station where the stringer orientation is defined for both the nose, cabin and first part of the wing (see Section 5.1.2). This specific frame itself will not be in the model created of the nose part, but instead will be in the part of the cabin. All the elements in the nose part (skins, stringers, floors etc) will be modeled up to this frame.

This part, dubbed "the nose" will be modeled using the fuselage template. This template requires the curves describing the outer surface of the structure at the frame locations. Other important template specifications are floor and stringer locations (by specifying planes), stringer run-outs, material properties, strut definitions and locations etc. Only one half of the curves (left or right) needs to be provided as an input, ZORRO-X will mirror the structure over the global x-z plane. As the mirroring is done by ZORRO-X itself, the element's label and attributes will all be allocated automatically and correctly, for both sides. Consequentially this one part will be a model of both the left and the right hand side of the nose.

The next part is called the cabin, it is located between the two red lines on the picture. As previously mentioned the first frame of this part is the one at the structural kink, the part continues upto and including the aft pressure bulk head. The curves used are those of the pressurized vessel, therefore it is partly coinciding with the outer surface and partly tapered, no longer on the outer surface. The cabin will be modeled using the fuselage template as well. As explained before only half of the outer surface curves are required. The template will mirror them to close the fuselage model. In a conventional aircraft the fuselage is in line of flight. In this case, the cabin is at an angle with the flight direction. So the mirroring of the curves around the global x-z plane is not correct in this case. To solve this issue the ZORRO-X program needed to be altered. ZORRO-X was updated by its developers to include the possibility to specify a local coordinate system in which the entities are mirrored. Thus the right hand cabin of the Flying V can be modeled using ZORRO-X too. To model the left hand cabin, another part is required with its own set of input curves. To create this part the curves were manually mirrored in the graphical input model. A new input deck of ZORRO-X was adjusted accordingly. By running this trough ZORRO-X as well the left hand cabin part is created.

The last part is the wing. It starts at the yellow indication line on the figure. This location is where the cabin starts tapering inwards. The part describes the outer surface and continues all the way up to the tip of the Flying V, including the winglet. This part is modeled as a wing in ZORRO-X, therefore it has ribs rather than frames, and it needs the upper and lower curves describing the wingbox at every rib station. Additionally the input deck requires material specifications and stringer orientations. This template in ZORRO-X offers the feature to mirror the wing (again automatically with correct labeling and attributes) over the global x-z plane. This is done too and thus this part, similar to the nose part contains the model of both the left and right hand side.

As can be seen from Firure 6.2 the wing part is overlapping with the cabin part. This was required to model the entire structure, namely both the tapering cabin and the overlapping wingbox. Consequentially some structural interference occurs; the first couple of ribs of the wing are run trough the tapering section of the cabin. Unfortunately there is no better way to model this transition part, nor can this be automatically improved. Manual remodeling of those local ribs will be required. Exactly what and how it's done will be described later in Section 6.2.4.

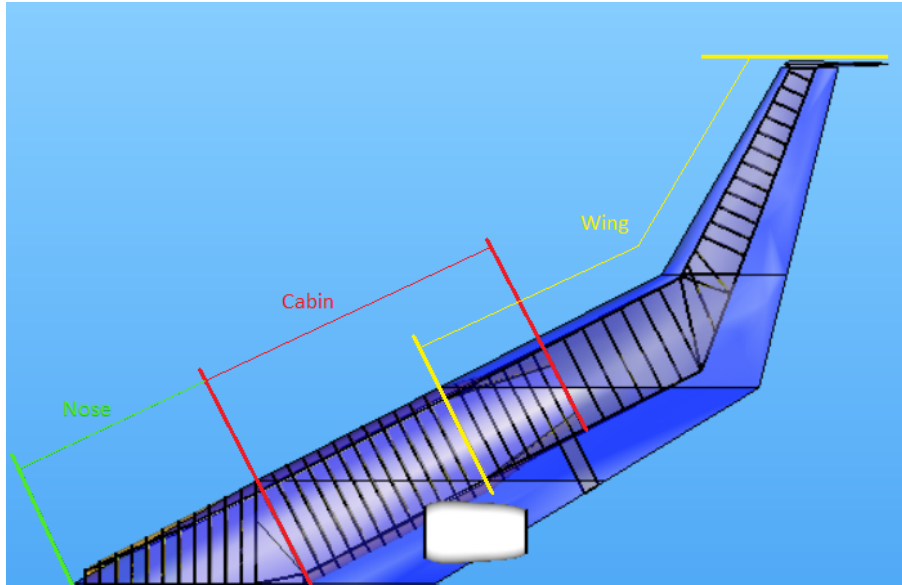


Figure 6.2: Flying V Parts Subdivision

Finally an overview of all the parts that are used, together with the modeling template is provided in Table 6.1.

Table 6.1: Flying V Structural Modeling Parts

Part	Template	Application Region
Nose	Fuselage	Both sides
Cabin Left Hand Side (LH)	Fuselage	Left side only
Cabin Right Hand Side (RH)	Fuselage	Right side only
Wing	Wing	Both sides

6.2.2. GRAPHICAL MODEL ADJUSTMENTS

When looking at the graphical model with the intention of creating a structural model and later performing a FEM analysis, two regions stand out immediately: both structural kinks. In the graphical model these regions have barely any elements. The first structural kink (called the nose kink and located at $\eta = 0.2$) only has skin and floor panels and a frame just before and just behind the kink, thus leaving quite a large gap between the two frames at the trailing edge (see Figure 6.1c). Additional frames are required here to cope with all the introduced forces and stresses. The second structural kink (called the wing kink and located at $\eta = 0.6$) has a couple of ribs in it, but these are intersecting (see Figure 6.1c). ZORRO-X can not model intersecting ribs, this is one of the limitations of the tool. But in reality intersecting ribs are not used either. They are too difficult to manufacture and install. So the region at the wing kink will need to be remodeled in the graphical model.

Furthermore, the winglets in the graphical model of ParaPy have only the profile, but no internal wingbox. So this will have to be created manually too.

These changes are made in PATRAN rather than in ParaPy, for two reasons. First, The PATRAN model is much cleaner (only the required curves) and therefore much easier to adjust. Second the model in ParaPy still has some bugs in it. The necessary elements are working but extending the model or significantly changing it would be troublesome.

NOSE KINK ADJUSTMENTS

The nose kink is fully located in the nose part. As has been explained in Section 6.2.1, the nose part goes up to the first frame of the cabin part. It was decided to continue the frames parallel to the ones already present in the nose part, and let them run up onto the first frame of the cabin part. Meaning that they do not go all the

way to the LE. The spacing of these frames is done as follows; first the same spacing of the previous frames is adapted. This leads to the last stringer being very short and close to the trailing end point of the cabin frame. So these frames were redistributed equidistant to get a better spacing. Finally, in order to be able to mesh the structure later on, each of the newly created frames was moved horizontally to align with the closest stringer node of the cabin. This way all of the elements (and parts) can be connected properly. The resulting spacing between the new frames varies between 0.677 and 0.611 meter. Remember the frame spacing of the ones already in there was 0.617 meter.

The frames in the nose part are half of the local oval. But the frames in the cabin are a full oval. Therefore the trailing points on the frame outlines of the cabin are lower compared to those of the nose. So the added frames must bridge this vertical gap too. By creating a temporary surface between the first frame outline of the cabin and the last full frame outline of the nose (a.k.a. the last of the original frames) and defining the new frames on this surface, it is made sure that the change is gradual. The change in height of the trailing points on the frame outlines can clearly be seen in Figure 6.3. This figure also shows how the added frame outlines (displayed in orange) are running only up onto the first cabin frame outline (displayed in blue). All the blue frames are the original exported frame outlines from ParaPy.

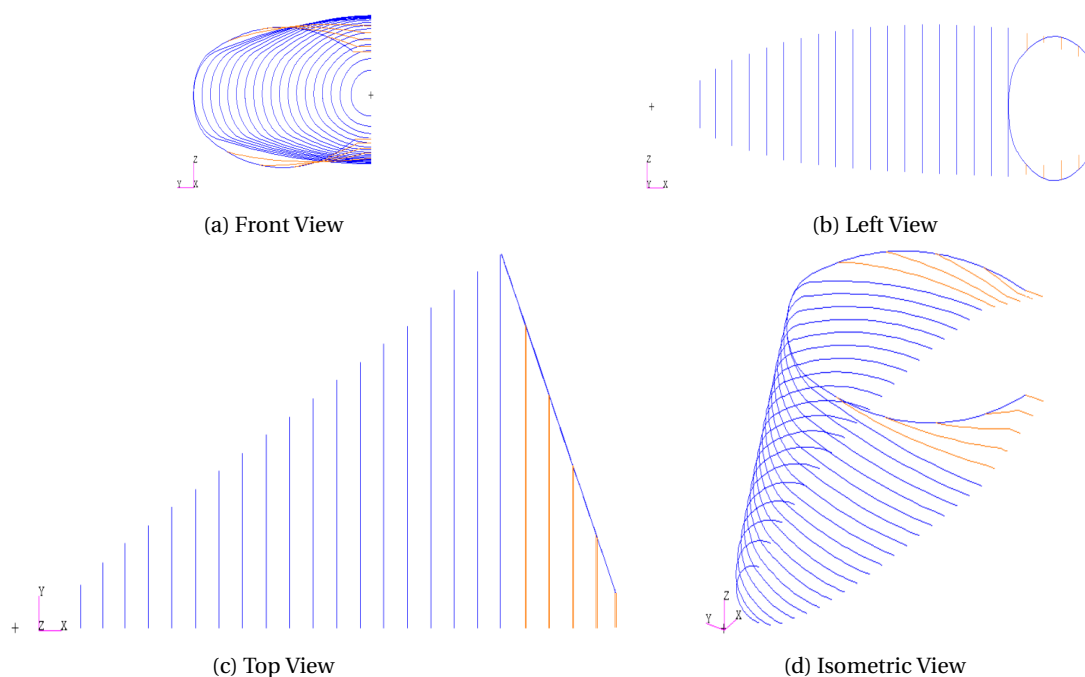


Figure 6.3: Adjusted Nose Part Flying V

WING KINK ADJUSTMENTS

New ribs are installed in the wing kink as well. Again these are shown in orange in Figure 6.4, and the blue ones are the original. Initially, to determine the orientation of these new ribs the same method as in the nose was considered. Namely, keeping the orientation parallel to those prior to the kink and running them up onto the first rib after the kink. This idea, while structural viable and manufacturable, is not possible, since ZORRO-X can not handle ribs that don't run between FS and RS. This is a known limitation of the tool. ZORRO-X will make the front spar by connecting the leading points of all the rib curves. So another solution needs to be implemented. The new ribs are now all angled and the orientation changes gradually between the ribs in front and behind the kink. Extra care has been taken to ensure that the ribs do not intersect at the leading edge, instead a minimum distance of 2.5 cm between the ribs is maintained. This is to avoid meshing errors. The number of new ribs is chosen so that the maximum spacing at the RS does not exceed 1 meter at any point. For this same reason two additional ribs are installed just behind the kink.

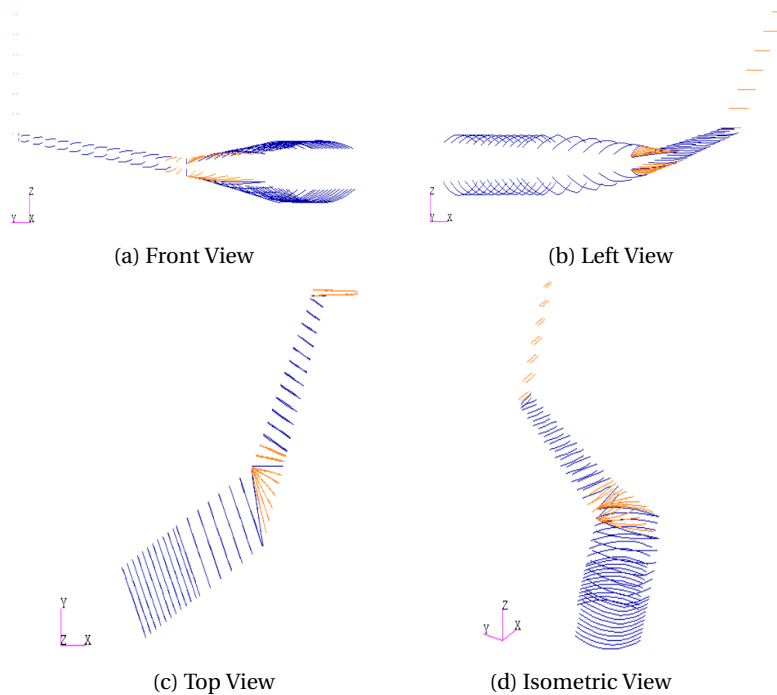


Figure 6.4: Adjusted Wing Part Flying V

WINGLET

To create the wingbox of the winglet the location of the FS and RS with respect to the local chord are kept constant to those at the wingtip. The stringers are made parallel to the RS and are continuations of the stringers in the wingtip. In conceptual design the orientation of these ribs is usually chosen to be perpendicular to the rear spar. While designing them this was not yet known, and by the time this became clear the overall design had already advanced too far to make this change. However, the final orientation will not be perpendicular to the RS either. Instead, orientation of ribs is usually subjected to optimization during detailed design.

The resulting winglet rib outlines are also shown in Figure 6.4.

6.2.3. INITIAL STRUCTURAL MODEL AND MESH

At this point every part is ready to be put through ZORRO-X. Before doing so, the labels of the curves and planes are checked one more time and the input templates are made for the different parts.

After every part has been designed by ZORRO-X, they are joined in an assembly. Pictures of the individual parts will not be generated here. Because the manual adjustments are relatively small scaled or on the internal structures, there is not much visual difference between the initial and final structural model. So these manual adaptations will be discussed first, and afterwards the final structural model will be presented, including some figures.

FUSELAGE TEMPLATE

For the fuselage templates the first thing that needs to be specified is the stringer range per frame range. In tapering sections this becomes a bit more complex. The planes are defined on a single curve and normal to that curve. The curvature, and occasionally the center, changes in the tapered sections, so the planes will intersect these curves at another location. This can be observed in the manual sketch in Figure 6.5. The black outer curve represents the one where the planes (marked red) are defined equidistant. The blue curve represents a structure outline at another location (in front or behind). Either the center is changed or the curvature. In both cases one can see that the resulting stringers at the other location are no longer equidistant. In addition to this phenomenon, in some instances the stringer orientation is not normal to the curve. For instance in the cabin part the stringer definition planes are either vertical (at the top and bottom curves of the oval) or

horizontal (at the front or back curves). In this case it was required to ensure that the stringers would be on the same locations with respect to the wing part. The different orientations further complicate the matter. So determining where the stringers intersect and thus where they should run out is challenging. As this process is not automated, eventually it is done by manual plane/curve intersection in PATRAN to identify the run-out location of each stringer separately, together with some trial and error until a good mesh was obtained.

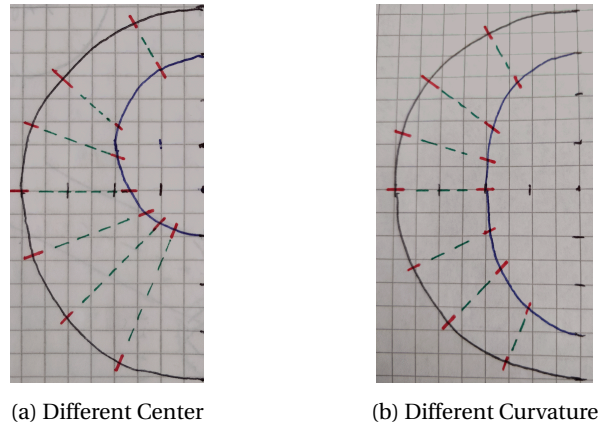


Figure 6.5: Stringer Pitch Variation

Furthermore the floor needs a stringer to be attached to, so a stringer should be at the same height as the floor. Rather than moving just 1 stringer and possibly creating a large local stringer pitch variation, all the stringers above and below the floors are redistributed to be equidistant. So once more, the stringer pitch of 0.2 meter is considered an ideal goal rather than an absolute must-achieve value.

The floor also needs supporting struts. This is defined in the template by specifying the longeron that needs the supporting strut, and the fuselages stringer that will connect to this strut. (the number of longerons is an input variable as well, spacing is automatically configured to the number of longerons and is non-adjustable). It is possible to define a plane in which the struts should be. But then the nodes of the longeron and stringer will be moved to fall in this plane. Since so much attention has been dedicated to proper spacing of the stringers, moving just one of them to get a very specific strut location is not desirable.

WING TEMPLATE

In the wing template the stringer run-outs are automatically done when intersecting either the FS or RS. What needs to be specified manually is how many elements should be in the spars. It is possible to vary the number of elements over the span, as the height of the spar will be decreasing drastically too. Furthermore skin, rib and spar thicknesses can be specified as well, for each entity separately or over a specified range. Obviously these thicknesses will be altered during the optimization, but an initial indication is important. Thicker elements will attract more of the loads from the start, so in the neighborhood of high loads these elements will be increased during the optimization. Thinner elements on the other hand are less likely to attract loads and thus will be less likely to increase in thickness.

At the wing kink the orientation of the stringers will change too. Consequentially the minimum distance between them is drastically decreased after the kink. To get a more realistic stringer pitch, only every other stringer is continued after the kink. The others run out at the kink rib. By doing this the resulting stringer pitch after the kink is once again very close to the desired 0.2 meter, namely 0.196 meters. Only the very first stringer behind front spar is kept at the smaller pitch (this stringer does not run out at the kink). This is done because at the kink there are a lot of ribs coming close together at the front spar. Having a stringer pitch of 0.2 meter at this location would result in very slender mesh elements. This can not give accurate results, so in order to make the individual elements viable, the local stringer pitch is made smaller as well. This is no problem because that specific first stringer runs out fairly soon after the kink. Both the stringer run-outs and the local smaller stringer pitch can be observed in Figure 6.6. This is an image of the top view of the wingbox structure at the wing kink.

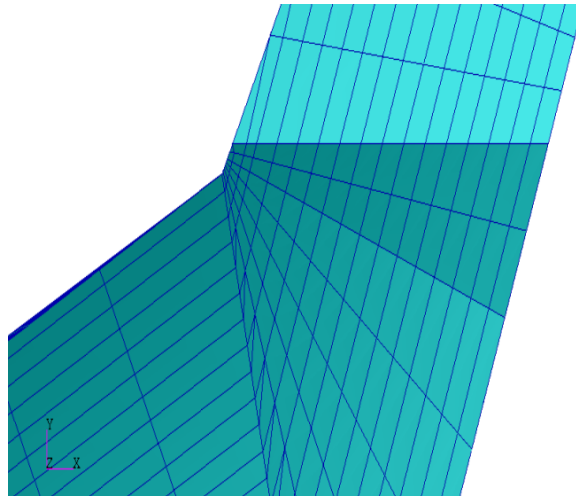


Figure 6.6: Flying V Wing Kink Structure

6.2.4. MANUAL ADJUSTMENTS

In order to connect the nose part to the cabin one needs to make the local nodes of both parts equivalent. During the modeling of the different parts special attention was paid in order to get the stringer alignment between the parts just right. Meaning that the stringer nodes of the different parts are nearly at identical positions. As a consequence these are easily connected. The floor elements need to be connected too. Here the number of elements (and thus nodes) is equal between the two parts, but their respective spacing (location) was not. This could not be avoided, the spacing was set automatically by ZORRO-X. Some quad-elements of the nose floor needed to be changed to multiple tri-elements to compensate for the different number of nodes. The properties of all the elements are kept in this process. More details and pictures can be found in Appendix B.1.

As mentioned before the first couple of ribs of the wing part interfere with the aft cabin. Ribs are fully closed entities, and thus form in effect walls inside the cabin at the transition. To resolve this issue the inner rib elements are deleted, while the outer ones (located between the wing and cabin surface) are connected to the cabin frames by moving and equivalencing local nodes. This way the two parts are connected structurally. Unfortunately the number of nodes between the ribs and frames was not the same, so in a similar fashion quad-elements were changed into tri-elements. Only this time only one tri-element was used as a replacement per initial quad. Every quad element is enclosed by supporting beam elements. Keeping those during the process of changing quad to tri-elements was exceptionally challenging, and by coinciding nodes zero length beams are created. This can not be handled by NASTRAN so they need to be identified and deleted from the model. More details and pictures can be found in Appendix B.2.

A final manual adjustment was required to define the attachment points for the engines and landing gear, and connect these to the structure. They are connected to the nearest ribs by very stiff rods. This way of connecting to the structure is a simplification compared to how it would be connected in reality. But at this point not enough is known about these parts to make a more detailed connection. Nevertheless, this is sufficient for a first analysis.

6.2.5. FINAL STRUCTURAL MODEL AND MESH

The final structural model is presented in Figure 6.7. The engine attachments atop the wing and landing gear attachment below are visible in this figure as well. In this model every element has the correct material properties and an initial thickness. The pressurized vessel is fully closed so this model is ready to be subjected to both the pressure and aerodynamic loads. How these loads will be applied and the obtained results from the FEM analysis will be covered in the final thesis paper. Furthermore a mass distribution will be proposed and the resulting center of gravity will be discussed as well.

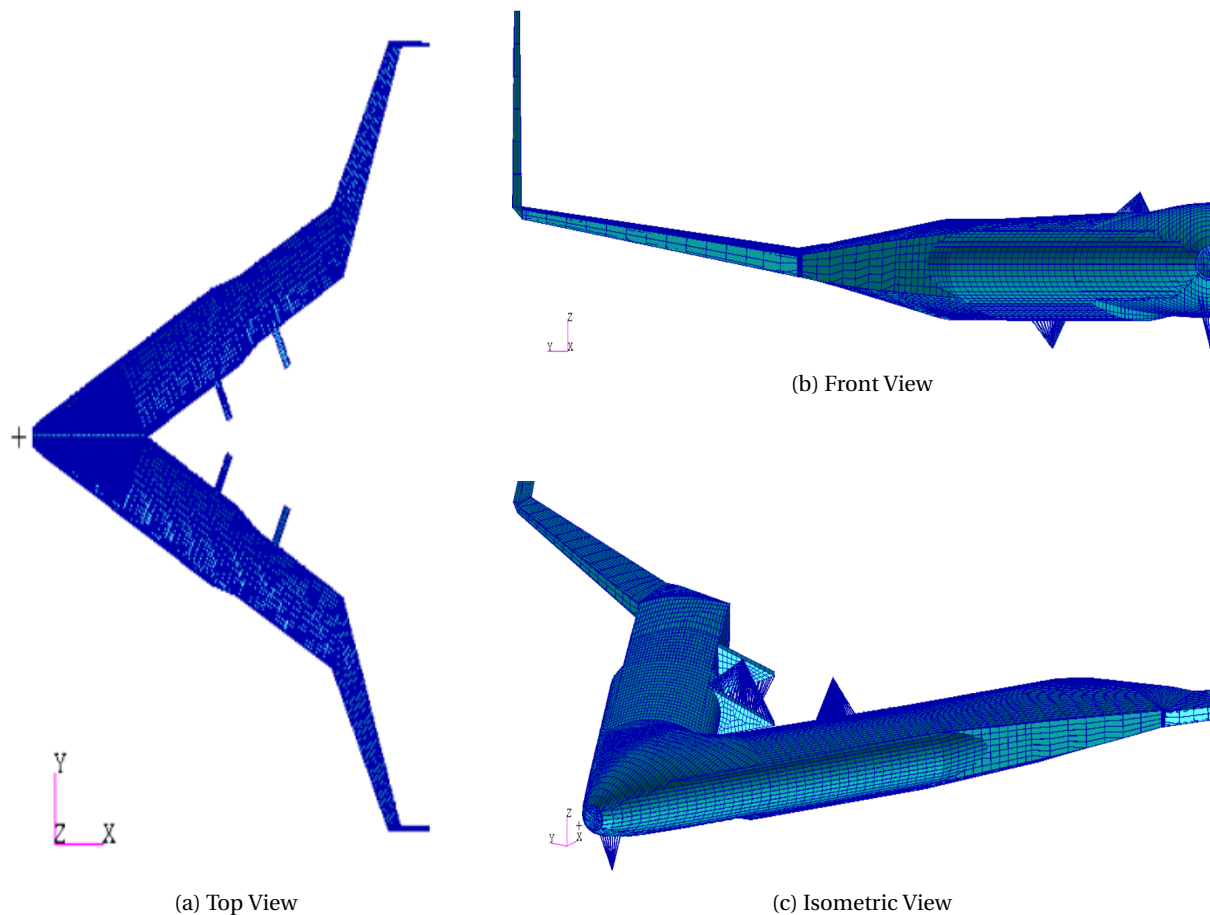


Figure 6.7: Flying V Structural Model

6.3. REFERENCE AIRCRAFT STRUCTURAL MODEL

To get the graphical model of the reference aircraft in PATRAN, the required curves and planes need to be exported from MARES. Because the combination of MARES and ZORRO-X/PATRAN was never used before, there was no direct way to do this. Thanks to the MARES developers such a feature was quickly established. With this new export feature the user can now select exactly what curves and planes are required and the model is exported to IGES. In this case all the required elements (including planes) could be imported by PATRAN and quickly re-labeled to use with ZORRO-X.

6.3.1. PARTS SUBDIVISION

The parts subdivision of the reference aircraft is straight forward. The wing, fuselage, VTP and HTP are each a part. ZORRO-X is developed for conventional aircraft, this makes that implementing the different parts in the correct template is much easier than for the Flying V. The lifting surfaces (wing, VTP and HTP) will be modeled using the wing template. Automatic mirroring of the wing and HTP is done, so only half of the graphical model is required. The fuselage will be modeled in its own specific template.

6.3.2. INITIAL STRUCTURAL MODEL AND MESH

Setting up the templates of the reference aircraft is done in the same way that it was for the Flying V, but for some minor differences. Here follows a quick recap.

FUSELAGE TEMPLATE

The planes that will be used for the stringer definition are normal to the a curve around the middle of the cylindrical fuselage length, where it is not tapered. A stringer was located at the passenger and cargo floor. In the three curve sections that result from this, the stringers were distributed equidistant. The number of stringers was chosen so that the obtained pitch is as close as possible to the desired 0.2 meter.

Floor struts are defined by specifying the longeron and stringer to which the strut will connect. The stringers used for the strut support of the passenger floor are the same stringers for the side support of the cargo floor.

In the reference aircraft a cut-out needs to be made for the wing integration and main landing gear storage. Making a cut-out is done by specifying the frame- and stringer range that will be left empty of structure.

WING TEMPLATE

As previously mentioned the wing template will be used for all lifting surfaces of the reference aircraft. Stringer run-outs happen automatically at the front spar. As there is not a drastic angle change required for the stringers (as there was for the Flying V) they remain at adequate spacing throughout all the lifting surfaces. As such no manual stringer run-outs are required at the wing, HTP or VTP.

Skin thicknesses and number of elements in the front and rear spars are given an initial estimation based on experience at Airbus. As explained before the thicknesses will be optimized, but initial indication can be an important factor.

6.3.3. MANUAL ADJUSTMENTS

WING FUSELAGE INTERSECTION

During the graphical design of the wing it was ensured that a rib was located at the intersection of the fuselage with the top cover. Because of this both structural models can now be connected by use of this rib. The nodes of the fuselage stringers at the top cover are moved to coincide with those of the mentioned rib and equivalenced. The bottom surface of the center wingbox can not be connected to anything, because there is no fuselage skin at this point. This can be seen in Figure 6.8b. In this subfigure the keel-beam and aft bulkhead are left out for visual convenience. To carry the moment introduced by the wing more connections to the the fuselage structure are required. Specifically connections with a different z position. So the front and rear spar will be connected to the pressure bulkheads. In addition the center wingbox will be connected to the keel-beam using some struts. This will be addressed in more detail in the following sections.

PRESSURE BULKHEADS AND FLOOR

In the model two pressure bulkheads are present, located at the cut-out for the center wingbox and main gear storage compartment. The nose and rear pressure bulkhead of the aircraft will not be modeled as structural elements but instead will be represented by a pulling force on the local frame. The bulkheads at the cut-out need to be connected to the local structure. So the front bulkhead is connected to the front spar of the wing. Every third supporting beam of the bulkhead is made to coincide with one of the ribs of the FS. The nodes of the bulkhead are moved accordingly and equivalenced.

The aft bulkhead can not be connected to the rear spar, as volume must be available for the main gear storage and hydraulic systems. A pressure floor is introduced at the top of the cut-out, between the rear spar and the aft bulkhead. This was already automated by ZORRO-X in the fuselage structural model. The longerons of the pressure floor are moved to coincide with the ribs of the center wingbox, and connected. Afterwards the nodes of the aft bulkhead were moved to those of the local longerons and they were connected as well.

KEEL-BEAM AND SPECIAL STRUCTURE

To help carry all the major loads at the cut-out, a keel-beam is introduced at the bottom, and triangular skin support from the rear spar and rear pressure bulkhead. All three were modeled manually, and the triangular support structures were mirrored to the other side. In order to minimize the out of plane deformation due to buckling on the keel-beam, it is connected with struts to the center wingbox. This is done at the rear spar and at the middle of the center rib. Both the special triangular skin supports and the keel-beam can be seen in Subfigure 6.8a and 6.8c.

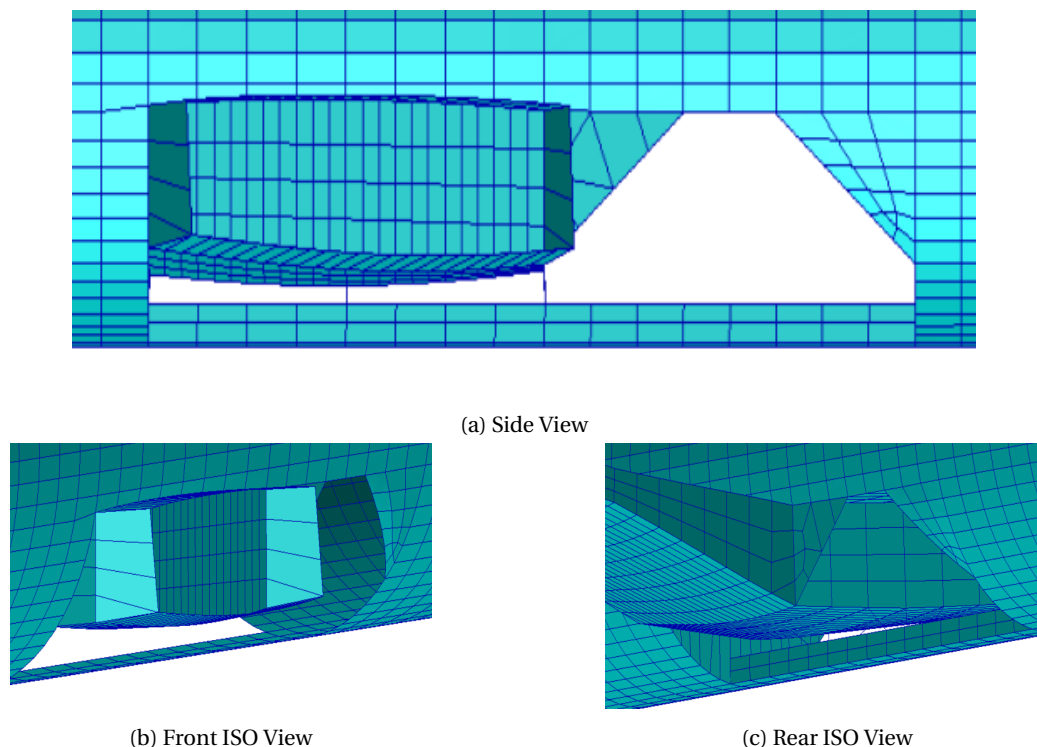


Figure 6.8: Center Fuselage Manual Adjustments

EMPENNAGE FUSELAGE INTERSECTION

The connection of the HTP to the fuselage is a bit more complex, for this time there is no rib nicely located at the intersection. So instead the local skin and stringer elements of the HTP were split at the intersection line and the resulting nodes were connected to the fuselage. This has been done for both the top and bottom of the HTP on both sides of the fuselage.

The VTP was designed so that the trailing edge of the root coincides with the fuselage skin. This means that the root itself is inside the fuselage. To solve this the nodes of the root were moved outward, onto the skin of the fuselage. The rib elements of the root were then moved to coincide with the local stringers of the fuselage. Finally all nodes were connected.

LANDING GEAR AND ENGINE CONNECTIONS

In order to find the location of the main landing gear, the spacing between the gears of the A350 was advised. This location was then moved into the middle of the two nearest ribs. The X-wise position was chosen to be at the center of the main gear bay, and the length of the strut was obtained by measuring the distance of the rib to a quarter of the fuselage width, at the center of the bay.

The engine location is estimated by the nacelle length and fan diameter. Both have been scaled from publicly accessible data from the A350. The engine location is at 30% semi-span.

Both engines and main gears were connected to the wing using very stiff beam elements. The engine will be attached to the front spar and front half of the local rib, and to a small extent to the two neighboring ribs. The main landing gear is connected to the rear spar of both neighboring ribs, and with a connection to the wing root to carry side loading. Finally the nose gear is connected to 4 frame stations.

6.3.4. FINAL STRUCTURAL MODEL AND MESH

In Figure 6.9 the final three-dimensional structure of the reference aircraft is depicted. The parametric values (span, length, box chord etc.) were checked and confirmed to be still correct. This figure also visualizes the engine and gear attachments. The engine attachment is displayed in orange, the gear attachment in blue.

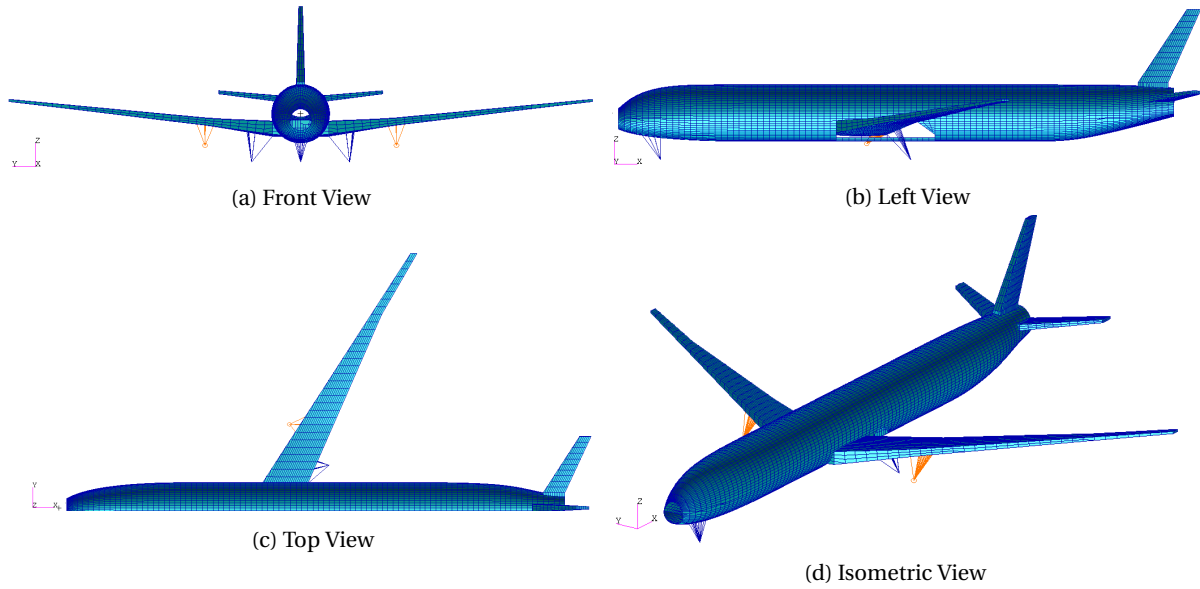


Figure 6.9: Reference Aircraft Structural Model

6.4. MATERIAL SELECTION

At this point the material selection gets addressed. It is desired to have the Flying V be a composite aircraft. Therefore both models will be using composites in this research. As no specific composite was suggested, the Airbus composite database was applied. Four commonly used composites were selected from this database, featuring different directional strength. The exact composites and their properties are used in Airbus and are considered confidential.

These composite materials were distributed over the elements based on initial load estimation, boundary conditions and manufacturing requirements. In this estimation the magnitude of the load is of minor importance compared to its direction. The direction with the most number of fibers should be the same as the direction of the main loads. Where the expected load is mainly in 1 direction (e.g. the stringers), the fibers can be more focused in that single direction, leaving the percentage of fibers in the other directions relatively low. However, in case of the stringers the boundary conditions dictate that the fibers can not be in longitudinal direction only. If this were to be done, the stringer would narrow when load is applied. Because the stringer is connected to the skin and other elements (boundary condition) this narrowing will tear the composite matrix, and the stringer will fail. This is just one example how boundary conditions can influence the selection of composite.

In places where bi-directional loads are expected (e.g. the skin elements on the wing) a more evenly distributed composite will be used. 3D internal loads should have an appropriate modeled composite too. Herein the fibers are more evenly distributed over all three directions. The used composites and their application regions are gathered in Table 6.2. Both aircraft will be using these.

Table 6.2: Used Composites

Composite	Application Region	Typical Elements
A	Mainly shear Large amount layers angled at 45 degrees	Spar and rib shells
B	Defuse load situation Quasi isotropic lay-up	Fuselage shells (outer skin)
C	Mainly compression and shear Layers angled mainly at 0 and 45 degrees	Wing shells (outer skin)
D	Mainly longitudinal loading and high required stiffness Layer orientation largely at 0 degrees	Beam elements (frames, stringers, etc.)

The individual plies will not be considered at this point. Ply optimization would prevent optimizing the structures and obtaining a weight estimate within the given time frame. But it can be beneficial, and it is therefore strongly suggested that full composite and ply optimization is performed at a later stage, when more resources become available. For now the composites are assumed to be scalable, meaning that if the thickness is increased, the fiber distribution remains the same. Furthermore the composite thickness will not be discretized (due to plies) but assumed continuous in order to run the automated optimization. The shell properties are applied as orthotropic properties, beams and rods use isotropic properties equivalent to the E11 property of the orthotropic lay-up.

7

LOAD MODELING

In this chapter all the loads will be obtained that will be used in the FEM analysis. First the structural and operational loads will be determined. This will be done for multiple sizing points, more on this later. Each of these points will have its own CG position. Because the CG positions differ between the sizing points, the aerodynamics will be different too. So the corresponding aero-loads will be determined. Other than aero and structural/operational loads, ground loads will be considered too. Combinations of all these loads will make up the different load cases to which the structure will be exposed.

7.1. METHOD

The aircraft are subjected to a rough mass breakdown to obtain the structural loads. The smaller components of the mass breakdown are placed at the coinciding locations on the respective aircraft and their CG's are obtained. These are all balanced out and the overall CG of the aircraft is determined. This process is repeated for multiple sizing points in the payload-range diagram. The obtained CG('s) are only a first indication; as the structural properties get iterated in the FEM optimization the obtained CG will change.

To find the aerodynamic loads Airbus's in-house software ODILILA is used. This software is developed by Klaus Bender and has been validated. Some parts of these validations are shared in Appendix D.3. The aerodynamics for 2.5g and $-1g$ maneuvers of the same sizing points as mentioned in the structural loads are obtained. To do this the (initial) CG is required, together with the respective weight. The ground cases are some of the standard book cases established by FAR25. The used loads are standard values.

7.2. STRUCTURAL AND OPERATIONAL LOADS

7.2.1. PAYLOAD RANGE DIAGRAM AND SIZING POINTS

In the payload range diagram shown in Figure 7.1, four points are indicated in total, called A through D. Each of these has a different CG location, as the CG moves when fuel increases or decreases and if the payload is changed. Even if the two balance each other out with respect to mass, (between point B and C) the CG will still move because the location of these masses is not the same. How much the CG moves is different for every aircraft. Different CG locations requires different trimming of the aircraft. Since the stability of the Flying V has not-so-good first guess estimations (based purely on visual aspects it is suspected that the CG will move a lot) it is a good idea to observe the CG locations at these four points. This will not be used to make a full fetched CG shift and stability analysis of the aircraft, but it can be used for a reasonable first indication, and can confirm or deny those bad expectations. In addition these CG positions will be required later on to determine the aerodynamic loads of the different load cases.

The presented diagram is the one of the Flying V. Since the reference aircraft has such similar masses, the diagrams will be very similar. Because the lift to drag ratio is slightly lower in the reference aircraft, the required fuel for the same range is slightly larger. For exact number please refer to Table 4.2 and 5.2. Other

slight differences can be found when comparing the volume available for fuel. The full tank capacity of the Flying V is 122 386 kg, compared to that of the reference aircraft at 116 504 kg. More on the fuel volume later in Section 7.2.2. Because of the different maximum fuel, the red line will not be as high for the reference aircraft. In addition line C in the payload range diagram of the reference aircraft will be at a shorter range of about 20 000 km, and likewise line D will be at 25 000 km. The magnitude of the blue and green lines will be the same for both aircraft. Because of the similarities between the two diagrams it was deemed unnecessary to include both in this thesis, even though both were made during the research. The numerical values of the fuel and payload mass of the different sizing points can be found in Appendix C.2.

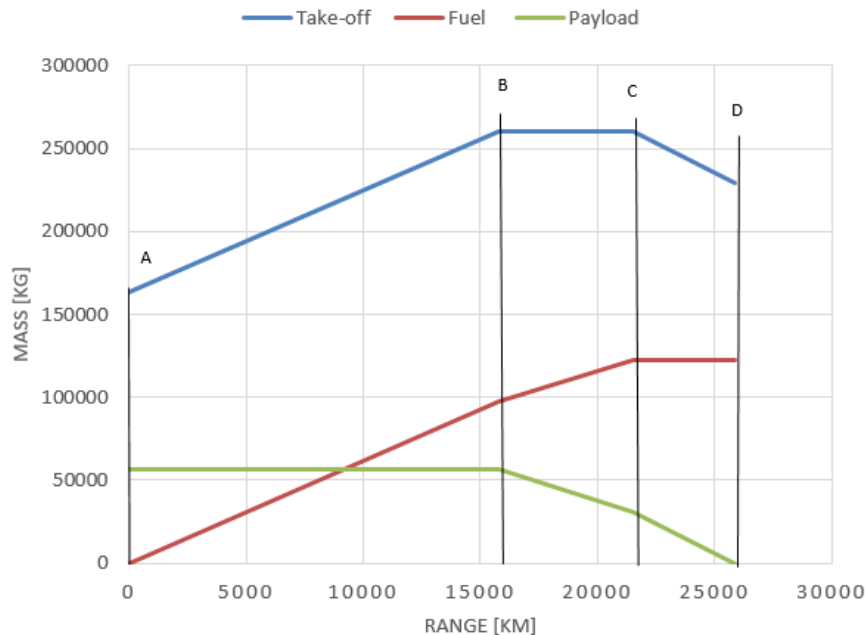


Figure 7.1: Payload Range Diagram of the Flying V

All the ranges indicated in the Payload Range Diagram presented in Figure 7.1 refer to absolute maximum range, not design range. This range amounts to the design range plus the extra range required for diverting.

Point A is the zero fuel point. This is encountered at the very end of the cruising phase, after already being diverted. Note that even at that point some fuel will still be in the aircraft in reality, but the worst case scenario is considered here.

Point B represents the aircraft when it has maximum payload and the fuel is added until the MTOW is achieved. This will occur when the aircraft is about to (or has just) take(n)-off, with the maximum number of passengers about to fly the maximum range.

Point C has a decreased number of passengers in order to extend the range that can be achieved. In this case all the tanks are filled up.

Finally, point D has decreased the number of passengers all the way to zero, while keeping the tanks filled up. This will result in the absolute maximum range the aircraft can travel. This is a once-in-a life-time operating point (i.e. first flight to operating base; the ferry flight).

7.2.2. FUEL LOCATION

As can be seen in the payload range diagram (Figure 7.1), the fuel amounts to a large portion of the overall mass of the aircraft. Where the fuel is located will thus have a large impact on the CG. As the fuel decreases in flight this will cause a CG shift. For handling qualities the magnitude of shift should be managed carefully.

REFERENCE AIRCRAFT

In the reference aircraft the fuel is located in the wings. This is standard practice for good reasons. Being at the wings means that the CG of the fuel will be close to the CG of the structure, and the shift due to fuel burn

is rather small. The available volume in the wing is generally the limiting factor for the maximum fuel that can be taken. Adding fuel tanks at other locations is possible but highly undesirable.

In this case the volume in the center wingbox (under the cabin floor) was required as well in order to fit the fuel necessary for the design mission. This is not ideal, but it was the best remaining option.

The fuel distribution of the reference aircraft can be found in Appendix C.4. The difference in fuel between MPLW and MFUW has been taken from the center wingbox tanks (ID 1-3). This moves the CG of sizing point B a bit more aft, compared to taking the fuel from the tip tanks. It will be shown in Section 7.2.3 that this moves the CG of sizing point B closer to that of A, thus reducing the CG travel during cruising with PAX and reducing the required trim deflections during this cruise.

FLYING V

Placing the Fuel in the Flying V is somewhat more challenging. In this report it is assumed that the only fuel tanks are aft of the pressure bulkhead, leaving 1 rib segment empty for safety, up to (but not including) the kink. This is considered the best available option to place the fuel. Other available volumes are underneath the passenger floor, or in the outboard wing. These were dismissed because under the full passenger floor (compared to the reference aircraft where it is only a small portion) is not safe in case of a crash or emergency landing. Placing fuel in the outboard wing will result in a much larger CG shift during cruise because of the reducing fuel mass. The theoretical best location of fuel is close to the CG location the aircraft would have without fuel. Taking safety in consideration, the mentioned location is what comes closest.

This is not taking the location of the engines into consideration. Fuel tanks should not be in line of engine shrapnel in case of failure. Relocation of the engines might be required to conform with this requirement. Naturally this will influence the CG and CG range too, so it is recommended to include all these considerations in a dedicated CG and stability of the Flying V research.

The fuel distribution of the Flying V can be found in Appendix C.4. The difference in fuel between MPLW and MFUW has been taken from the outboard tank (ID 5). This moves the CG of sizing point B a bit more forward, compared to taking the fuel from the inboard tanks. It will be shown in Section 7.2.3 that this moves the CG of sizing point B closer to that of A, thus reducing the CG travel during cruising with PAX and reducing the required trim deflections during this cruise.

7.2.3. MASS AND CENTER OF GRAVITY ANALYSIS

MASS BREAKDOWN

The mass breakdown is required to find the overall CG of the aircraft. The main aspects of the breakdown are already known; the payload mass, the fuel mass, the maximum take-off mass and the operational empty mass. The latter has a number of important contributors to it, such as the wing structural mass, the engine mass, empennage mass, furnishings etc. It is important to distinguish these, as each of them causes a moment on the aircraft depending on the part's location.

Usually a large number of part masses is obtained in the mass breakdown; more parts will result in a better CG location estimation, provided that the individual masses are correctly estimated. Obtaining the values is done using empirical relations to the the MTOM, and (local) surface area. Note that more detailed equations are available but pose a number of issues. They are outdated (based on older databases since more recent databases are not publicly available), and require many more input variables. Many of the required input variables are not (yet) known at this point in the design. Therefore the more fundamental relations using only surfaces, thrust or MTOW are considered.

In case of the Flying V some of these relations might not be correct, as they are typically valid for conventional aircraft. For instance, when considering using those for the Flying V model, the structural wing mass will be underestimated by such methods, while fuselage mass will be over estimated. This limits the number of breakdown parts that can be obtained for the Flying V. Only those masses that are not specifically related to the configuration of the aircraft can be used. These are the landing gear mass, engine mass, operational

mass (pilots, water, oil, etc.) and furniture mass. The remaining part of the (operational) empty mass will be smeared over the entire structure, as it can not be subdivided further while remaining accurate. The mass breakdown of the Flying V is represented in Table 7.1 and visualized in Figure 7.2a. In this figure all the CG locations are indicated. The size of the CG logo is indicative of the magnitude of the load.

For the reference aircraft more parts can be distinguished and the full operational empty weight can be accounted for using these equations. Because no remaining weight needs to be smeared over the entire structure, the obtained CG of the reference aircraft can be assumed to be more accurate. The mass breakdown of the reference aircraft can be found in Table 7.2 and Figure 7.2b. For the numerical locations of each CG, form both aircraft, the reader is referred to Appendix C.1

Table 7.1: Flying V Mass Breakdown

Group	subgroup	Part	Group Mass	Sub Mass	Part Mass	Location	
$MTOM$			260 000	[-]	[-]	Overall CG	
M_P			56 190	[-]	[-]	Cabin CG	
M_f			97 065	[-]	[-]	Fuel CG	
M_e	Landing Gear	Nose	[-]	[-]	2 493	NG CG	
		Main*	[-]	[-]	4 985	MG CG	
		Total	[-]	12 463	[-]	[-]	
	Engines	Left	[-]	[-]	9 900	L. Eng. CG	
		Right	[-]	[-]	9 900	R. Eng. CG	
		Total	[-]	19 800	[-]	[-]	
	Operational Items			[-]	12 255	[-]	Cabin CG
	Furniture			[-]	3 770	[-]	Cabin CG
	Remaining			[-]	58 457	[-]	Structural CG
	Total M_e			106 745	[-]	[-]	[-]

*All masses are represented in [kg]
* mass per individual gear*

Table 7.2: Reference Aircraft Mass Breakdown

Group	subgroup	Part	Group Mass	Sub Mass	Part Mass	Location	
$MTOM$			260 000	[-]	[-]	Overall CG	
M_P			56 190	[-]	[-]	Cabin CG	
M_f			96 690	[-]	[-]	Fuel CG	
M_e	Landing Gear	Nose	[-]	[-]	2 493	NG CG	
		Main*	[-]	[-]	4 985	MG CG	
		Total	[-]	12 463	[-]	[-]	
	Engines	Left	[-]	[-]	9 900	L. Eng. CG	
		Right	[-]	[-]	9 900	R. Eng. CG	
		Total	[-]	19 800	[-]	[-]	
	Operational Items			[-]	12 255	[-]	Cabin CG
	Furniture			[-]	3 770	[-]	Cabin CG
	Wing Structure			[-]	24 925	[-]	Wing CG
	Fuselage Struct.			[-]	19 445	[-]	Fus. CG
empennage	HTP	[-]	[-]	1 230	HTP CG		
	VTP	[-]	[-]	770	VTP CG		
	Total	[-]	2 000	[-]	[-]		
Systems	APU	[-]	[-]	3 900	APU CG		
	Rest	[-]	[-]	8 562	Cabin CG		
	Total	[-]	12 462	[-]	[-]		
Total M_e			107 120	[-]	[-]	[-]	

*All masses are represented in [kg]
* mass per individual gear*

As can be seen in Table 7.2, the mass distribution in the empty mass (M_e) group has more subgroups compared to the Flying V. The values above the horizontal line are the same for both the Flying V and the reference aircraft, since the same equations are used. The values below the horizontal line could only be computed for the reference aircraft. In the Flying V these are all grouped together in the subgroup called "remaining".

CG RANGE

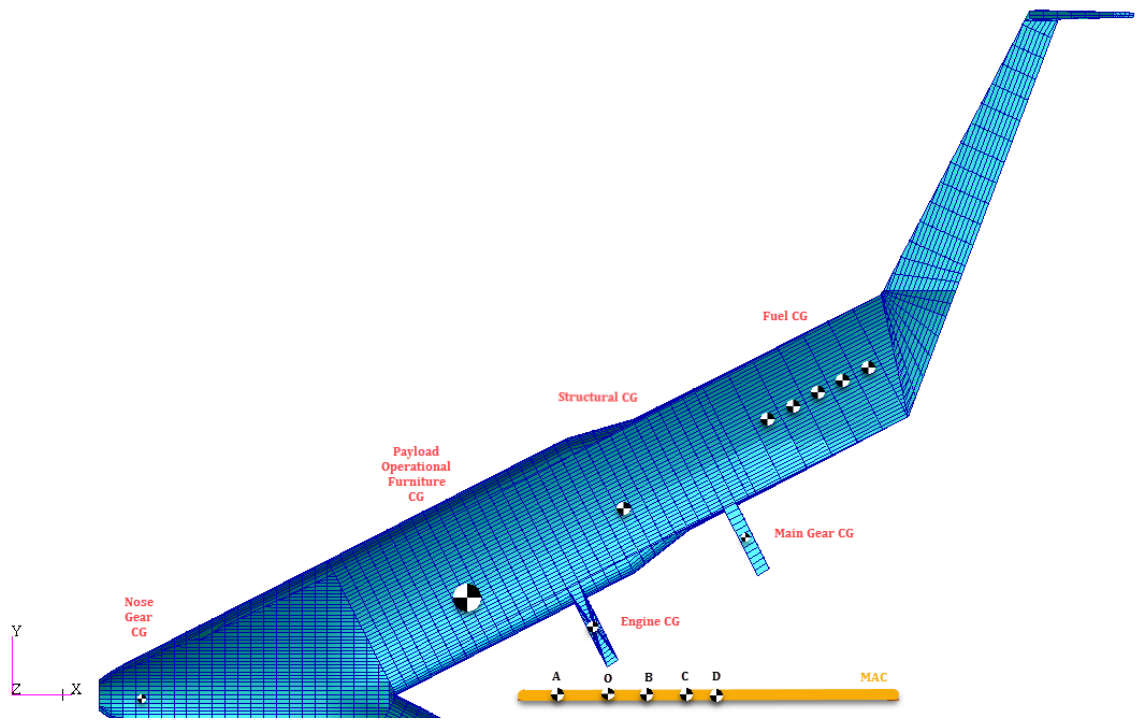
All the masses mentioned in the above tables have their respective CG location assigned. From these locations and masses the overall CG location is determined using ZORRO-X. As mentioned before, four points in the payload range diagram are considered (A through D in Figure 7.1). The CG location for each of these points will be different. The next tables show the CG locations of each of these four points, for each aircraft numerically, a visual representation is given in Figure 7.2. The fuel and payload mass of the different sizing points can be found in Appendix C.2. Herein the respectively obtained overall CG positions are presented as well. Graphical representation of the resulting CG shift can be found in Appendix C.3.

Table 7.3: CG Locations for Sizing Points of the Flying V

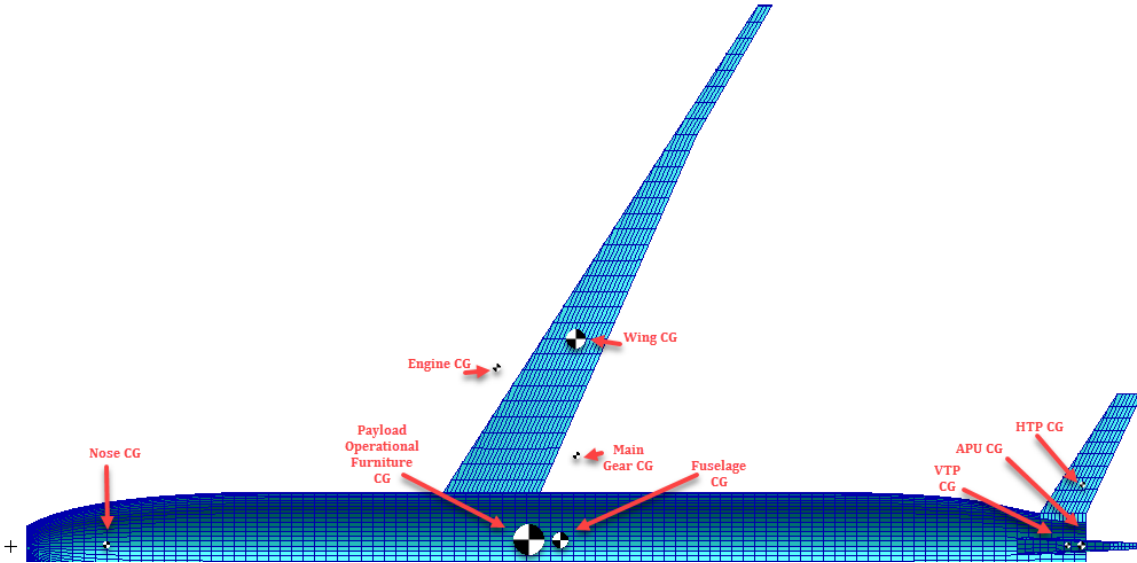
Sizing Point	CG location [% MAC]	Comment	Abbreviation
A	9.64	No fuel left in the tanks	MZFW
B	33.95	Max. range (fuel) for max. payload	MPLW
C	44.44	Max. payload with full tanks	MFUW
D	52.62	Full tanks with no payload	MZPW
O	23.26	Operational empty weight CG	OEW

Table 7.4: CG Locations for Sizing Points of the Reference Aircraft

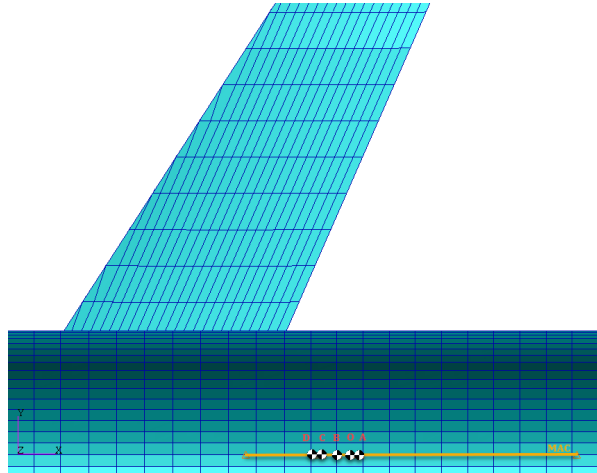
Sizing Point	CG location [% MAC]	Comment	Abbreviation
A	34.52	No fuel left in the tanks	MZFW
B	27.89	Max. range (fuel) for max. payload	MPLW
C	23.19	Max. payload with full tanks	MFUW
D	20.53	Full tanks with no payload	MZPW
O	31.88	Operational empty weight CG	OEW



(a) Flying V Mass Breakdown & CG Range



(b) Reference Aircraft Mass Breakdown



(c) Reference Aircraft CG Range

Figure 7.2: Mass Breakdown and Resulting CG Ranges

When analyzing the CG locations of the Flying V in Table 7.3, one will see that the CG can, in the worst case scenario, move over 43% of the *MAC* during the flight. This is much larger than what is observed with a well balanced conventional aircraft, as is the case for the reference aircraft (Table 7.4) where the CG shift is 14%. When these points occur during flight, the aircraft needs to be trimmed accordingly. Consequentially the different CG's will result in a different pressure distribution over the wing. The required aileron deflection and resulting drag penalty will be shown in Section 7.3.

STABILITY

With such a large CG shift for the Flying V, stability might become a problem. A full stability analysis is out of scope for this thesis, but a quick look at the location of the neutral point can and will be done. This will give an indication of the stability and safety margin of the Flying V at the different sizing points.

The location of the neutral point depends on the mach number. For increasing speed it is found that the neutral point shifts aft. At lower speed for landing and take-off (0.2 Mach) the neutral point is at its most forward location of 46% of the *MAC*. At cruising speed it moves back to 53% *MAC*.

Comparing this to the different CG locations it becomes clear that for low speeds, sizing point D is unstable. The CG of sizing point C remains in front of the neutral point by 2.6% *MAC* (corresponding to about 46 cm), and this remains stable. When considering cruising speeds the margins increase so that sizing point D now becomes (marginally) stable too. Its CG position was found to be in front of the neutral point by 0.4% *MAC* (corresponding to about 7 cm). The location of the neutral point has also been visualised in the CG diagram of the Flying V, which can be found in Appendix C.3.

The same analysis has been done for the reference aircraft. Here the neutral point is always aft of the sizing points and the aircraft will always be stable. The found neutral point starts at 50% of *MAC* for low speed.

CONTROLLABILITY

Another possible consequence of such a large CG shift is that the Flying V might become hard to control. Large CG shifts will require large flap deflections to trim the aircraft. While the required flap deflection during cruise is not analyzed in this research (out of scope) the flap deflections for the maneuvering cases (see 7.3) have been found. Those have been added to the overview of important aerodynamic results found in Appendix E. From these results it can be seen that occasionally very high flap deflections are required to maintain the current maneuver. While for the analyzed maneuvers the flap can still be deflected sufficiently, this might not be the case for the full flight envelope. a detailed controllability analysis is therefore suggested.

7.3. AERODYNAMIC LOADS

7.3.1. GENERAL INFORMATION

The aerodynamics of both aircraft will be determined with the same software; ODILILA. By using the same software inconsistencies between both aerodynamic models are avoided. The software has been developed by Klaus Bender. It is a lattice-vortex penal method which can quickly analyze and optimize aerodynamic performance. To verify the accuracy of this tool an in depth analysis verification has been made by Klaus in the years past. Some of the verification data (specifically those comparing to modern real modern aircraft data) is confidential. But validation with respect to public accessible data could be shared in this report. This can be found in Appendix D.3. This appendix also includes the working principles of ODILILA (D.1) and the implementation methods (D.2).

In order to reduce the computation times of the optimization later on the number of load cases that will be used should be kept low. Therefore the aerodynamics are limited to two maneuvering cases; at 2.5 and $-1g$. These are maneuvering loads that are most likely to be the most critical in the overall flight envelope. Using only these specific maneuvering loads is common practice at this stage.

As maneuvers can take place at any point during flight, all the sizing points are considered and each of them was subjected to the two loads. This leads to a total of 8 aerodynamic load sets.

7.3.2. PROCEDURE

Initiating ODILILA is easy, the input file is based on code words. By this code word the software knows what will be specified in the next couple of lines. Each code word has a template for the following lines. By simply following this specific template everything can be defined. The turn order in which the code words are used can be changed, the only requirement being that the full geometry definition needs to be completed before computational request can be inserted.

MODEL INPUT

The graphical input of ODILILA is straight forward, by using code words such as WING, HTP, VTP or FUSELAGE the tool knows what part will be defined. But before the individual parts are inserted the reference wing is defined. Herein the wing area, MAC, span, MAC_y coordinate, MAC_z coordinate are specified in that specific order.

For lifting surfaces the trailing edge points are defined for a number of sections. The first line gives a series of x-coordinates, the second line y-coordinates and the third line z-coordinates. The fourth line describes the chord length, and the last line gives the respective thickness. The HTP and VTP require one additional input line compared to the main wing; its relative location. In case of the HTP this is done by defining the y-coordinate of the root, for the VTP the z-coordinate at the root is defined.

For the fuselage the following variables need to be specified in turn order, each on its own line. The length, nose x-coordinate, nose z-coordinate, width, height, depth, Z-coordinate of the HTP, x-coordinate of the wing root trailing edge and lastly, the wing root chord.

Finally the camber is specified. This can be done by simply implementing the airfoils (as was done for the Flying V) at specific locations in the wing, or by manually setting the camber (as was done for the reference aircraft; 1%, 2%, 2% at $\eta = 0, 0.3, 1$ respectively).

OPTIMIZATION

The next step in obtaining the aero loads is optimizing the wing. The speed and attitude of the aircraft need to be defined. This is the same for both aircraft; 0.85 Mach and a common cruising Angle of Attack (AoA) of 2.5 degrees.

The optimization in ODILILA will optimize the wing (and HTP) lift distribution by changing the twist for a certain flight condition. The optimization can be done towards lift only or to the combination of lift and pitch. The first one will not try to balance the aircraft, but instead will just determine the best possible lift distribution and its location (at quarter MAC). The latter will get the best possible lift distribution while the aircraft remains trimmed. In this case the lift and pitch will be optimized, to get the aerodynamic loads of the trimmed aircraft.

In both cases the c_L value and the X-CG should be specified. The optimization will be done for the mid-cruise conditions of the aircraft. This way the trim drag can be reduced. If one were to use the beginning or end of the cruising phase to optimize the lift distribution, this would lead to higher trim flap deflection angles and thus higher drag. Optimizing for mid cruise will result in the same delta between flap setting at the beginning and end of cruise, but this time half of the deflection will be negative and the other positive. Thus the magnitude of the flap deflection will be lower resulting in lower drag. Moreover this would mean that during half of the cruise there will be a slightly higher lift, while in the other half the lift will be a bit lower.

$$c_L = \frac{W}{0.7 * P * M^2 * S} \quad (7.1)$$

$$W = \frac{M_a + M_b}{2} \quad (7.2)$$

The x-CG can be found by taking the average of the CG position at sizing point A and B. To find the corresponding lift coefficient the following equations are used. M_a (MZFM) and M_b (MPLM) are the masses at the end and start of the cruising phase respectively, P is the pressure, M is the mach speed and S is the wing surface area.

To quickly see the effect of trimming the aircraft on the aerodynamics the optimization is done for lift only as well. This is just for additional information on the aerodynamic efficiency. For the structural optimization later on only the trimmed loads will be used. To see the effect the drag counts for both the trimmed and non-trimmed aircraft will be compared in Table 7.5.

Table 7.5: Trim Drag Penalty

	Not Trimmed		Trimmed	
	C_D	C_{D_I}	C_D	C_{D_I}
Flying V	88	26	100	38
Reference Aircraft	209	72	211	74

Expressed in drag counts 10E-04

As can be seen the drag penalty required for the reference aircraft is small; 2 counts. For the Flying V the penalty is noticeable higher; 12 counts. This is because of the poor CG location mentioned before. When comparing the reference aircraft and Flying V it is clear that the drag coefficient of the Flying V is lower. This was to be expected, as the wing area is so much larger, and consequentially the lift coefficient too is smaller compared to the reference aircraft. Having a lower drag coefficient does not mean that the Flying V will definitely perform better. The drag (rather than the drag coefficient) can still be substantial.

MANEUVERING LOADS

As mentioned before 8 aerodynamic load sets will be computed. for each of the following input needs to be provided on the same line in this specific order; the mass, load factor, x-coordinate of the center of gravity, lift coefficient, maneuvering mode, control surface ID, and trim mode. The mass and X-CG's have already been determined (Section 7.2.3), the load factor too, has already been discussed (2.5g and -1g). The maneuvering mode that has been used in this research is gust loading (specified in ODILILA by the term c_Z). The trim mode will be lift and pitch, in order to keep the aircraft trimmed during these maneuvers.

Each of the resulting maneuver cases can be analyzed in an automated ODILILA report. In such an automated report the loads are visualized and parametric data such as control surface deflection, AoA, c_L and c_D and many more are presented. In addition the loads are exported to Excel sheets, whom will be imported to the PATRAN models later. This thesis report includes the most important data in Appendix E.

In this entire process the VTP (reference aircraft) and winglets (Flying V) remain unloaded. This is because they have a symmetrical profile in a symmetrical flow, so no lifting force is created. To size these parts a load is introduced here as well. This load was not obtained by ODILILA, nor was a lift distribution made. Instead a load was estimated based on (confidential) Airbus regression data. This provided a maximum load per area. The load is modeled as a single force acting at the MAC of the respective part, in positive Y-direction. From this position the load is distributed over the outer surface using a PATRAN feature.

7.4. GROUND LOADS

Four ground load cases were included in the analysis. All of them are standard bookcases as regulated by FAR. The first is a braking case. Herein 0.8g braking is applied at the landing gears. The second and third ground case are take-off cases, one regular take-off and another with crosswinds. The final ground case is a turning case, which introduces a side force to the gears. The overview of the ground cases and their respective directional accelerations are given in Table 7.6.

Table 7.6: Ground Loading Definitions

Ground Case	Acceleration [g]		
	x	y	z
Braking	-0.8	[-]	1
Take-off 1	[-]	[-]	1.7
Take-off 2	-0.3	0.3	1.5
Turning	[-]	0.5	1

Accelerations represented in gravitational acceleration

7.5. LOAD CASES

All the aforementioned loads, being aerodynamic or ground loads, are the so called load sets. They are grouped together in the following list and given an appropriate load set number, in order to easily distinguish them.

1. Pressure differential ($dP = 575Pa$)

11. Zero Fuel at 2.5g limit load (sizing point A)
12. Maximum Payload at 2.5g limit load (sizing point B)
13. Maximum Fuel at 2.5g limit load (sizing point C)
14. Zero Payload at 2.5g limit load (sizing point D)

21. Zero Fuel at $-1g$ limit load (sizing point A)
22. Maximum Payload at $-1g$ limit load (sizing point B)
23. Maximum Fuel at $-1g$ limit load (sizing point C)
24. Zero Payload at $-1g$ limit load (sizing point D)

31. Ground braking
32. Ground Take-off 1
33. Ground Take-off 2
34. Ground turning

41. Side gust

The aircraft will be subjected to a combination of these sets during flight. Not all of them can be acting on the aircraft at the same time, while others must be. So to distinguish what load sets are acting on the aircraft at a given time, load cases are introduced. These load cases will be used during the sizing. They are presented in Table 7.7. The PATRAN Labels are shown here as well, these will be used later on in the visual representation of the active load case of the final results. (Figures 9.7, E.2 and G.2) The first two load cases are only used for aluminum models. As it is possible aluminum models will be considered later, these load cases are already created.

Table 7.7: Compiled Load Cases

Load Case	Load Set(s)	PATRAN Label
1	1 scale 1	
2	1 scale 1.15	
3	1 scale 2	Over-pressure
4	11	2.5g MZFUW
5	11 & 1	2.5g MZFUW Pressurized
6	12	2.5g MPLW
7	12 & 1	2.5g MPLW Pressurized
8	13	2.5g MFUW
9	13 & 1	2.5g MFUW Pressurized
10	14	2.5g MZPLW
11	14 & 1	2.5g MZPLW Pressurized
12	21	-1g MZFUW
13	21 & 1	-1g MZFUW Pressurized
14	22	-1g MPLW
15	22 & 1	-1g MPLW Pressurized
16	23	-1g MFUW
17	23 & 1	-1g MFUW Pressurized
18	24	-1g MFUW
19	24 & 1	-1g MFUW Pressurized
20	31	Ground Braking
21	32	Ground TakeoffD1
22	33	Ground TakeoffD2
23	34	Ground Turning
24	41	Side Gust

8

FEM IMPLEMENTATION

In the previous chapters everything was prepared for the FEM analysis. At this point all of this needs to be joined together in a NASTRAN deck and the optimization can begin. Joining the loads (called mapping) is done by ZORRO-X. Exactly how can be found in the first two sections. Next ZORRO-M is initiated with the applicable sizing constraints.

8.1. AERO MAPPING

The exported aero load distribution of ODILILA contains coordinates of different attachment points and the corresponding force. The attachment points do not yet coincide with the structural nodes. In order to map the aero loads to nodes ZORRO-X is used. Other than the previously used features ZORRO-X can also create MPC's between given coordinates and existing nodes in the neighborhood. MPC's are nodal relations. They can be configured so that the forces on one node are distributed to the other nodes so that the total force and moment is zero. The number of nodes that the MPC uses is an input variable in ZORRO-X. Because the number of nodes on the structural modal is many times higher than the number of attachment points obtained by ODILILA this variable is between 10 and 50, depending on the local part. Choosing this number is not easy, too much will result in a too uniform load distribution. Too few will result in large local loads. In the end a visual inspection and trial and error lead to the selection of the number of nodes used per attachment point of ODILILA.

During the process of mapping the aero loads of the reference aircraft a problem was discovered. At the fuselage-wing intersection some of the aero wing loads belonging to the wing were (partly) attached to the fuselage nodes by the aforementioned automatic generation of MPC's. When this was discovered an attempt was made in solving this issue. The idea was to split the MPC generation by ZORRO-X into different steps for each part. First the MPC's for a single part (e.g. the wing) are created, next the ones for the following part (e.g. fuselage) and so on. Thus all MPC's are connected to the to the correct part only. To map all the different aero loads (eight sets) the created MPC's are re-used. However this caused another problem. The obtained loads from ODILILA are for one half of the model only. So ZORRO-X processes all the loads in order of the data file. Once all of them are modeled, ZORRO-X will mirror them to the other side to get the full loads. If the MPC's are subdivided into parts, one part will run, and its MPC's will be mirrored, and then the next part will be run. But the loads are not arranged in the same order. They still disrobe each part in turn and are mirrored at the very end. Thus the loads of the second part are actually mapped on the MPC's of the mirrored side of the first part. This issue is not easily resolved. In theory one could also subdivided the load data files. But the load mapping by ZORRO-X can not be done for batches. Therefore every part should be run individually in ZORRO-X, for every load-set. This would result in 24 individual runs (three parts, each having eight load sets). This way the mirroring would occur correct. But 24 runs of ZORRO-X is too time consuming. In addition manual subdivision of the eight load databases would not be convenient either. So the idea of subdividing MPC's and loads to solve the small local mapping issue is abandoned. The possible gains are so small, and not proportional the the required effort at all. The expected error from these few partly incorrect connected MPC's is not expected to be a driving factor in the optimization.

If in the future batch mode is enabled in the ZORRO-X load mapping, and the ODILILA load data files can be generated for each part individually and automatically, it is recommended to map the loads as was attempted here. As long as these features are not available, it is not worth the effort. Especially not if there are a lot of load sets and or parts.

8.2. INERTIA MAPPING

The inertia is required during the optimization process as well. It represents the operational mass of the aircraft and are obtained from the mass breakdown. They are created by an inertia response to external loading, and are scaled to 1g mass of the aircraft. Once obtained, the forces are mapped as 1g loads and distributed evenly along the correct nodes (i.e. payload is only mapped to the floor nodes etc.) To do this structural groups are introduced in PATRAN. These are made with respect to the required CG positions mentioned in the mass breakdown. The same ZORRO-X feature as mentioned before is used to do this distribution.

The inertia mapping in ZORRO-X also features a balancing method. If the structural CG and the center of pressure are not at the same (x) location, the program will introduce a rotational acceleration to counter this offset and balance the aircraft. In ODILILA the loads were specified to have the CoP at the CG. So this feature was not necessary for either model. This has been verified by checking the value of the rotational acceleration (in all directions). They proved to be negligible every time. This re-affirms too that the loads and inertia were correctly sized and mapped to the structure.

8.3. BOUNDARY CONDITIONS

Now that all the loads are mapped to the respective models, the compiled load cases can be introduced to the models as well. Other than the aero-, ground-, and pressure loading combination specific to each load case (as specified in Table 7.7) they require proper boundary conditions as well.

In ODILILA the forces are optimized in order to trim the aircraft, so it is aerodynamically balanced. The inertia loading will ensure that the aircraft's lift and weight are balanced as well. If both these intentions succeeded, the location of the boundary conditions (the fixed attachment points) should not influence the optimization. This is verified by checking the magnitude of the loads at the boundary conditions. They show that indeed the loads at these points are negligible. Both aircraft can now be considered balanced and ready for optimization.

One load case is the exception however; load case 24, the side gust acting on the winglet (Flying V) or VTP (reference aircraft). This load was manually introduced and is therefore not balanced. Consequentially, the loads at the boundary conditions are not zero. This is no problem, as long as the boundary conditions of this specific load case are selected in a smart matter. This will ensure that no large local deformations are introduced at the BC's. Selecting them was based on trial and error, guided by Airbus colleagues whom have many years of structural modeling experience.

8.4. ZORRO-M

Up to this point only ZORRO-X has been used. This is the pre-processing part of the tool. For the processing itself another extension of ZORRO will be utilized; ZORRO-M. In ZORRO-M the sizing constraints are specified. This is done with respect to dedicated PATRAN groups. Each element within a group will be subjected to the same criteria.

8.4.1. SIZING CRITERIA

Two major failure modes are considered in this sizing procedure; failure in strength of the material and failure in stability of the material.

STRENGTH CRITERIA

In isotropic material optimization the design criteria specify a maximum allowed stress. If this stress is reached during FEM analysis the thickness of that specific element will be increased in the next iteration, consequently the area will increase too. Now that specific element can carry a higher load while keeping at or below the allowed stress. For multi-directional loads Von-Mises stress can be used as a driving design constraint.

When considering composite materials, everything becomes more complicated. Composites have plies each having different orthotropic material properties. So in attempting to use the same design criteria as is used in isotropic materials, the stress needs to be analyzed in each ply individually. Furthermore failure might also occur between plies rather than in a specific ply. So this needs to be analyzed as well. Micro cracks of one ply might also influence neighboring plies as they need to carry more loads etc. All this will require a large amount of extra time. But that's not even the main issue. According to Airbus personnel, modern material theory is not yet able to provide a single theory that can describe or predict all the failure modes of all the plies and all the inter-ply connections correctly. While some interesting studies exist, as well as theoretical methods and models to predict and analyze the aforementioned properties, these theories all require some level of regression data input to describe physical material behavior.

So another design criteria is required for composite materials. Analyzing all the plies and ply connections is foregone. Instead the composite element is considered as a whole. As theory is not sufficient yet, measurements are used to determine the limits of the material. These are done in a controlled environment. Different composite lay-ups are subjected to a range of loads and boundary conditions that are known to occur during flight and the strain of the top ply is measured up to failure. This way the strain of the top ply can be used as a reference for when this specific composite will fail. The strain is not constant for all the plies, but this is of no consequence. If any of the plies fail the coinciding strain of the top ply will be documented. This method does not indicate what kind of failure has occurred, or at what ply.

The reason strain is measured rather than stress, is because the measurement itself is easier for strain. In addition the strain distribution is more uniform than that of the stress.

The maximum allowed strain for the shell elements is set to 2667 and 2333 $\mu\epsilon$ in tension and compression respectively. This is for limit loads, so a safety factor of 1.5 has been applied to the allowable strains. (equivalent ultimate load amounts to 4000 and 3500 $\mu\epsilon$ allowable strain respectively.) The measured strain is a combination of strain in x and y direction, shown in Equation 8.1. More details about this definition and other options can be found in ZORRO-M documentation [12]. Because the constraint is not bound to a single direction, different composites with different fiber orientations can use the same maximum allowed strain.

$$\frac{1}{Rf_{x,y}} = \sqrt{\left(\frac{\epsilon_{x,y}}{\epsilon_{xmax}}\right)^2 + \left(\frac{\gamma_{xy}}{\gamma_{xy\ max}}\right)^2} \quad (8.1)$$

The maximum allowed strain for bar and beam sizing is a combination of the axial and bending strain at all recovery points and average between node A& B.

STABILITY CRITERIA

The stability of the different elements is kept in check by a buckling sizing criteria. Buckling onset can be defined in two ways, either by a constant offset factor with respect to the limit load or by a variable offset factor with relation to the panel thickness. The latter is of interest when the thickness of the panel becomes significant; thicker panels are more resilient towards buckling. Which definition is used depends on the expected load direction. With the help of more experienced colleagues the buckling onset criteria was set for different directions in different design groups. When the buckling onset is breached, the panel thickness will be increased in the next iteration. The method used to calculate buckling is in accordance with ESDU [13]. For stiffened panels it is assumed that stringer and skin occur at the same level. The stringer itself is not checked because its physical properties are unknown.

The elements are all clamped to a certain extent, so clamping factors need to be implemented as well. A simply supported element would have a clamping factor of one, while a fully clamped would be 1.73. The value depends on the rotational stiffness of the stringer. This value is not known, but the stringer should have a positive impact to the buckling behavior. This is why 1.3 is assumed by Airbus engineering judgment.

Buckling is checked for compression and tension in combination with shear. The dominant influence is kept so that it can be used in post processing. For more information about the implemented criteria and other implementation possibilities, the reader is referred to the ZORRO-M manual [12].

8.4.2. SIZING CONSTRAINTS

The general sizing constraints are specified in Table 8.1. These are the same for the Flying V and the reference aircraft. These constraints can be changed locally. This has been done occasionally. To do this sizing groups are introduced in PATRAN. These are not exactly the same as the structure groups mentioned before. All the elements in a specific sizing group will have the exact same sizing constraints and criteria. So if a local change is required in either of these properties a dedicated group is required. As such it was found that the frames at the bulkheads of the reference aircraft required specific sizing constraints, as well as the first 4 frames in of the Flying V. They are but a small example of the total number of sizing groups. Not all the constraints for all the groups will be stated in this report, that would be too much to clearly report on. Instead the most common constraints are specified in the following table. They account for the sizing of more than 80% of the groups. All the groups will be summarized in the results, as they will be used there as well to establish convergence 9.6.1.

Table 8.1: Geometric Sizing Constraints

Fuselage Beams					
BAR_B_LIM	Bar width	Lower & upper limit	30	100	[mm]
BAR_T_LIM	Bar thickness	Lower & upper limit	1.5	5	[mm]
BAR_H_LIM	Bar height	Lower & upper limit	100	200	[mm]
(T/B)	Relative thickness	Desired & upper limit	0.05	0.167	[-]
(H/B)	Relative height	Desired		3.33	[-]
Wing Beams					
BAR_B_LIM	Bar width	Lower & upper limit	20	100	[mm]
BAR_T_LIM	Bar thickness	Lower & upper limit	1.5	5	[mm]
BAR_H_LIM	Bar height	Lower & upper limit	60	200	[mm]
(T/B)	Relative thickness	Desired & upper limit	0.075	0.167	[-]
(H/B)	Relative height	Desired		3.33	[-]
fuselage Skin					
REL_A	Relative Stringer Area	Required		0.35	[-]
T_LIM	Thickness	Lower & upper limit	1.625	NONE	[mm]
A_LIM	Cross section area	Lower & upper limit	150	NONE	[mm^2]
Wing Skin					
REL_A	Relative Stringer Area	Required		0.5	[-]
T_LIM	Thickness [mm]	Lower & upper limit	2.5	12	[mm]
A_LIM	Cross section area	Lower & upper limit	150	NONE	[mm^2]

8.4.3. SMOOTHING

To facilitate manufacturability a smoothing has been implemented on the thicknesses of the skin and spar elements. Other elements aren't likely to have high thicknesses or thickness outliers. If they do that this needs to be analyzed carefully as there might be something wrong with the model in that region.

Smoothing can be defined in three different ways. All of them limit the thickness of a shell relative to the thickness of its neighbors. The definition can specify a maximum ramping ratio (defining a maximum slope), or it can specify absolute or relative thickness ratios between elements. In this sizing procedure a ramping ratio was used.

The ratio needs to be defined in three directions; local x and y direction, and diagonal (xy). The implemented ratio is 1 mm up or down for every 100 mm in the analyzed direction. This has been done for all directions in both the Flying V and reference aircraft, with one exception; the span direction at the reference aircraft, which was set at only 1 mm per 10. This is quite steep, and was just an initial value. Results indicated however that thickness distribution in span direction of the reference aircraft was already smooth enough not to warrant a more constricting criteria.

8.4.4. CONVERGENCE

ZORRO-M will run for a given number of iterations. It will keep track of the convergence but it will not stop automatically. So initially 15 iterations were run. After these it will be checked if further iterations are required. If this is the case, then the process can continue from the last iteration.

Convergence is expressed in terms of change in mass between iterations. If this number has become sufficiently small according to the user sizing can be halted. The exact convergence of both models will be addressed in the results (Section 9.6.1). This goes hand in hand with the obtained FEM masses and is therefore placed at the end of the results in this report, even though it was checked first.

8.4.5. TEST RUN

Before both models were subjected to the iterative sizing procedure an initial test run was made to ensure the model is behaving correctly. This way there is a final check of the load implementation, the selection of the boundary conditions and the connectivity of the model. Four load cases were checked individually; the pressure load (LC 3), an aerodynamic load (LC 6), ground load (LC 20) and side gust (LC 24).

For both models it was found that some regions still lacked proper connectivity between elements, so this was addressed. Other than connectivity the reference aircraft behaved correctly, the Flying V however showed some additional problems.

The combination of the aerodynamic load distribution and the configuration of the Flying V introduces a torsional moment in the cabin skins, together with the wingtip deflection. Because of the torsion the leading edge is deforming upwards, and the trailing edge down. This phenomenon intensifies when the two cabin parts get closer together and reaches a maximum when they connect together with the nose part, where there is a suddenly large open space.

The magnitude of this deformation becomes rather large. This might be because the elements are not yet correctly sized to handle all the loads that converge in this region. So (only) this load case was sized until convergence. It became clear that the structure simply is not sufficient in this region, as the displacement remained rather large even after sizing. The sized elements all reach their maximum allowed value and will still fail under the current loads. So in order to solve this issue the structural concept needs to be adapted.

Figure 8.1a shows how the initial deformation was. The undeformed (jig) shape is displayed in pink. Note that in this picture the floor structure was left out to enhance the visualization. In this case the LE moves upwards about 15 cm while the trailing edge moves down 35 cm. Both are measured at the intersection frame of the cabin and nose parts. Therefore the height difference between LE and TE at this frame station is 0.5 meter. The induced torsion is indicated in this figure by the purple and pink arrows (left and right cabin respectively). From these it becomes clear how both of them will push the TE intersection down (indicated by the red arrow). Figure 8.1b shows the implemented reinforcements in order to cope with this force convergence. The original frames are displayed in blue, the reinforcement structure in orange.

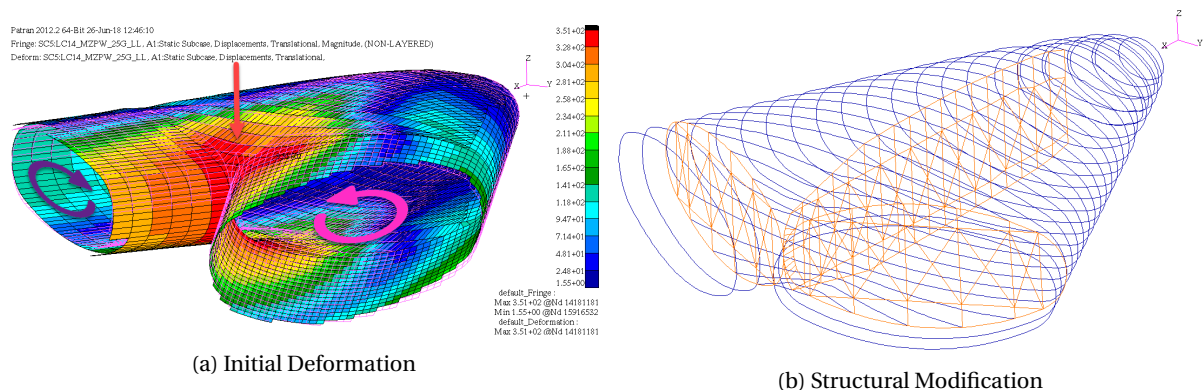


Figure 8.1: Flying V Center Deformation and Implemented Solution

9

RESULTS

In this chapter all the results will be summarized and analyzed. First the obtained thicknesses will be presented, followed by the frame sizes. Next the critical load cases and design criteria are discussed. These all lead to certain deformations, which is what will be discussed next. Finally the convergence is shared together with the final FEM weight estimations and new CG locations.

9.1. THICKNESS

9.1.1. INITIAL RESULTS

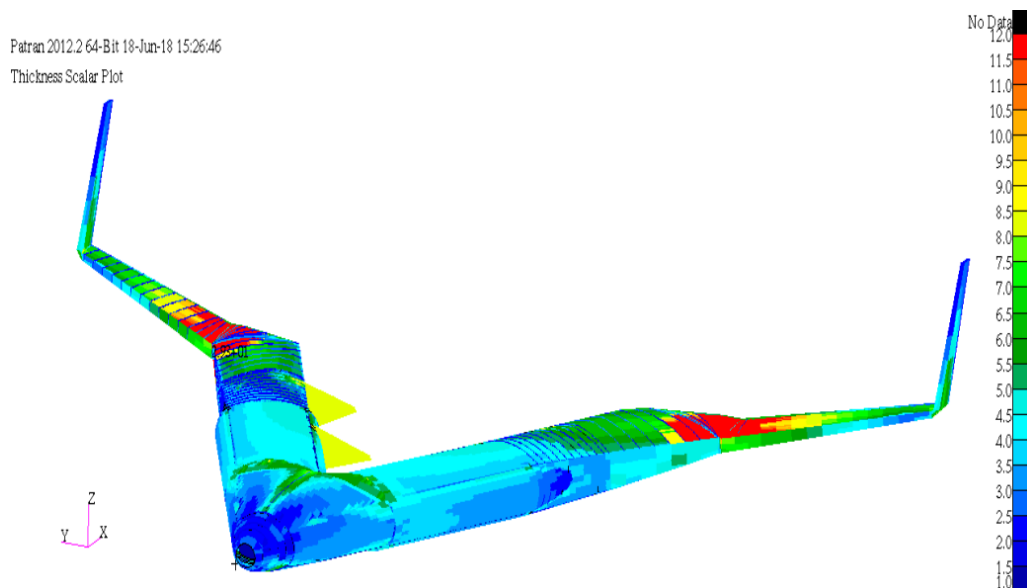


Figure 9.1: Flying V Thickness Distribution

The obtained thickness distribution of the Flying V is displayed in Figure 9.1. It can be seen that the highest thickness occurs just behind the kink. Upon analyzing this region it was found that the thickness increased to almost 30 mm. The upper bound of this picture is set to 12 mm just to give an indication of the thickness distribution in other regions. As thickness of 30 mm is not realistic this region will be analyzed in more detail.

9.1.2. KINK ANALYSIS

It was found that the cause lies with only 8 elements; one at the FS and RS of both the top and bottom skin, on both sides. Due to the smoothing all the neighboring elements were made thicker as well. The required

thickness of these eight elements was addressed next. This region was made automatically by ZORRO-X so no manual mistakes can be present here. Furthermore the results are mirrored as well, further indicating that the loads and modeling in this region is correct and the the FEM was correctly implemented. The required thickness comes from strength requirements.

This can not be explained by element size. Some of the elements indeed are rather small in this region, together with high stress gradients at the kink, the average stress in elements does increase. However, looking more closely to the region (see Figure 9.3a) one can see that the 8 outlying elements are in fact not those that have small sizes, quite the opposite these extreme elements have the same size as most of the other elements of the wing.

The loads of the outer wing result in bending moments. The strain increases with each element traveling inboard. Since the dimensions of the wingbox are not increasing much the thicknesses of the elements needs to increase to provide the necessary inertia to carry the (bending) loads. At the kink the dimensions of the wingbox increase rapidly, therefore the thickness does not need to increase as much inboard of the kink. In other words; as a consequence of the large increase in box dimensions at the kink, the area just outboard of it is made more sensitive to all the forces converging it that region. This is why, from a structural point of view the change of box dimensions should always be gradual, unlike the present example.

Nevertheless having such a beefed up region for a couple of square meters just for the sake of 1 element is not realistic. For this reason the sizing is done again, this time by limiting the skin thickness to 20 mm. This limit was chosen by observing the required element thickness of all the elements near the eight outliers mentioned before. All of these were between 16 and 18 mm. Choosing the limit slightly higher ensures that all these elements will be sized correctly.

9.1.3. UPDATED RESULTS

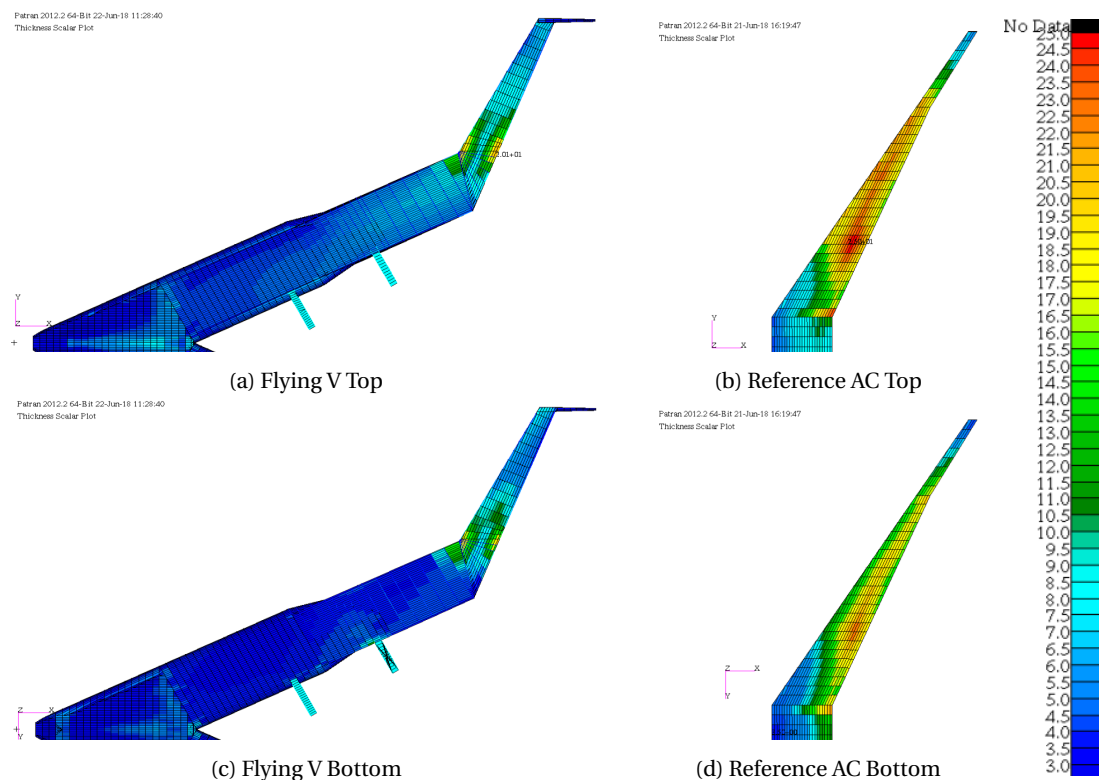


Figure 9.2: Thickness

In order to compare the thicknesses both aircraft have the same color scale indicator. From the new results shown in Figure 9.2 it can be seen that the overall thickness of the Flying V is lower than the obtained values for the wing thickness of the reference aircraft. All the sub-figures are on the same scale, so geometric comparison is possible too. It is clear that the chord of the Flying V is bigger at every location. It is because of this higher chord (and consequentially thickness) that the (bigger) box can provide more of the required inertia, and a lower thickness is required. For both the Flying V and the reference aircraft the required thickness on the top is slightly higher than that of the bottom.

For the reference aircraft one can observe that the thickness increases towards the rear spar. This is generally speaking the case for conventional aircraft, due to the loads taking the shortest load path.

The thickest points of the Flying V are still at the wing kink. A closer look has been provided in Figure 9.3. In this figure the wing is at its maximum deflection (more on the maximum deflection later on in Section 9.5). The jig shape (no deflection) is presented by the pink wire-frame. The blue arrows indicate the direction to the root and tip. The front and rear spars are removed in this picture, so that the thickness of the internal ribs can be seen as well.

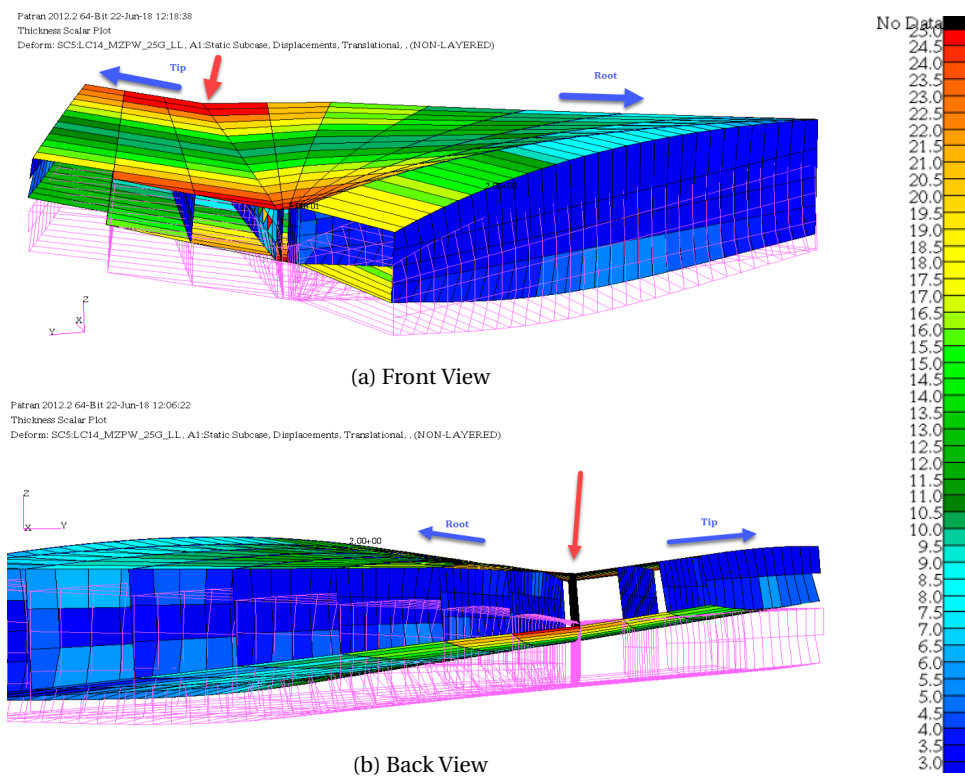


Figure 9.3: Flying V Kink Thickness Distribution

As explained before the sudden increasing box dimensions lead to a localized load convergence. But there is more going on than just dimensional changes. At this location the front spar is kinked (see Figure 9.3a) and in addition, the top cover is kinked as well making the kink 2D. (Indicated by the red arrow in Figure 9.3b.) It is the combination of these three elements that really drives the increasing thickness of the 8 extremities. All of which are located exactly at this indicated rib. Ideally the kink should be smoothed out so that the very noticeable angle of the top cover and front spar are reduced if not eliminated. One way to achieve this is to introduce (large) curvatures rather than angles. However, according to Klaus Bender this would drastically deteriorate the aerodynamic performance of the Flying V. So this solution is likely not possible. The remaining option to address this is to perform a detailed stress and strain analysis (with possibly a finer mesh) in this region to define the major load path directions and design a very specific composite lay-up to be used in this region. Or a dedicated topology optimization can be used here to truly optimize the structure. Topology will place

material only where it is needed. If implemented correctly, topology optimization will have the exact amount of strength required for the specified loads, while at the same time obtaining the minimal structural weight. As things stand now it must be accepted that this region will introduce a weight penalty to the structure of the Flying V. Even with the penalty the obtained FEM weight is still lower than that of the conventional reference aircraft. So this penalty might be deemed acceptable.

From Figure 9.2a it can be deduced that the skin thickness at the structural adaptation of the nose-fuselage intersection is still noticeable higher (by a factor of 2) than the surrounding elements. So the loads converging in this region are still quite large. Most of these loads will be carried by the frames and beams. They will be analyzed later on (9.2 and Section 9.5.2), and special attention will be payed to this region.

From this point onward only the results of the latest optimization will be discussed. The limited thickness is believed to give a more realistic results.

9.2. FRAME SIZE

9.2.1. NOSE-CABIN INTERSECTION FRAME

Earlier on (Section 8.4.5) it was explained why additional structure was required at the intersection between the nose and cabin parts. The proposed structural solution was implemented in the model of the Flying V and the resulting will now be analyzed. In the thickness analysis it was seen that the skin elements at this location are higher than the surrounding elements, but still acceptable. One of the remaining attributes that needs to be analyzed are the profiles. It is required to check if the thickness of the bars and frames is sufficient to carry the converging loads. To do this Figure 9.4 is introduced.

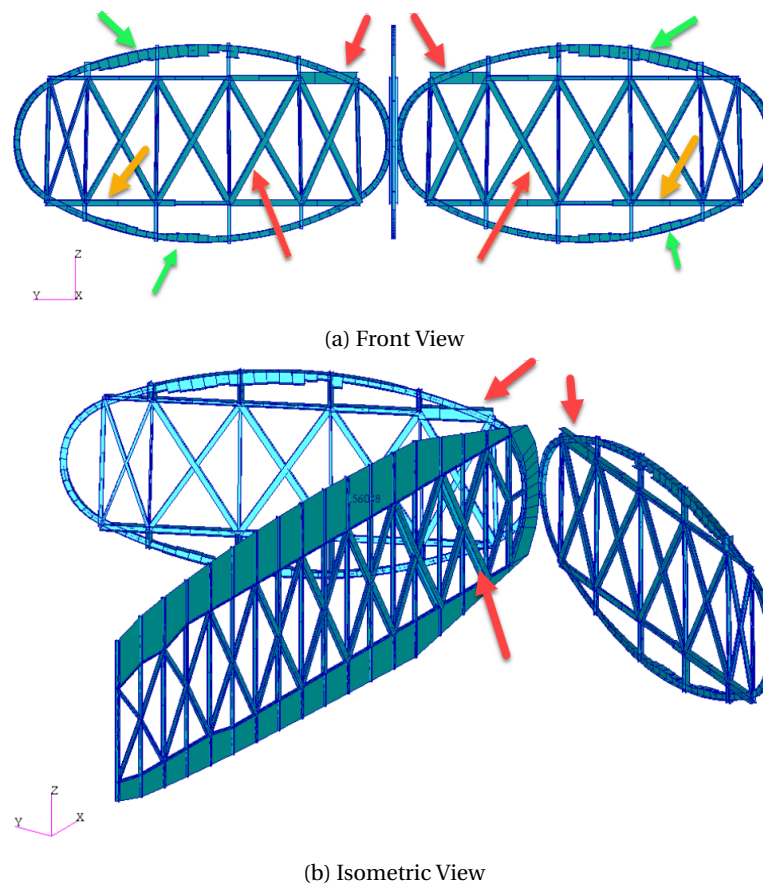


Figure 9.4: Flying V Center Frame and Ribs

These images reveal some interesting aspects. Starting with the most comprehensive; the floor beam, indicated by the yellow arrow. This beam is under compression. This is a consequence of the cabin pressure pushing (the bottom shell) outwards. This was fully expected. The reason that the thickness of the beam increases from center on outwards is that the end points of the beam are fixed to other structure. This introduces a hard point in the structure where more loads converge.

The same logic would hold for the side struts, only they are much smaller and cover a shorter curvature, so they do not require as much thickness. The top (ceiling beam) is another story. While the same would be expected as was seen at the floor beam, here the size distribution is not symmetrical. The outboard beam dimensions are smaller, possibly because of the thicker frames at this position. The inboard beam becomes very large due to the convergence of forces and torsional moment described before.

The green arrows indicate increases in frame size. All of these are introduced by the pressure in the cabin. This has been verified by visualizing (and magnifying) the deformation due to pressure at the first design loop (before sizing). It would appear that the highest deformations (and stains) occur at the same locations that have the increased frame size. A more symmetrical distribution was expected initially. The reason we see this effect might be that the (top and bottom) curvature is not perfectly constant in this specific section. Remember that this is a transition frame between two ovals, so this is not impossible. Another (perhaps more likely) explanation is that multiple structures are converging at the intersection point of the cabins, making this region stiffer and thus less effected by the pressure.

There are some beam elements that have reached their geometric size limitation. Some of those are indicated by red arrows. This is not a good sign, it means that these bars might not have obtained the value they require to carry the local loads. So even though the thickness of the skin and the local deflections are now within acceptable ranges, the structure itself is not yet strong enough at every location. It has become clear by now that the load paths and convergence in this specific frame is very complex. A more detailed analysis is required to fully understand them and the structure might need an enhancement to solve the issue of oversize beams. The easy solution would be to introduce a sheer wall at this frame station. This would drastically decrease the required beam dimensions and would further limit the deflections. It might even result in a lighter overall structure, though this can not be guaranteed. A wall introduces material every where, even if it is not required. The best solution is more complex but has the advantage that every bit of introduced structure will be ideally distributed and utilized, loading to the lowest possible weight and a structure strong enough to cope with all the forces. This method would be a localized topology optimization.

9.2.2. CENTRAL NOSE FRAME

Observing the frames at the nose might be interesting too, as the size of the oval is quite a bit larger here. All the frames have been checked in PATRAN and they proved very similar. In this report one of the frame is included as a representative frame for the nose. This can be seen in Figure 9.5. The frame does behave as expected. The smooth size distribution suggest a uniform (pressure) loading. Even though it might not be very obvious in this figure, somewhat thicker elements can be found at the hard points introduced by the supporting beams. The most significant frame size is found at the extremities of the oval curve segments. Here the strains are highest, and in addition there is a hard point created by the (beam of the) center frame. The thickest frame elements are still within the design constraints, and thus fully sized.

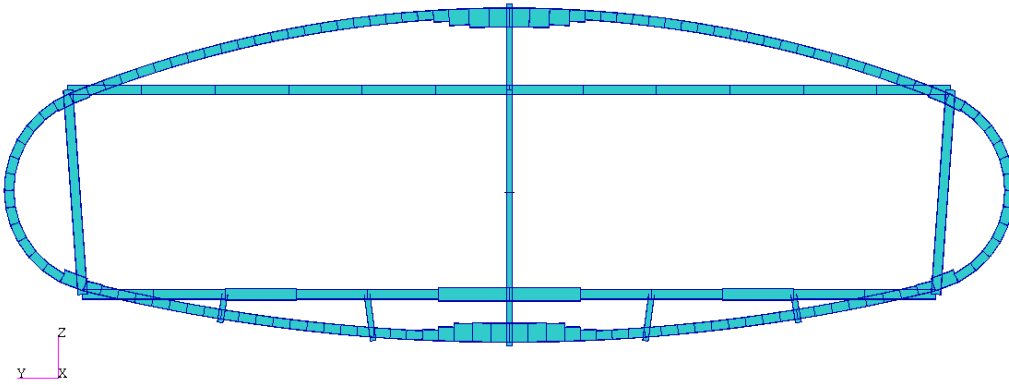


Figure 9.5: Nose Frame

9.2.3. CENTRAL CABIN FRAME

The representative frame for the cabin yields the same results; nice, smooth and symmetrical size distribution, with slight increments at the introduced hard points.

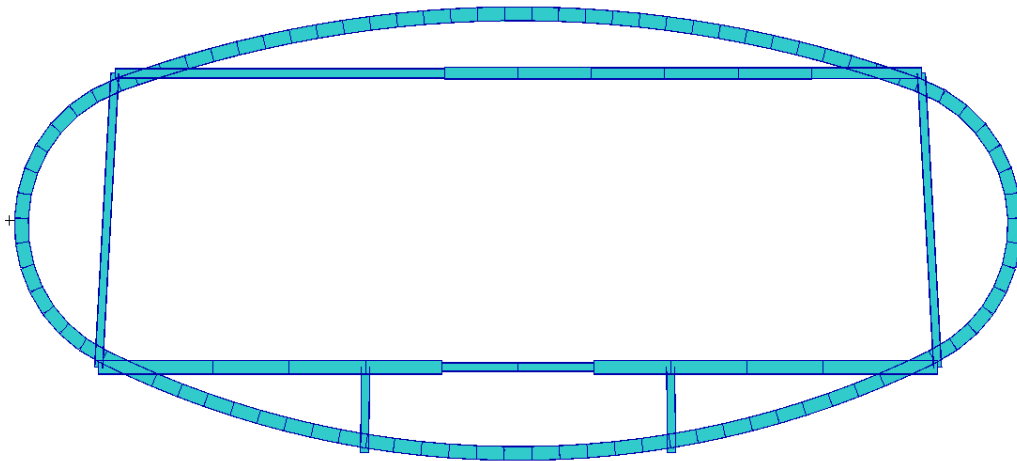


Figure 9.6: Cabin Frame

9.3. CRITICAL LOAD CASES

The critical load cases per element are shown in Figure 9.7. Herein the Flying V is compared to the wing of the reference aircraft. The results of the entire reference aircraft (including fuselage and empennage) can be found in Appendix G. The 22 used load cases do not fit in one color range without making the colors hard to distinguish. So two color ranges are used.

In the first color range (figs. 9.7a to 9.7d) the pressure and all the 2.5g load cases are presented, as well as the first $-1g$ load case (LC 12 and 13; MZFW, labeled as LC21. The labeling "LC" in this figure refers to load set). It would appear that the latter is not critical in any region, so in effect only the pressure and 2.5g load cases are visible in these four sub figures. The regions that have critical load cases not represented in this color scale are marked in red, and can be found in the next four subfigures (figs. 9.7a to 9.7d).

The last four subfigures thus represent all the remaining $-1g$ load cases, the four different ground load cases and the side gust. This time the load cases that could not be represented in this color bar are displayed in blue.

When analyzing the results of the Flying V it becomes clear that most of the skin elements at the top are sized by the 2.5g load-cases. The bottom skin elements are sized mostly by ground cases or again the 2.5g aero loads. $-1g$ load cases are almost never critical, and are only found at the bottom of the nose part, or at the bottom skin near the FS aft of the pressure bulkhead. The wingtip and winglet is sized by the side gust.

At the results of the reference aircraft no ground cases can be found anywhere. This is because the main landing gear is connected to the rear spar and ribs. So the influence of the ground cases will be seen there and the effect on the top and bottom skin elements is rather limited and not critical. The results of the full reference aircraft, including spars, can be found in the (Appendix G). The only critical $-1g$ load case can be found at the root bottom front spar skin elements and to a minor extent at the very wingtip bottom skins. The most common 2.5g load cases are MFUW and MPLW. These are the two cases where the aircraft has the highest loading.

Comparing the Flying V to the reference aircraft wing one can conclude that the Flying V uses more different load cases to size. This was to be expected as not all the forces are introduced in the wing of the reference aircraft. Some (such as payload mass and side gusts) are introduced in the cabin and empennage instead. If the full reference aircraft is analyzed (Appendix G) it can be seen that the number of critical load cases in both models is more or less the same. Either way the 2.5g aero load cases seem to dominate over the $-1g$ load cases with respect to sizing. This is true for both the Flying V and the (full) reference aircraft.

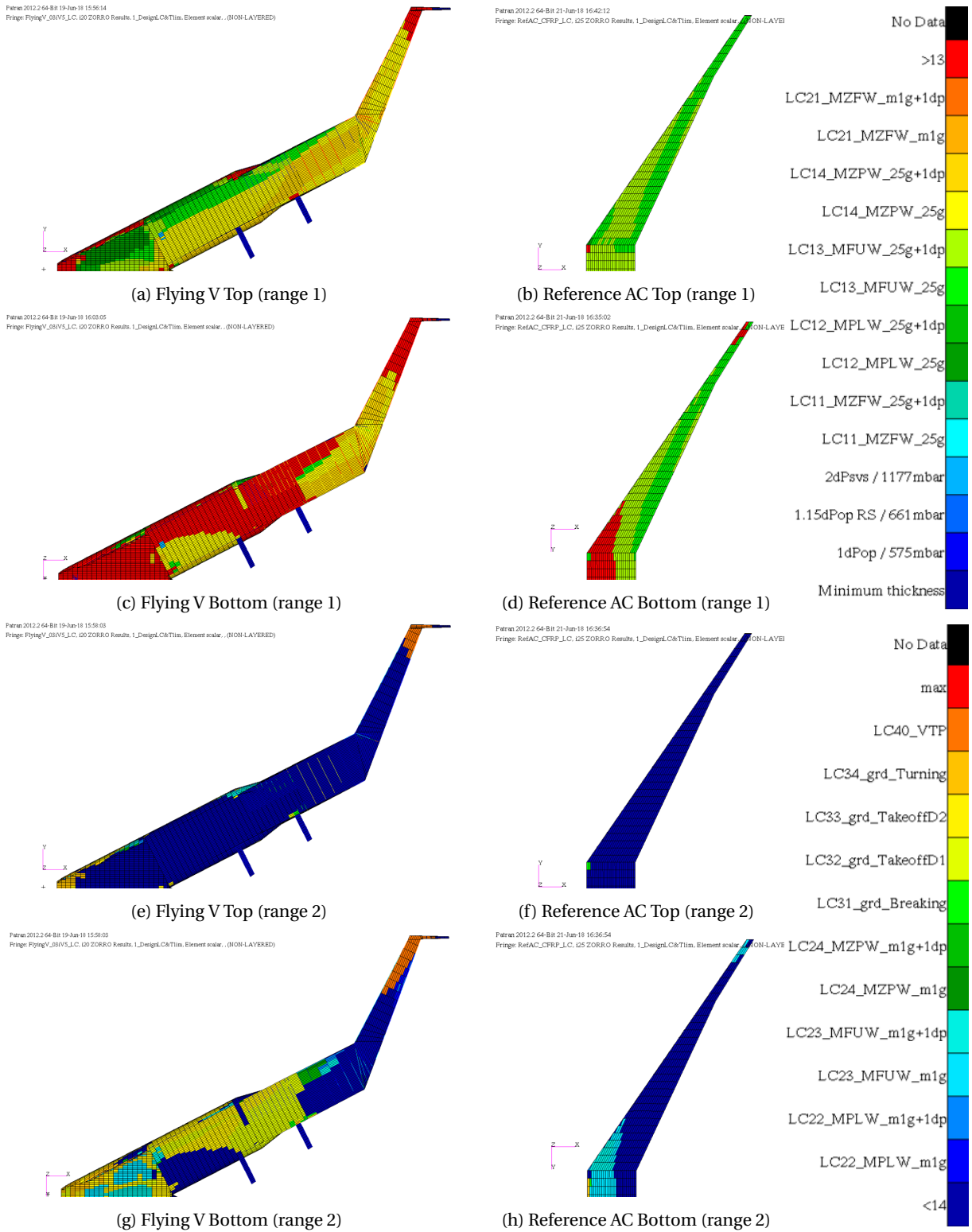


Figure 9.7: Critical Load Case

9.4. CRITICAL DESIGN CRITERIA

Figure 9.8 indicates which design criteria was driving the elements. Again the Flying V top and bottom is compared to the wing of the reference aircraft. Even though both criteria (buckling for stability and strain for strength) are combinations of multiple directions (see Section 8.4.1), the main contributor has been kept track of. By doing this it is now possible to visualize what criteria is used and in what direction its main contributor can be found.

As can be seen from the figure the Flying V is sized mostly by buckling, except for the area aft of the kink. This is true for both top and cover panels. The wing of the reference aircraft on the other hand is mainly sized for strength. When looking at the other areas of the reference aircraft (see Appendix G) this statement does not hold any longer, as the entire fuselage is sized by buckling. This might lead one to believe that the presence of pressure can influence what of the design criteria becomes more critical.

Note that the attachment structure of the engine and main landing gear on the Flying V is not minimum thickness, but it is not sized.

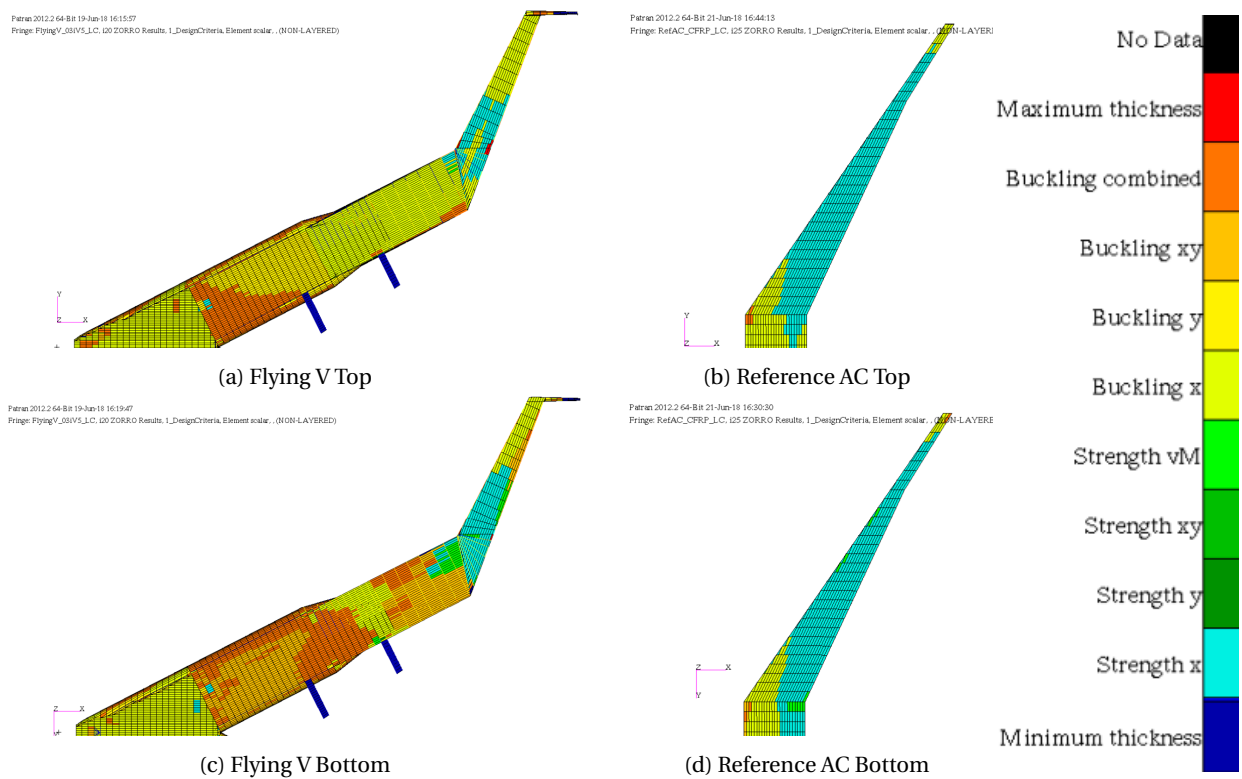


Figure 9.8: Critical Design Criteria

9.5. DEFORMATIONS

9.5.1. TIP DEFLECTION

Next the maximum wingtip deflection is analyzed. For the Flying V the max deflection occurs at sizing point D (no payload), for the reference aircraft it is at sizing point C (max fuel). They are represented in Figure 9.9. The jig shape of both aircraft is represented by the black wire-frame.

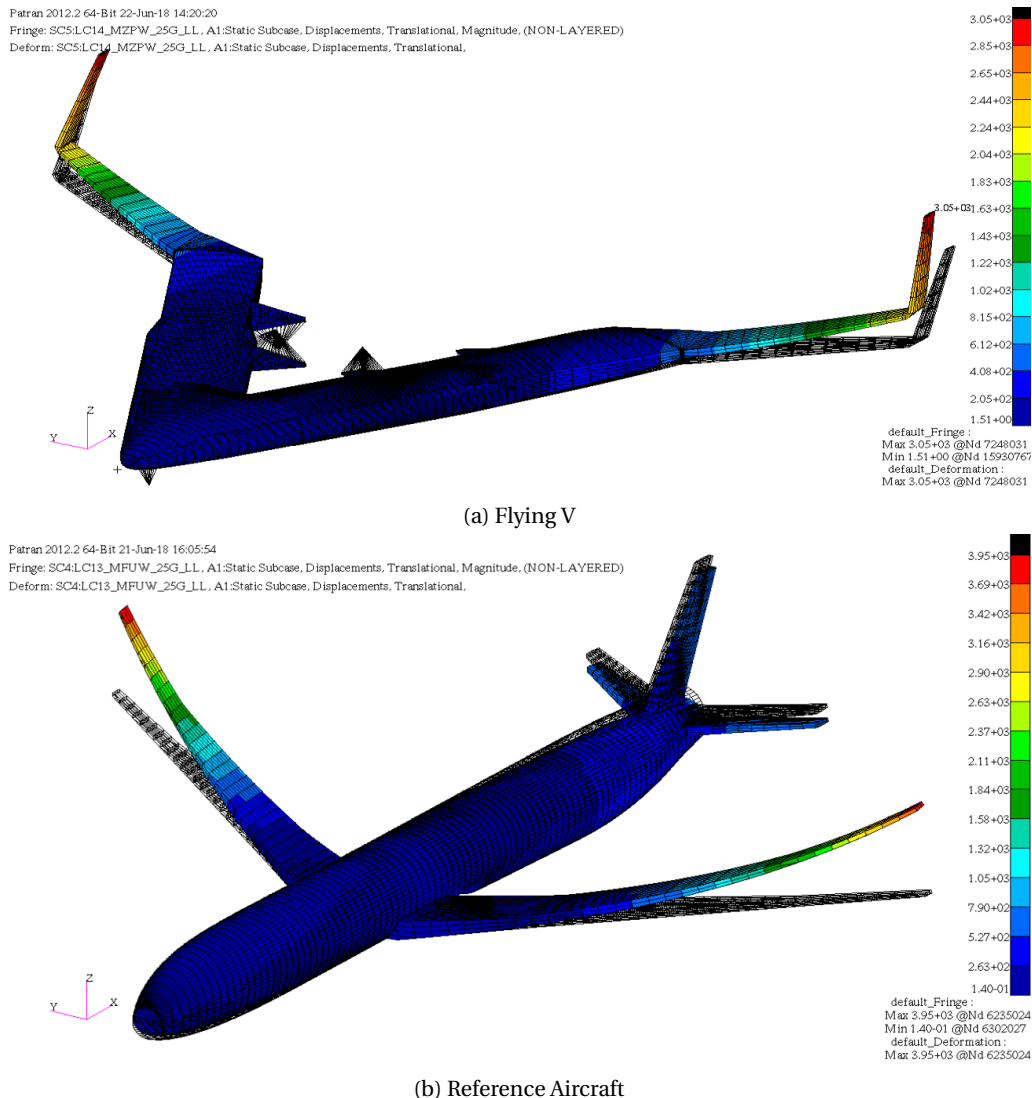


Figure 9.9: Maximum Tip Deflection

The tip deflection of the other sizing points are given in Table 9.1. These deflections (and the ones in the above figures) are measured with respect to the unreformed jig shape.

A couple of interesting things can be noted from this data. First off, the tip deflections of the reference aircraft all have higher magnitude compared to the Flying V. This was to be expected; the wingbox of the Flying V is much larger than the one of the reference aircraft. A bigger box has more stiffness and thus less deflection.

Another interesting phenomenon is that the zero fuel case does not have the highest deflection. In fact it has the lowest deflection, and the highest is obtained at maximum fuel (ref AC) and maximum payload (Flying V). This can be explained by the variance in height. As the speed, weight and lift coefficient are all specified, the altitude is implicit. The weight is the only changing variable and thus the altitude will be different for each of the maneuvers. Another way to look at this is that if more weight needs to be lifted, the wing will be loaded more and the deflection will be higher.

Table 9.1: Wing Tip Deflection [m]

Load Case	Flying V	Reference Aircraft
# 4: MZFUW at 2.5g	0.22	2.64
# 6: MPLW at 2.5g	1.91	3.89
# 8: MFUW at 2.5g	2.78	3.95
# 10: MZPLW at 2.5g	3.05	3.32
# 12: MZFUW at -1g	1.07	-1.09
# 14: MPLW at -1g	1.12	-1.62
# 16: MFUW at -1g	0.99	-1.64
# 18: MZPLW at -1g	0.84	-1.38

Last but not least, it should be noted that the wing tip deflection of the Flying V is always positive. Unlike those of the reference aircraft, which produce negative displacements for the $-1g$ load cases. This can be explained by the required flap deflection. In order to obtain the nose down attitude the flaps need to be deflected down. This increases the lift on the aft wing resulting in a positive deflection. For the reference aircraft the attitude is obtained by the deflection of the aileron, so the wingtip deflection is not influenced in the same manner.

The deflections that would occur at the wing tip of the Flying V if the thickness were not limited are slightly (3 cm or less) lower compared to the values of the limited thickness sizing results shown here. Higher thickness will give more resistance against tip deflections.

9.5.2. CENTER DEFLECTION

At this point it is necessary to address the effectiveness of the implemented structural adaptation at the nose-cabin intersection with respect to the deflection. Remember that it was made to cope with the introduced torsional moment (see Section 8.4.5) and prevent the large local deflection. Even though some bar elements were maxed out, the effect might still be seen. In Figure 9.10 the maximum deformation of the beam elements and frames of this specific region is shown (this is for MZPLW at 2.5 g, load case 10). It is clear that the deformation is still most prominent at the intersection of the three parts, but the magnitude has decreased drastically. The downward deflection at the intersection is now just over 5 cm. So with respect to limiting the deflection magnitude the implemented structure appears to be working properly. In Section 9.2 the profiles of the beams will be addressed as well, in order to see if they do not fail under the converged loads.

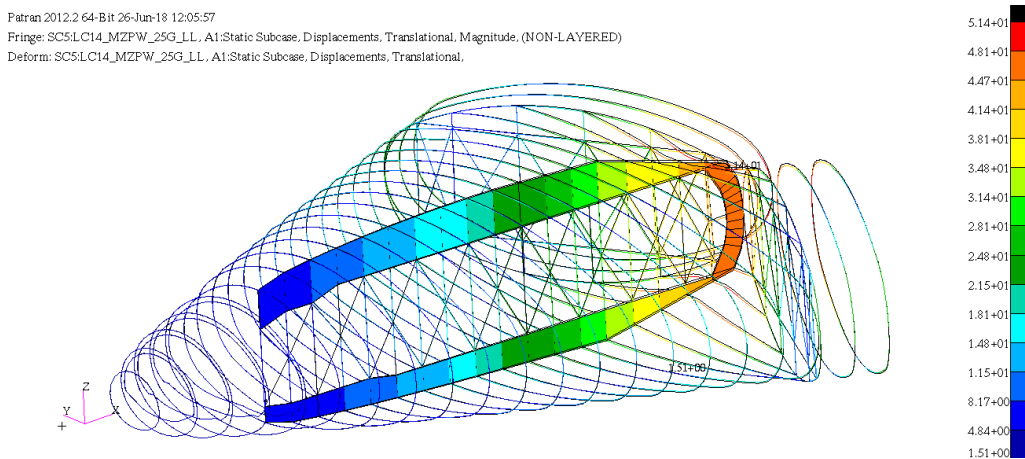


Figure 9.10: Maximum Frame and Beam Deflection [mm]

9.6. WEIGHT

9.6.1. CONVERGENCE

Convergence is established when the change in mass falls below a certain threshold. To increase the level of accuracy not only the total structural weight is tracked, but even the change of weight per design group is monitored. Table 9.2 shows the change in weight per design group by indicating how many percent of the structure falls in a specific range of mass change between iterations. The presented results are those of the last iteration (20 for the Flying V and 25 for the reference aircraft.) It can be seen that even though the reference aircraft has more iterations, the level of convergence is about the same for both models and full convergence has been established. The mass changes that fall in 10 or 20 % change category are small, furthermore the design groups that have the most of these changes are low in structural mass, meaning that even the marginally larger mass change in that group has no significant impact on the overall structural mass. This has been visualized by including the weighed average over all the design groups for the mass change intervals. The obtained mass per design group will be shared in the next section.

Table 9.2: Group Convergence

Group	Flying V					Reference Aircraft				
	+20%	+10%	±5%	-10%	-20%	+20%	+10%	±5%	-10%	-20%
Floor Struts	0.0	0.5	99.5	0.0	0.0	0.0	0.0	100	0.0	0.0
Floor XBeam	0.0	0.6	98.3	1.0	0.0	0.0	0.2	99.4	0.4	0.0
Frames Center	0.0	0.0	100	0.0	0.0	0.0	0.0	99.8	0.0	0.2
Frames Nose	0.0	8.8	91.2	0.0	0.0	-	-	-	-	-
Frames	0.0	1.6	97.3	1.1	0.0	0.0	0.4	97.4	2.2	0.0
Frames Rear	-	-	-	-	-	0.0	7.2	97.8	1.0	0.0
Pressure Bulkhead	0.0	0.3	99.5	0.3	0.0	0.0	0.0	99.7	0.2	0.0
Ribs	0.2	0.4	98.9	0.5	0.0	0.5	0.8	98.6	0.1	0.0
Skin Cabin	0.0	0.0	99.9	0.0	0.0	0.0	0.5	99.5	0.0	0.0
Skin Wing	0.0	0.0	100	0.0	0.0	0.0	0.0	100	0.0	0.0
Skin Emp.	-	-	-	-	-	0.0	0.1	99.9	0.0	0.0
Spars	0.0	0.0	100	0.0	0.0	0.0	0.0	100	0.0	0.0
Triangular Elm.	0.0	0.0	100	0.0	0.0	-	-	-	-	-
Keelbeam	-	-	-	-	-	0.0	0.0	100	0.0	0.0
Special Struct.	-	-	-	-	-	0.0	0.0	98.5	1.5	0.0
Weighted Av.	0.02	0.17	99.66	0.15	0.00	0.02	0.19	99.73	0.07	0.00

9.6.2. FINAL MASS DISTRIBUTION

Figure 9.11 showcases the weight change over the first 15 iterations of both the Flying V and the reference aircraft. The groups are given the same color indication between both graphs, but the vertical mass scale is not the same. The mass range of the reference aircraft is twice that of the Flying V. It can be seen that for both aircraft the wing and fuselage skin amount to the bulk of the weight, with the ribs coming on noteworthy lower third place and spars on fourth. The most important difference between the two is without a doubt the wing skin weight.

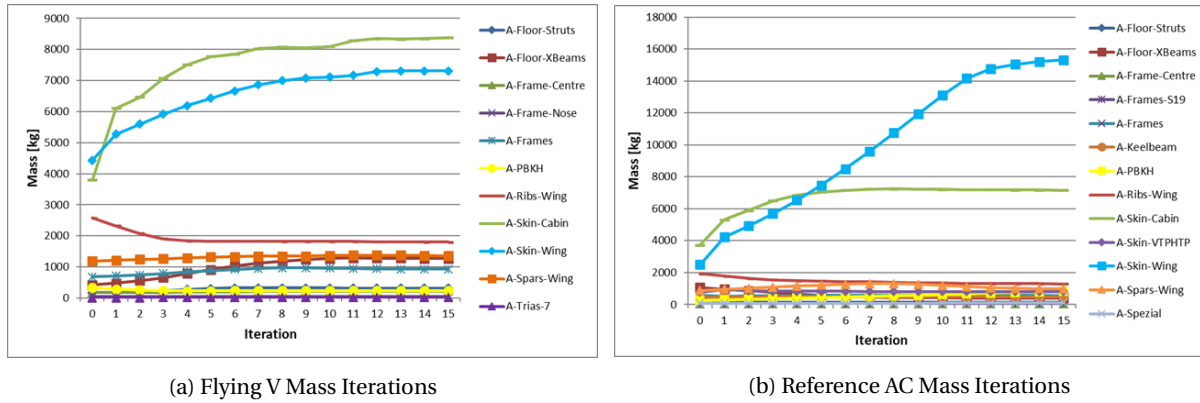


Figure 9.11: Group Mass Iterations

The reason only the first 15 iterations are shown here was because after this the scale of the figures negates every variation in weight after this point. As mentioned before the model optimization was continued until all design groups showed proper convergence. This took 20 iterations for the Flying V and 25 for the reference aircraft. The resulting masses of the groups at the respective final iteration of both models is shared using Table 9.3.

Table 9.3: FEM Design Group Mass Distribution [kg]

Group	Flying V	Reference AC	Description
Floor Struts	309	131	
Floor XBeams	1 268	415	
Frames Center	222	40	Structural adaptation (see Section 8.4.5)
Frames Nose	55	[-]	First four frames
Frames	930	557	
Frames Rear	[-]	68	Last nine frames
Pressure Bulkheads	241	826	
Ribs	1 807	1 299	
Skin Cabin	8 487	7 149	
Skin Wing	7 304	15 446	
Skin Empennage	[-]	810	
Spars	1 335	955	
Triangular Elements	11	[-]	
Keelbeam	[-]	494	
Special Structure	[-]	114	Triangular skin support to rear spar and pressure bulkhead
Sized Total	21 969	28 304	
Rest	2 770	1 480	Not sized (e.g. floor panels)
Total	24 739	29 784	

From this data it is clear that the Flying V has a significant lower FEM mass than its reference aircraft. Meaning that the difference between the two is larger than the expected margin of error of FEM analysis such as was applied here. The difference of approximately 5 tons can be explained by tree phenomena. First, in the Flying V all of the structure is contributing to the generation of lift. In a conventional aircraft the fuselage is not (significantly) doing so, while it does contribute to the overall mass (amounting to about 30% of the total). The second explanation for the lighter mass of the Flying V is the overall decreased thickness. The reference aircraft has obviously more elements with high thickness, driving its weight up. The last reason is simply because the Flying V has no longer an empennage.

9.7. CENTER OF GRAVITY

Now that the FEM mass and FEM mass distribution have been obtained, the new center of gravity can be found. Initially all the elements were assumed to have the same thickness. As this is no longer the case, it is to be expected that the CG positions of the different sizing points will be slightly altered. Consequentially the CG shift might have a marginally change as well. The following tables (Table 9.4 and 9.5) show how the new CG positions of each sizing point relates to the initial estimate. The CG location is expressed as a percentage of the MAC, measured from the LE.

In order to obtain the CG locations of the sizing points, the same method and mass breakdown were applied as initially (see Section 7.2.3). The only thing that has changed is the location of the structural CG based on the obtained results.

Table 9.4: CG Locations of the Flying V

Sizing Point	Abbreviation	Estimated CG [% MAC]	Final CG [% MAC]
A	MZFW	9.64	6.88
B	MPLW	33.95	32.22
C	MFUW	44.44	42.77
D	MZPW	52.62	50.79
O	OEW	23.26	24.04
CG Shift		42.98	43.91

Table 9.5: CG Locations of the Reference Aircraft

Sizing Point	Abbreviation	Estimated CG [% MAC]	Final CG [% MAC]
A	MZFW	34.52	38.47
B	MPLW	27.89	30.36
C	MFUW	23.19	25.91
D	MZPW	20.53	24.17
O	OEW	31.88	39.13
CG Shift		13.98	14.96

As can be seen from the tables both the Flying V and the reference aircraft have a slightly larger CG shift, 1% higher than initially estimated. Therefore the previously drawn conclusions are still valid; the CG shift of the Flying V is too large. A dedicated CG analysis is suggested and a new mass breakdown might be required. Possible solutions include, but are not limited to, a trim tank, engine relocation, detailed weight allocation etc. As for the reference aircraft, the CG shift has increased here as well but it is still within the accepted range of magnitude.

When looking at the CG locations rather than the CG shift, it can be seen that in every case the final CG is more forwards compared to the initial estimate. This is beneficial in terms of stability, as the neutral point has not changed (see Section 7.2.3). For the reference aircraft, which already was stable by a big margin, this change in CG locations isn't very influential. For the Flying V on the other hand, it is. With this new mass distribution and resulting CG locations sizing point D is now stable at high speeds with a more comfortable safety margin of 2.2% MAC (39 cm), compared to the initial margin of 0.4% (see Section C.3). Unfortunately, sizing point D is still unstable at low speeds. All other sizing points of the Flying V are stable both for low and high speeds.

IV

CONCLUSION AND RECOMMENDATIONS

10

CONCLUSION

The goal of this thesis was to establish the feasibility of the Flying V as a structural concept, by obtaining its preliminary structural weight and comparing it to a conventional aircraft design for the same mission. In order to enable comparison between the (conventional) reference aircraft and the Flying V some assumptions and design decisions were made. It was decided to use a constant span between the models, and area coefficients with respect to the A350 were used to design the empennage of the reference aircraft. The payload for both models was obtained by scaling down that of the A350, in function of the total available floor area. As the floor area of the Flying V (obtained from the Parapy model) is slightly smaller to that of the A350, the payload will be smaller too. As such, the two aircraft have been designed with the same span (65 m), *MTOM* (260 000 kg), design range (14 850 km), payload mass (56 190 kg), specific fuel consumption (15 g/kN/s) and speed requirements (0.85 mach). Additional steps were taken to enable comparison of the models included using the same stringer, rib and frame pitch. Finally, from making the structural models onward, the same software was used for both aircraft.

This report specifies exactly how both models and their loading was established (again using the same software packages). Afterwards both were subjected to the same structural optimization process using ZORRO-M and NASTRAN.

It was found that the current model of the Flying V is not yet fully stable. Due to the location of payload and fuel the obtained CG shift is rather large at 44% *MAC*. Consequentially the most aft CG position ends up to be 4% *MAC* or 71 cm behind the neutral point at low speeds. At high speeds the neutral point shifts to the back and even the most aft CG position becomes stable. It should be noted too that the most aft CG position is obtained only for ferry configurations (maximum fuel without payload). Therefore this issue can be resolved by adding some ballast. This will also reduce the ferry range somewhat. Another consequence of the large CG shift of the Flying V is that controllability might become an issue. This has not been analyzed in the current research, but, based on found flap deflections for maneuvering, a detailed analysis is strongly suggested. The obtained CG shift might be reduced by a number of actions, like relocating the engines, implementing trim tanks and providing more detailed weight allocations. This has the potential of solving both the controllability and stability issue.

Results of the FEM analysis show that the Flying V still has some challenges ahead with respect to its structural model. These include the structure at the wing kink and at the nose-fuselage intersection.

The wing kink features eight skin elements (at the front and rear spar, of both top and bottom cover of both wings) that require a very high thickness. The neighboring elements do not require these extreme values (18 mm versus 25-30 mm). Yet because of the symmetry of the extreme thick element's locations, together with detailed load analysis, it can be concluded that this is not due to a problem with the modeling or optimization. The phenomenon is explained by the geometric properties at the kink, which are required for aerodynamics. Proposed solutions include designing a very specific composite lay-up in this region, or implementing a local topology optimization.

The deflection and skin thicknesses at the nose-fuselage intersection have improved noticeably by introducing struts and x-beams over the entire frame. After this implementation the deflection is reduced to 5 cm where first 0.5 m was measured. However, it became clear that the used beams and struts to obtain this, became very large. Some of them even reaching the pre-set geometric limits. Reaching this limit means that they are not yet fully sized and will likely fail under the currently assessed loads. One of the proposed solutions is implementing a shear wall rather than beams and struts. This wall may still contain a door opening to connect the different sections in the cabin. It can be used for class separation or lavatory placement in (future) internal cabin design. A wall will drastically decrease the required thicknesses of the supporting beams, since the loading can be distributed more evenly throughout the frame section, it is possible this reduces the weight of the (local) structure. The downside of a wall is that material might be introduced where it is not actually necessary. If this needs to be avoided, the best alternative is again a localized topology optimization.

Even though the proposed structural model is not yet ideal, the feasibility of the Flying V structure is favorable. The obtained FEM mass of the Flying V is lower than the one for the comparable conventional reference aircraft. If aforementioned issues can be addressed in further development, the Flying V shows good promise for not only being structurally viable, but preferable.

11

RECOMMENDATIONS AND PROPOSALS FOR THE FUTURE

11.1. PROJECT RECOMMENDATIONS

- Make a metallic analysis and sizing
- Make a dedicated study to optimize rib orientation
- Make a more detailed engine and landing gear structure
- New structural proposals;
 - At the wing kink use localized and dedicated composite lay-up for the high loaded elements
 - At the nose-fuselage intersection use a shear wall over the entire frame
- Establish cabin lay-out and window/door placement
- Include the holes in the structural (FEM) analysis
- Limit Flying V CG range by;
 - Relocate engines
 - Implement trim tank at the nose
 - Detailed system weight allocation
 - Detailed payload weight allocation (passengers vs. cargo)
- Make a detailed controllability and stability analysis for the (new) CG range
- Establish an estimation for factor between FEM and real weight. (broken down to rib/frame/.. level and obtained by statistical data)
- Close design loop by;
 1. Feed back structural weight (with factor to get from FEM to real)
 2. Obtain new MTOM
 3. Obtain new mass breakdown
 4. Obtain new CG range
 5. Obtain new loads
 6. Sizing

11.2. SOFTWARE RECOMMENDATIONS

- ParaPy
 - Establish a working export feature for the curves and planes
 - Label the required curves and planes according to the ZORRO-X used standard
 - New model of the Flying V without complicated fuselage-wing transition
 - Implement stringers on the front and rear facing curvature of the fuselage
- MARES
 - Establish working export feature to ODILILA
 - Implement easily adjustable rib orientation (e.g. paralleled to spar option)
- ZORRO-X
 - Implement location definition of floor longerons
 - Establish batch mode for creating and mapping multiple load case data sets
 - Enable the user to specify explicitly what node groups can be used to map forces to.
- ZORRO-M
 - Implement post processing feature to visualize elements that are at the specified maximum constraints
 - Clarify some parts of the user manual
- PATRAN*
 - Implement automatic window sizing to get a correct aspect ratio visual

PATRAN can use a lot more recommendations in order to make it more user friendly, and have more logical implantation options. These however can not be made by Airbus personnel or TUD students and staff, nor are they really relevant to the current study. Therefore these numerous recommendations are not mentioned here.

A

CONCEPTUAL DESIGN

A.1. USED EQUATIONS

The following equations are used to obtain the conceptual design of the different aircraft.

A.1.1. WING PLANFORM

$$S = \frac{M_0}{W/S} \quad (\text{A.1})$$

$$A = \frac{b^2}{S} \quad (\text{A.2})$$

$$S_{wet} = C_1 * S \quad (\text{A.3})$$

$$c_r = \frac{2 * S}{b * (1 + \lambda)} \quad (\text{A.4})$$

$$c_t = c_r * \lambda \quad (\text{A.5})$$

$$MAC = 2/3 * c_r * \frac{1 + \lambda + \lambda^2}{1 + \lambda} \quad (\text{A.6})$$

$$MAC_y = \frac{b/2}{1 - \lambda} * \left(1 - \frac{MAC * b/2 * (1 + \lambda)}{S} \right) \quad (\text{A.7})$$

$$MAC_{.25} = \tan(\Lambda_{.25}) * MAC_y + c_t/4 \quad (\text{A.8})$$

$$(L/D)_{max} = C_2 * \sqrt{\frac{A}{S_{wet}/S_{ref}}} \quad (\text{A.9})$$

$$(L/D)_c = C_3 * (L/D)_{max} \quad (\text{A.10})$$

A.1.2. WEIGHTS

$$M_e/M_0 = C_4 * M_0^{C_5} \quad (A.11)$$

$$M_e = \frac{M_e}{M_0} * M_0 \quad (A.12)$$

$$M_1 = \frac{M_0}{e^{R * \frac{sf c}{(L/D)_c * M * a}}} \quad (A.13)$$

$$M_{f1} = M_0 - M_1 \quad (A.14)$$

$$M_{f2} = M_{f1} * C_6 \quad (A.15)$$

$$M_f = M_{f1} + M_{f2} \quad (A.16)$$

$$MTOM = M_e + M_f + M_P \quad (A.17)$$

A.1.3. FUSELAGE PLANFORM

$$l = C_7 * MTOM^{C_8} \quad (A.18)$$

$$d = \frac{l}{l/d} \quad (A.19)$$

A.1.4. HTP PLANFORM

$$S_{HTP} = S * C_9 \quad (A.20)$$

$$b_{HTP} = \sqrt{\frac{S_{HTP}}{A_{HTP}}} \quad (A.21)$$

$$c_{r,HTP} = \frac{2 * S_{HTP}}{b_{HTP} * (1 + \lambda_{HTP})} \quad (A.22)$$

$$c_{t,HTP} = c_{r,HTP} * \lambda_{HTP} \quad (A.23)$$

A.1.5. VTP PLANFORM

$$S_{VTP} = S * C_{10} \quad (A.24)$$

$$b_{VTP} = \sqrt{\frac{S_{VTP}}{A_{VTP}}} \quad (A.25)$$

$$c_{r,VTP} = \frac{2 * S_{VTP}}{b_{VTP} * (1 + \lambda_{VTP})} \quad (A.26)$$

$$c_{t,VTP} = c_{r,VTP} * \lambda_{VTP} \quad (A.27)$$

A.1.6. USED CONSTANTS

As could be seen in the previous equations, some constants are used. These constants are all obtained by historical data, and adjusted for modern capabilities and developments. The process is fully explained in Section 4.1. The exact databases or trend-lines can not be shared because of confidentiality.

Table A.1: Used Constants in Conceptual Design Equations

Variable	Value	Comment	Variable	Value	Comment
C_1	4.5		C_6	0.05	
C_2	16		C_7	0.306	
C_3	0.866		C_8	0.43	
C_4	0.93		C_9	0.1841	HTP to wing area ratio
C_5	-0.065		C_{10}	0.1154	VTP to wing area ratio

A.2. PROPERTIES FLOW DIAGRAMS

In all the following diagrams the same logic has been applied to facilitate understanding them. Inputs are grouped in a blue frame, parameters with respect to the wing planform in a yellow, fuselage parameters are in a red frame and weight parameters are in green. Finally the empennage planform is represented in a purple frame. All the input parameters are connected to the output parameters that require them in its equation using an arrow. When a parameter is required for multiple computations the arrow is split using a black dot. An open circle represents the locations where two parameters join and will continue in a single arrow rather than two separate ones. Finally comparisons are marked by a diamond, and will always have a yes or no result. The specific consequences of these results are added in text.

A.2.1. A350

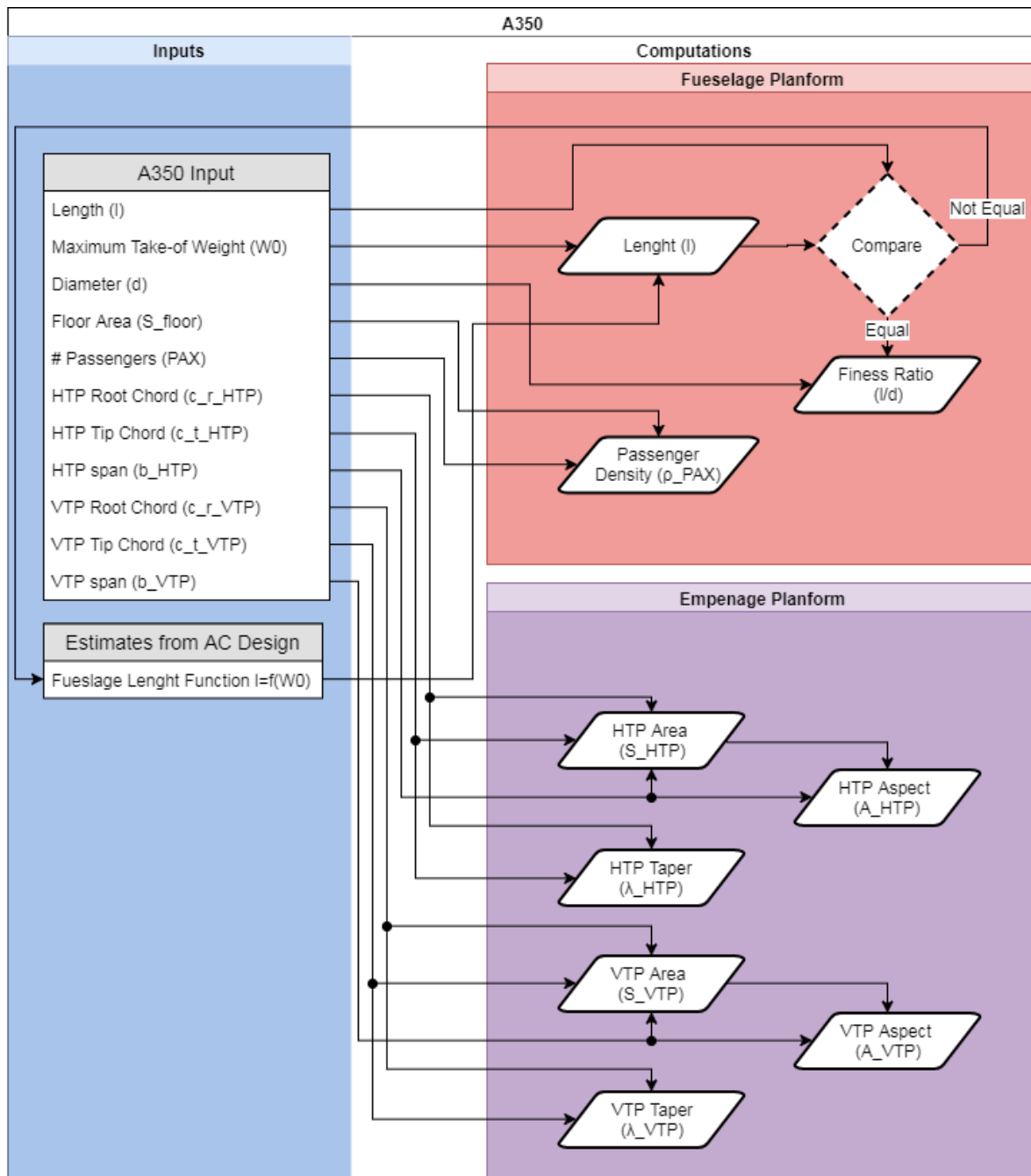


Figure A.1: Process Flow of Conceptual Design of the A350 Model - Part 1

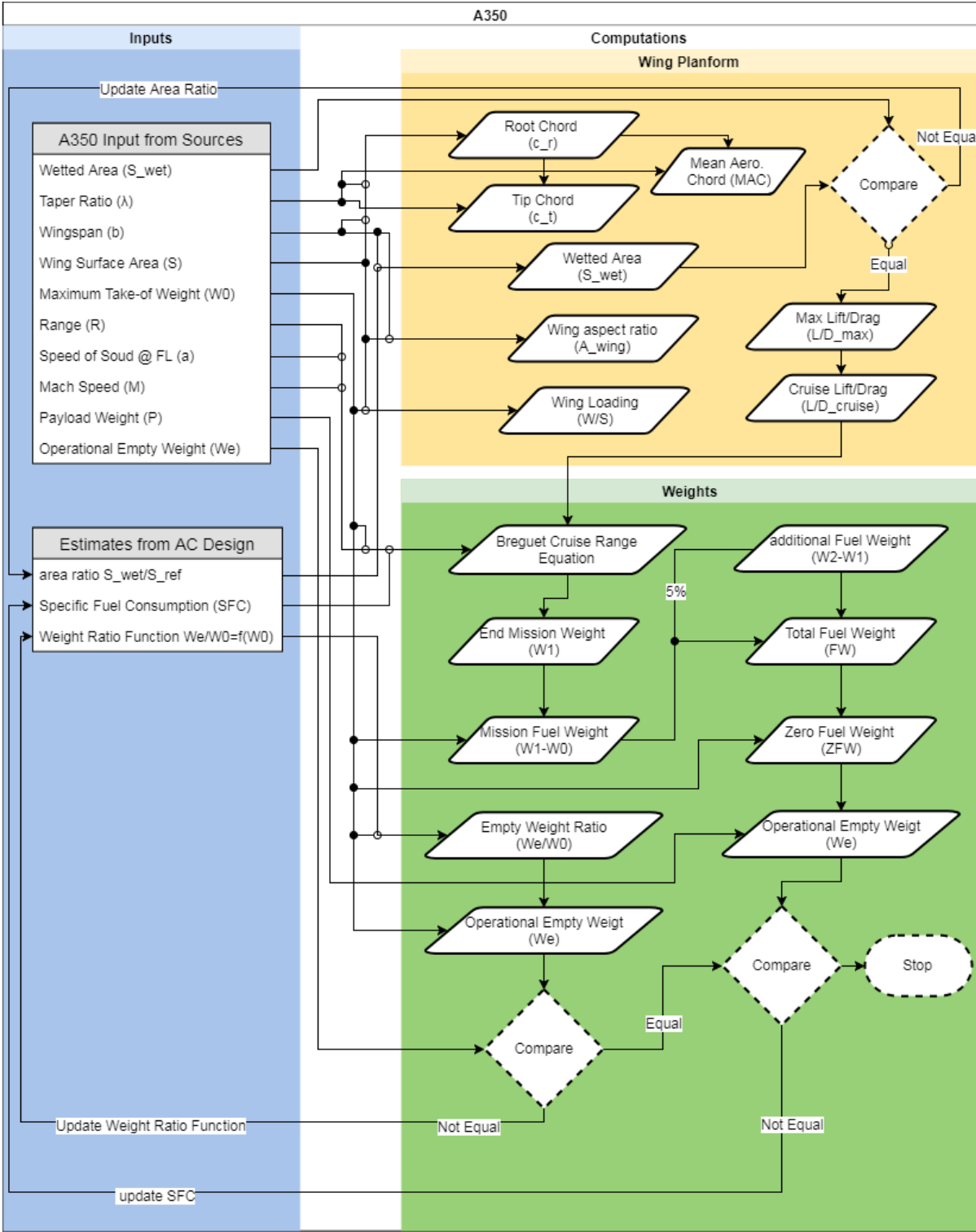


Figure A.2: Process Flow of Conceptual Design of the A350 Model - Part 2

A.2.2. FLYING V

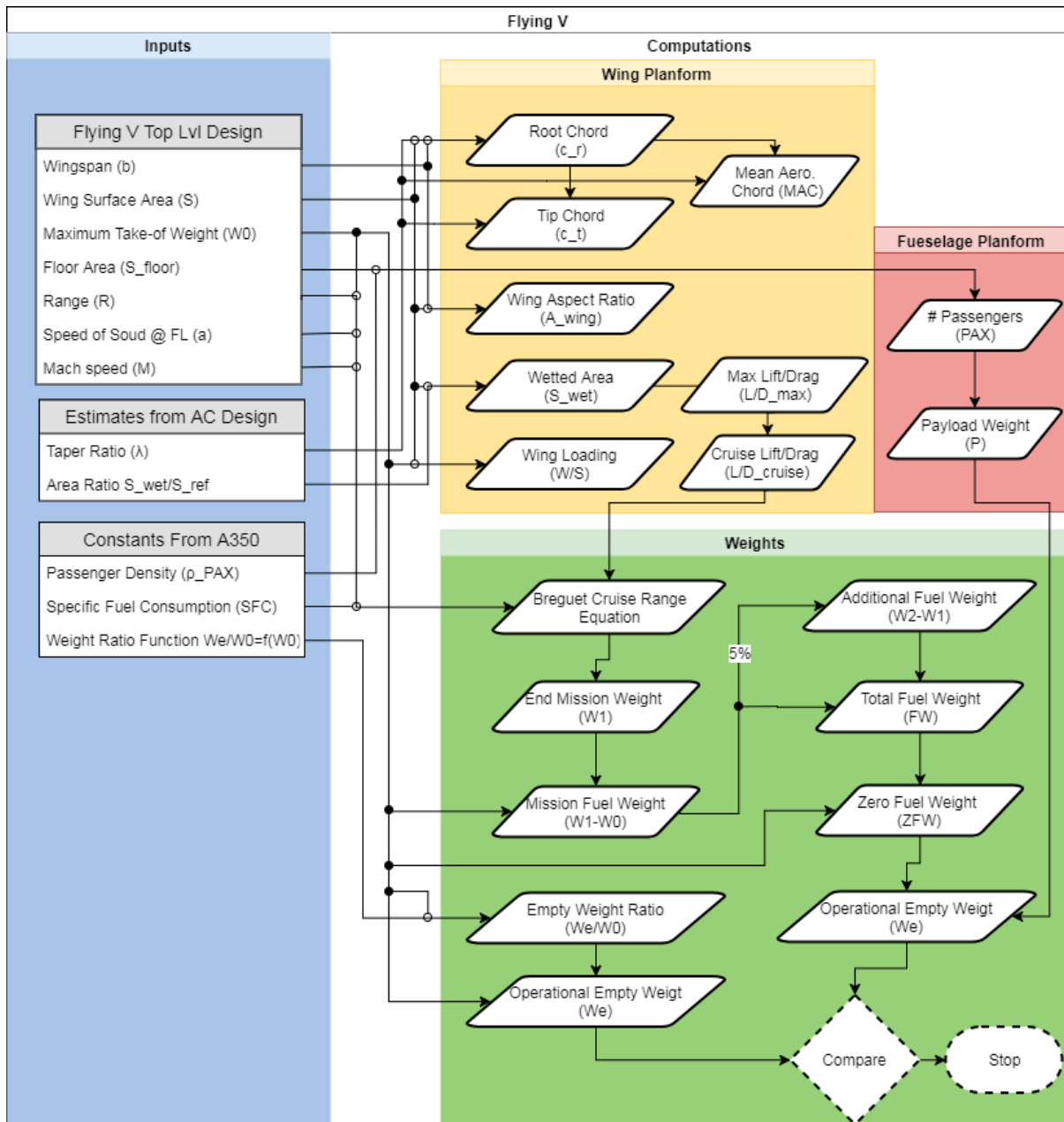


Figure A.3: Process Flow of Conceptual Design of the Flying V Model

A.2.3. REFERENCE AC

The flow diagram of the reference aircraft hasn't been given separately. This is because it is exactly the same as the one of the Flying V. The empennage naturally is extra, but the flow diagram for designing that is the same as specified for the A350, so it can be observed in Figure A.1.

B

FLYING V STRUCTURAL MODEL PARTS ASSEMBLY

B.1. NOSE AND CABIN CONNECTION

Figure B.1 shows how the nose part is connected to the right hand cabin. In Subfigure B.1a it can be seen how the top skin stringers of both parts nicely align, as they were intended to. Subfigure B.2b shows the internal floor connection. As explained in the main text (Section 6.2.4), the number of floor elements was initially not the same. So some tri-elements were introduced, this way all the longerons of the cabin floor could be connected to the nose.

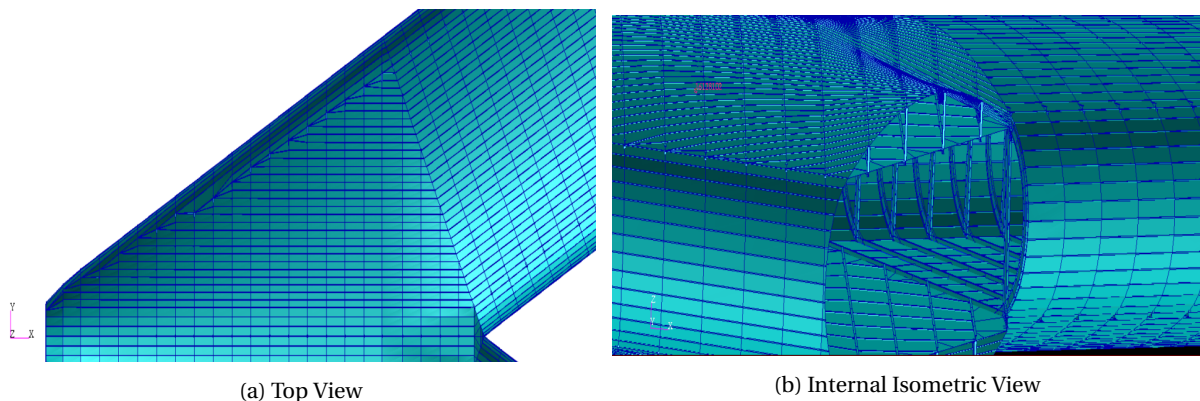
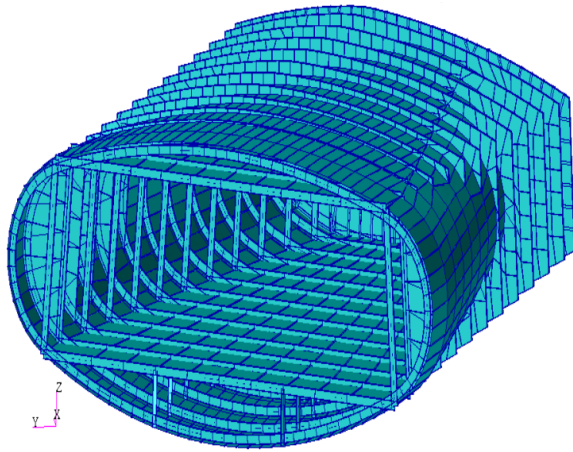


Figure B.1: Flying V Nose-Cabin Connection

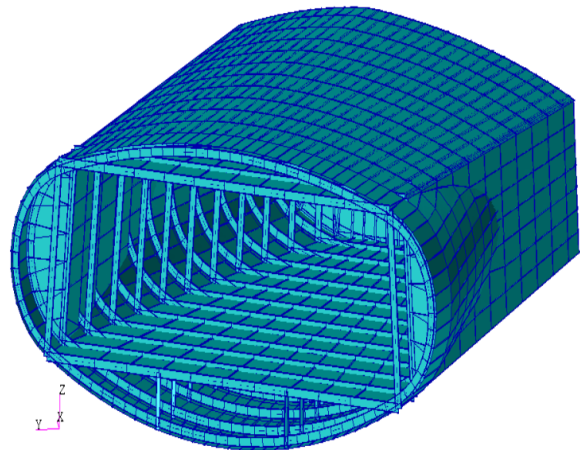
Apologies to the reader if these pictures appear grainy, this is due to the graphic limitations of PATRAN. Better images of the 3D structure could not be made.

B.2. CABIN AND WING CONNECTION

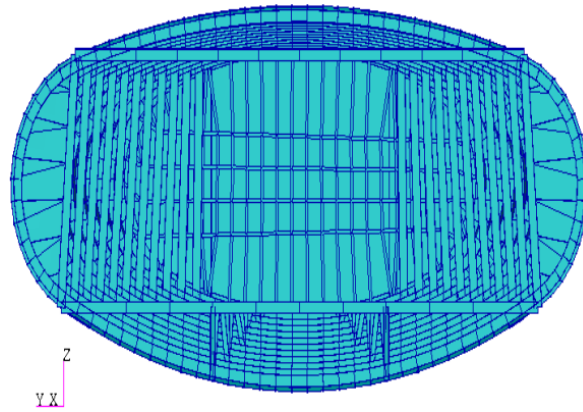
The cabin-wing transition is shown in Figure B.2. This region required extensive manual adjustments. As explained in the main text of this report (Section 6.2.4) the segments of each rib that fell within the cabin needed to be deleted manually. To connect both parts together the local nodes of each rib were moved to coincide with the local pressure wall nodes of the cabin. This way the pressure vessel gradually tapers into the wing. So at each rib station both parts are connected. Between rib stations the structure is intersecting but not physically connected. In reality either the pressure vessel or the spars would be continuous and the other one split in two parts that are connected to the intersection line (visible on the right side of Subfigure B.2b). But it is believed that the proposed modeling solution is sufficiently adequate. Modeling it like it would be in reality is not a realistic option when considering the time this would take.



(a) Transition Rib Adjustments



(b) Transition with Wing Skin Elements



(c) Transition Front View

Figure B.2: Flying V Cabin-Wing Transition

C

MASS BREAKDOWN AND CG RANGE NUMERICAL PROPERTIES

C.1. CG LOCATIONS

Table C.1: Flying V CG locations

CG	Location (from nose) [m]
Cabin	19.2
Nose Gear	4.1
Main Gear	33.0
Engine	25.6
Structural	27.0

Table C.2: Reference Aircraft CG Locations

CG	Location (from nose) [m]
Cabin	28.7
Nose Gear	5.4
Main Gear	31.8
Engine	27.1
Wing	31.3
Fuselage	30.4
HTP	59.3
VTP	58.7
APU	59.2

C.2. MASS DISTRIBUTION VARIATION OF SIZING POINTS

Table C.3: Flying V Mass Variation of Sizing Points

Sizing Point	Abbriviation	Fuel Weight [kg]	Payload Weight [kg]	CG location (from nose) [m]
A	MZFW	0	56 190	23.9
B	MPLW	97 065	56 190	28.2
C	MFUW	122 386	30 870	30.1
D	MZPW	122 386	0	31.6

Table C.4: Reference Aircraft Mass Variation of Sizing Points

Sizing Point	Abbriviation	Fuel Weight [kg]	Payload Weight [kg]	CG location (from nose) [m]
A	MZFW	0	56 190	31.1
B	MPLW	96 689	56 190	30.5
C	MFUW	116 504	36 376	30.2
D	MZPW	116 504	0	30.0

C.3. CG DIAGRAMS

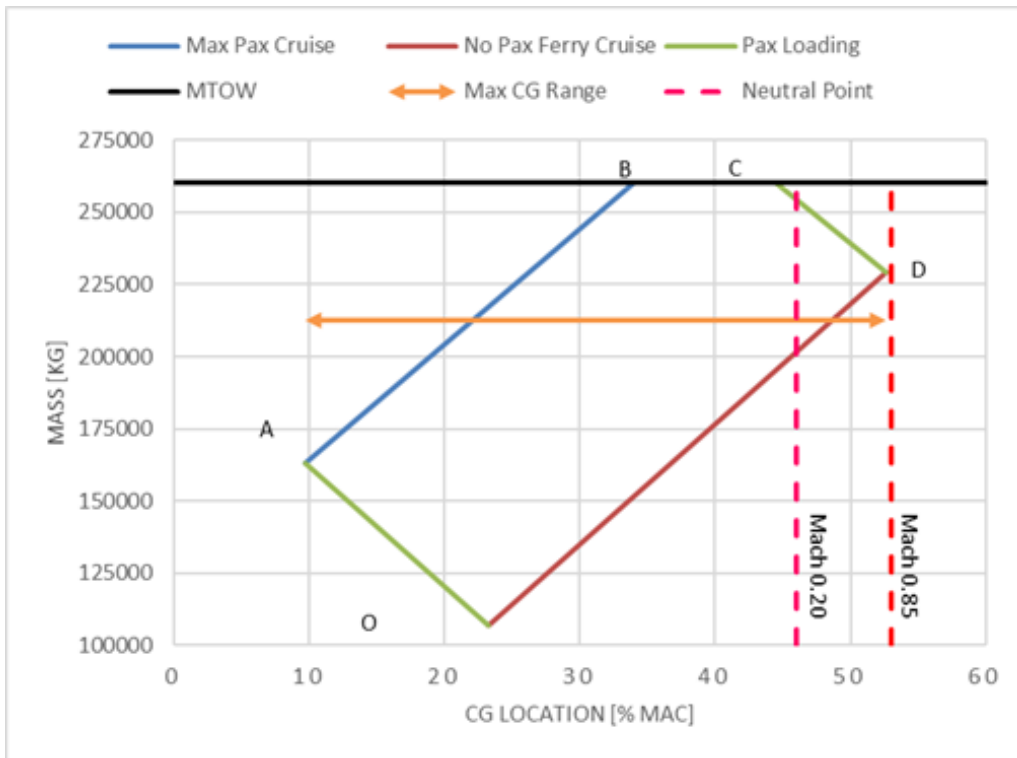


Figure C.1: Flying V CG Diagram

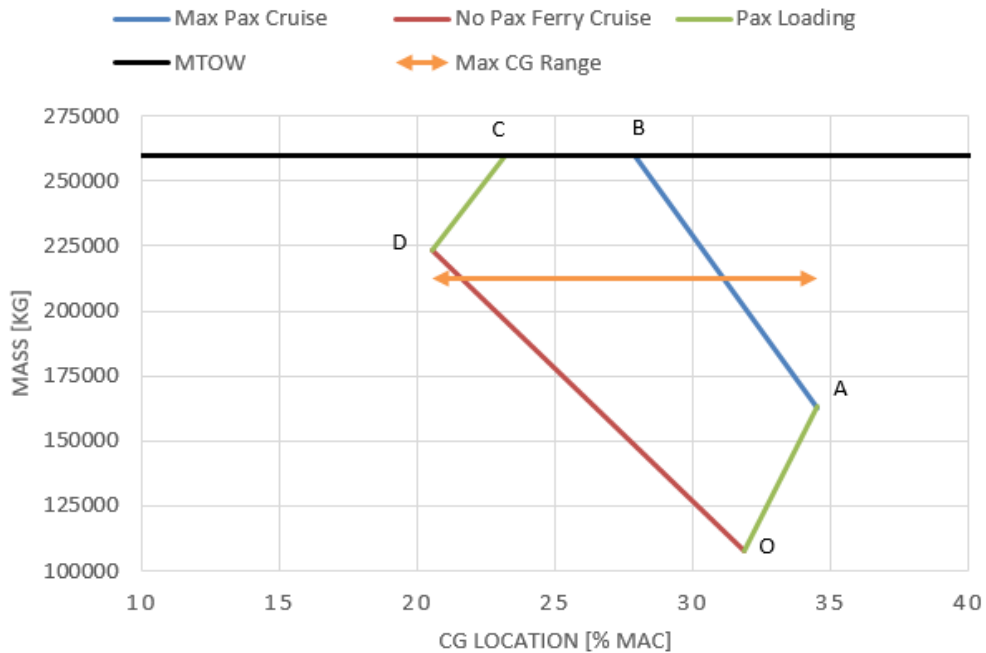


Figure C.2: Reference Aircraft CG Diagram

C.4. FUEL DISTRIBUTION

The fuel per tank has been calculated using a density of 800 kg/m^3 and a usable volume of 90%.

Table C.5: Flying V Available Tank Volume

Tank ID (front to back)	CG Location (from nose) [m]	True Volume [m^3]	Usable Mass [kg]
1	33.9	20.16	14 515
2	35.2	18.97	13 658
3	36.4	17.39	15 521
4	37.6	15.41	11 095
5	38.8	13.06	9 403
Total		84.99	61 193
Both Wings		169.98	122 386

Table C.6: Reference Aircraft Available Tank Volume

Tank ID (front to back)	CG Location (from nose) [m]	True Volume [m^3]	Usable Mass [kg]
1	26.6	8.45	6 086
2	26.6	8.05	5 800
3	26.6	7.63	5 492
4	26.8	6.50	4 681
5	27.3	5.88	4 231
6	27.7	5.23	3 762
7	28.2	4.59	3 301
8	28.7	3.98	2 867
9	29.1	3.43	2 473
10	29.6	2.96	2 130
11	30.1	2.55	1 835
12	30.6	2.28	1 639
13	31.0	2.12	1 524
14	31.5	1.96	1 413
15	32.0	1.81	1 305
16	32.4	1.67	1 200
17	32.9	1.52	1 097
18	33.4	1.38	996
19	33.8	1.25	898
20	34.3	1.12	805
21	34.8	0.99	715
22	35.2	0.87	630
23	35.7	0.76	549
24	36.2	0.66	473
25	36.7	0.56	401
26	37.1	0.46	334
27	37.6	0.41	296
28	38.2	0.37	266
29	38.7	0.32	233
30	39.3	0.29	211
31	39.8	0.26	186
32	40.4	0.23	162
33	40.9	0.20	141
34	41.5	0.17	122
Total		80.91	58 252
Both Wings		161.81	116 504

D

ODILILA DOCUMENTATION

The following text and data has been obtained from Klaus Bender, the developer of ODILILA. He made a report on his software in order to show its capabilities and validity. From this report the non-confidential parts were copied and inserted here. Some minor changes were made in the text to ensure continuity but other than those minor changes this is a one-to-one copy. As most of the original text is confidential it can not be states as a source.

D.1. WORKING PRINCIPLES

D.1.1. AERO DATA FOR PERFORMANCE

Induced drag is predicted by analyzing the down- and side-wash and the lift in the Trefftz-plane. Lift for performance data is predicted as well in the Trefftz-plane to be numerical consistent with the induced drag. The circulation for this method is taken over from the trailing edge circulation of the lattice-vortex method. Optimization and lift distribution setting is done as well in the Trefftz-plane. The lift is then related to twist or camber and applied to the lattice vortex method.

D.1.2. AERO DATA FOR HANDLING QUALITIES AND LOADS

Moments are predicted by calculating the lift of single bound vortex elements (the leading edge of panels) on the geometry.

D.1.3. GEOMETRY

All components of the aircraft are modeled with lattice vortex elements. The component geometry is described by its trailing edge in 3D and chord (always parallel to the x-axis). All panels from leading edge to trailing edge in one row are linked to a section. The section has additional characteristics as twist, camber and others. Sections are assigned to (wing) entities.

D.2. IMPLEMENTATION

D.2.1. INDUCED DRAG AND LIFT

Lift for performance calculation is predicted in the Trefftz-plane. It is derived from the trailing edge circulation of the lattice-vortex method.

D.2.2. COMPRESSIBILITY

So far only the KLM method is available. It is off by default and must be activated by setting the KLM k-factor to a value > 0

D.2.3. OPTIMIZATION

Optimization of lift distribution is done by directly manipulation of twist or camber. The optimizer is of the SQP type and uses numerical differentiation. It can be used for trimmed and untrimmed configurations, minimizing complete drag or any component of it. The lift distribution optimization can be subjected to CoP, cL, xcg and max local cn -constraints.

D.3. VERIFICATION

ODILILA predicts lift gradient and induced drag as expected. The predicted lift gradient matches well with wind tunnel test data. The inverse down-wash method (the desired down-wash is defined and the needed twist or camber is calculated by ODILILA) is accurate by less than 1% error in k-factor if the span-wise discretization is reasonable selected (25 to 200 panels per span).

For the verification of the lift prediction the lift gradient of straight untapered wings of different aspect ratio are compared with measurement and test results. [14], [15]

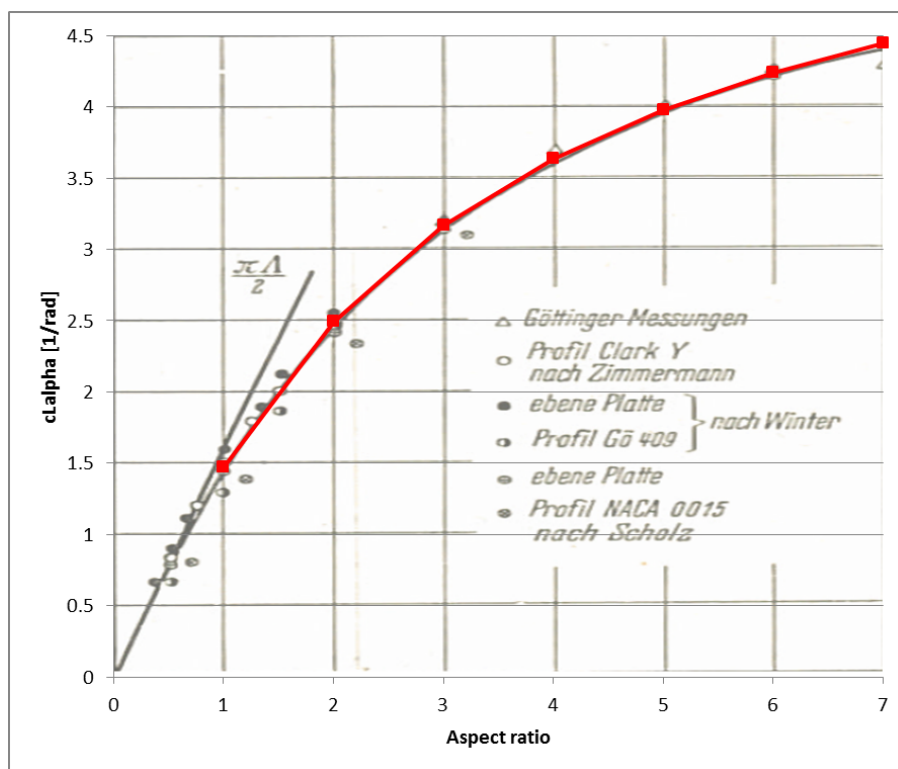


Figure D.1: Lift Gradient Vs. Aspect Ratio

pan

Figure D.1 shows the lift gradient as function of aspect ratio compared with various wind tunnel testing [14], [15]. The red line is the ODILILA calculation for unswept untapered wings. Circles and triangles indicate WTT. ODILILA shows very good matching to the WTT results even for very low aspect ratios. Span-wise discretization of this verification was 50 elements per half wing and chord-wise 6 elements. Note that the lift gradient is expressed in function of radians in this figure.

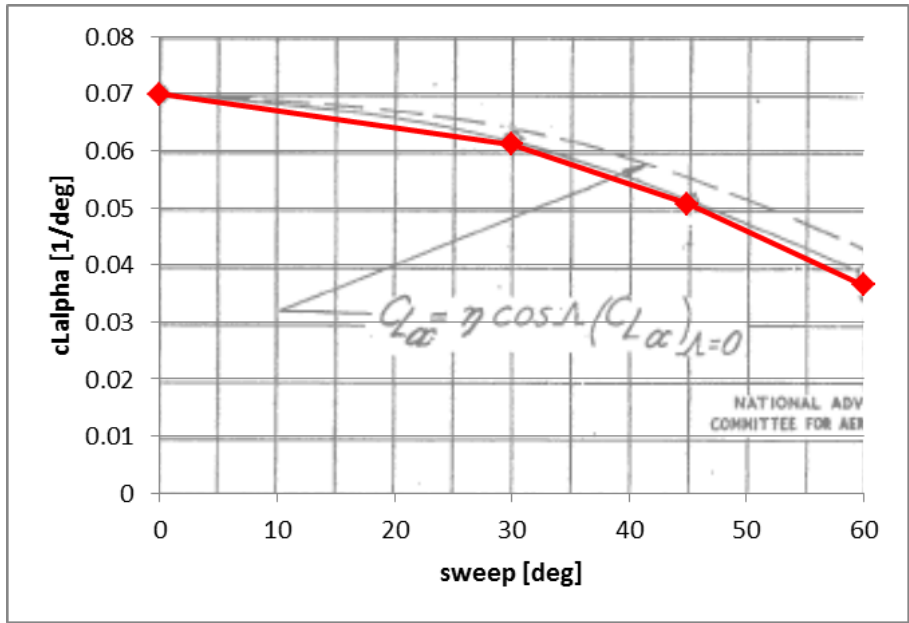


Figure D.2: Lift Gradient Vs. Sweep Angle

The lift gradient as function of sweep compared with NACA wind tunnel testing [NACA TN 1046] can be found in Figure D.2. The red diamonds are from ODILILA calculations of untapered wings. The discretization is 50 elements per half span and 6 per chord. Aspect ratio varies with span in this particular investigation (see NACA TN 1046 for more details) which is taken into account in ODILILA. The software shows good matching up to 45 degrees sweep and slightly underestimates the WTT at 60 degrees. In this figure the lift gradient is expressed in function of degrees.

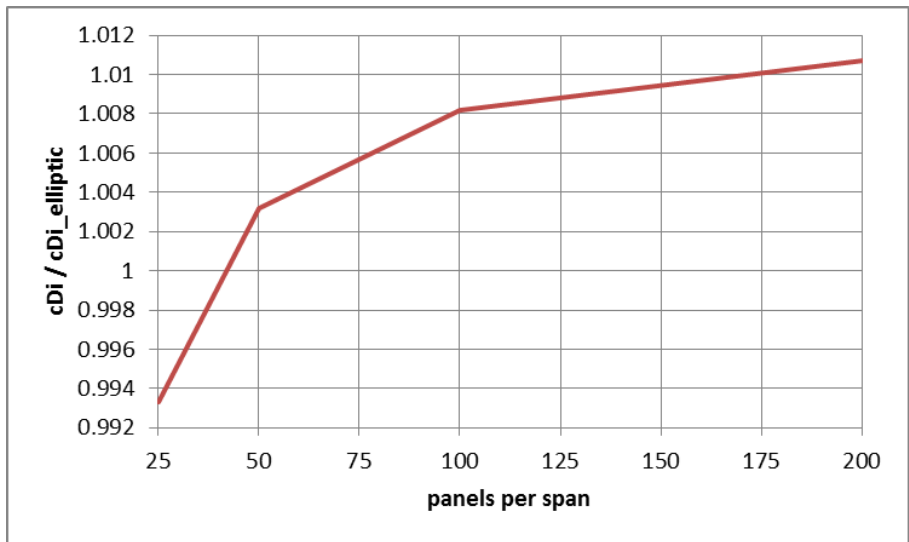
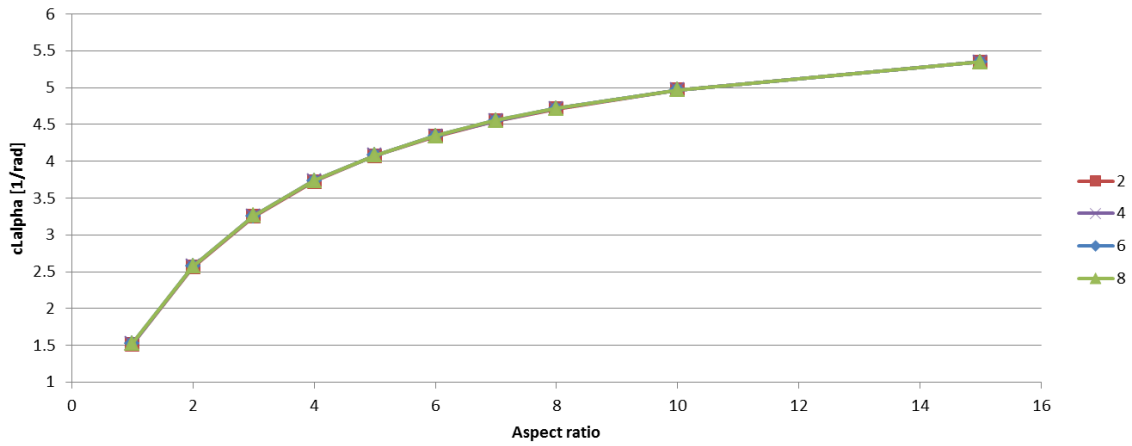
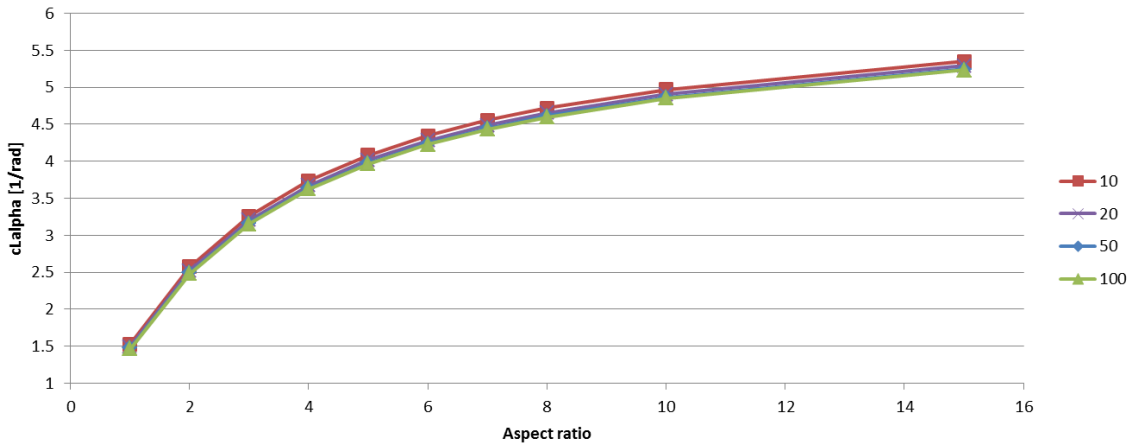


Figure D.3: Induced Drag Vs. Number of Span-wise Panels

Finally Figure D.3 shows the induced drag as function of span-wise discretization. In this case a rectangular wing of aspect ratio 10 was twisted to have a constant down-wash using ODILILA's inverse normalwash calculation feature. The induced drag was compared of the theoretic induced drag. Low discretization underestimates by 1% and high discretization overestimates the induced drag by 1%.



(a) Chord Discretization



(b) Span Discretization

Figure D.4: Discretization Effect on Lift Gradient

The curves in Figure D.4 represent the number of panels per chord- (Figure D.4a) or span- (Figure D.4b) section. The legend shows the color coding of the number of panels. It is clear that changing the number of panels per chord section has no visible distinguishable effect on the lift gradient. Changing the number of panels per span section does have a small effect on the lift gradient. At high aspect ratios increasing the numbers of panels from 10 to 100 will result in lower lift gradient of about 1%. At lower aspect ratios this offset decreases. Note that the lift gradient is expressed in function of radians in this figure.

E

SUMMARY OF IMPORTANT ODILILA RESULTS

The maneuvers are all calculated for a set lift coefficient and speed. In case of the Flying V the used CL values are 0.5 for 2.5g and -0.1 for -1g. The speed is 0.6 mach.

Table E.1: Flying V Aerodynamic Results

Load Factor [g]	Load Set	Sizing Point	q [Pa]	α [deg]	CD	CD_i	δ [deg]
2.5	11	A	8 927	11.7	396	324	-29.2
	12	B	14 244	8.6	237	169	-2.8
	13	C	14 244	7.3	226	156	7.6
	24	D	12 553	6.3	240	168	16.0
-1	21	A	17 853	-5.0	101	41	20.1
	22	B	28 489	-4.4	85	28	19.9
	23	C	28 489	-4.1	81	24	12.8
	24	D	25 106	-3.9	79	22	11.1

In case of the reference aircraft the used CL values are 1 for 2.5g and -0.5 for -1g. The speed is 0.6 mach.

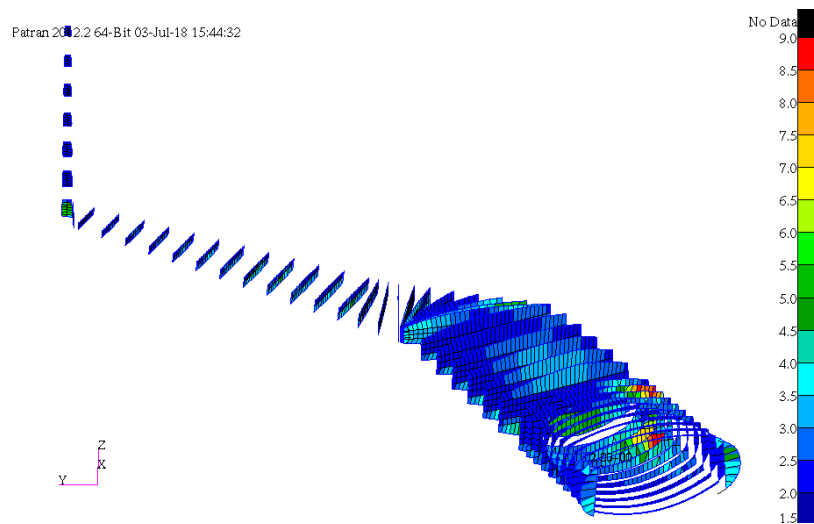
Table E.2: Reference Aircraft Aerodynamic Results

Load Factor [g]	Load Set	Sizing Point	q [Pa]	α [deg]	CD	CD_i	δ [deg]
2.5	11	A	9 588	9.0	484	315	-2.1
	12	B	15 264	9.2	476	314	-3.7
	13	C	15 264	9.4	477	314	-4.8
	24	D	13 128	9.5	481	314	-5.5
-1	21	A	7 670	-7.1	235	84	4.34
	22	B	12 211	-7.2	226	82	5.0
	23	C	12 211	-7.3	225	81	5.7
	24	D	10 503	-7.3	227	81	6.0

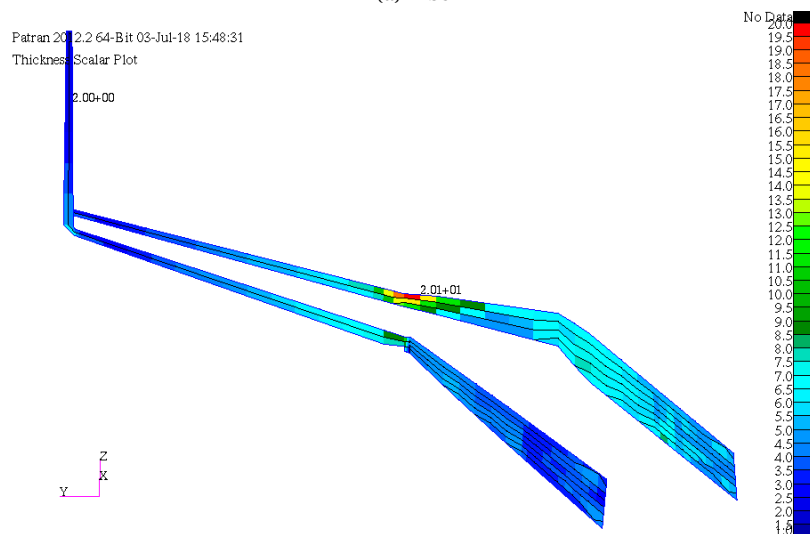
F

ADDITIONAL FLYING V RESULTS

F.1. THICKNESS



(a) Ribs



(b) Spars

Figure F1: Flying V Additional Thicknesses

F.2. CRITICAL LOAD CASES

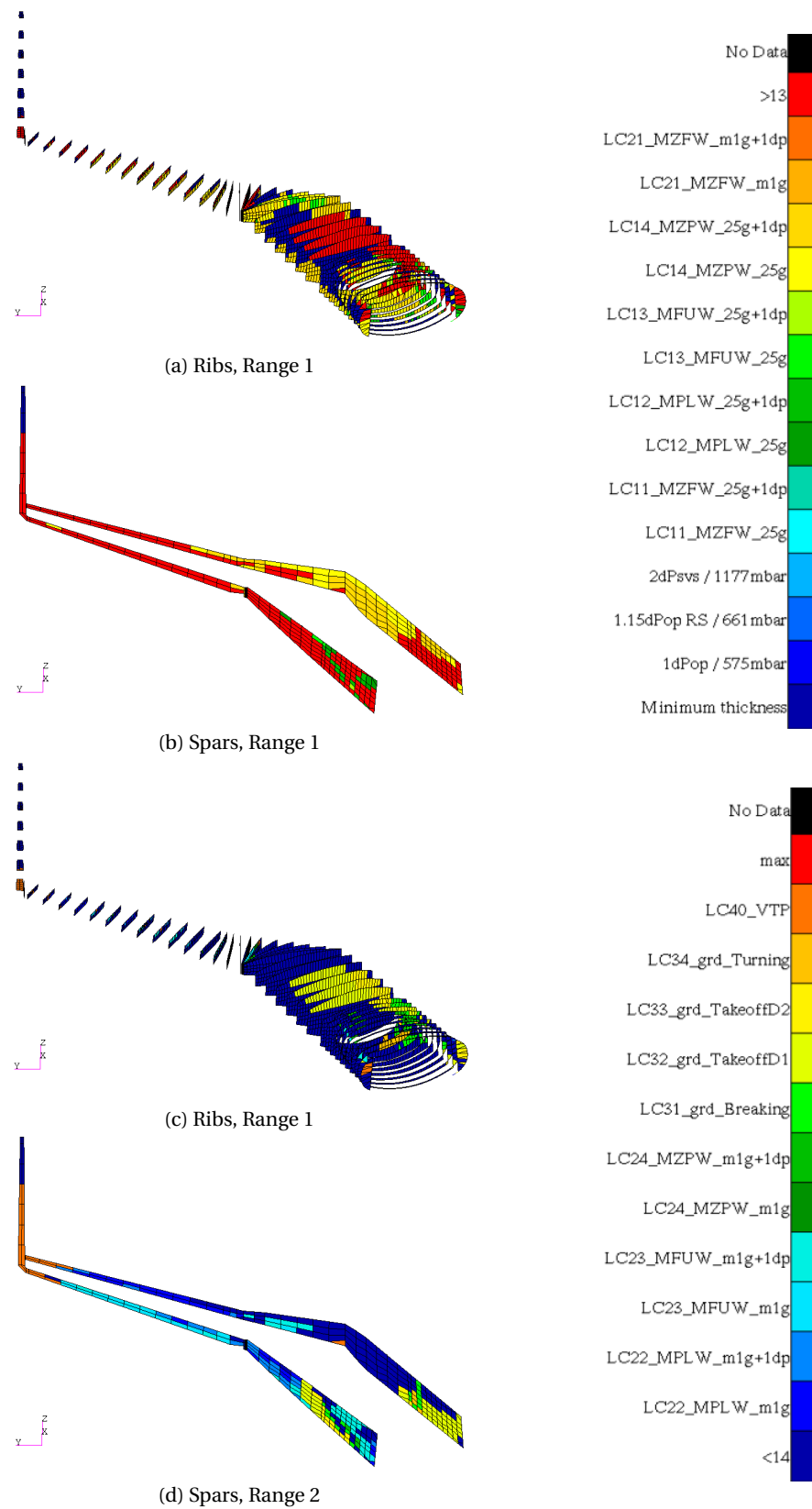


Figure F2: Critical Load Conditions

F.3. CRITICAL DESIGN CRITERIA

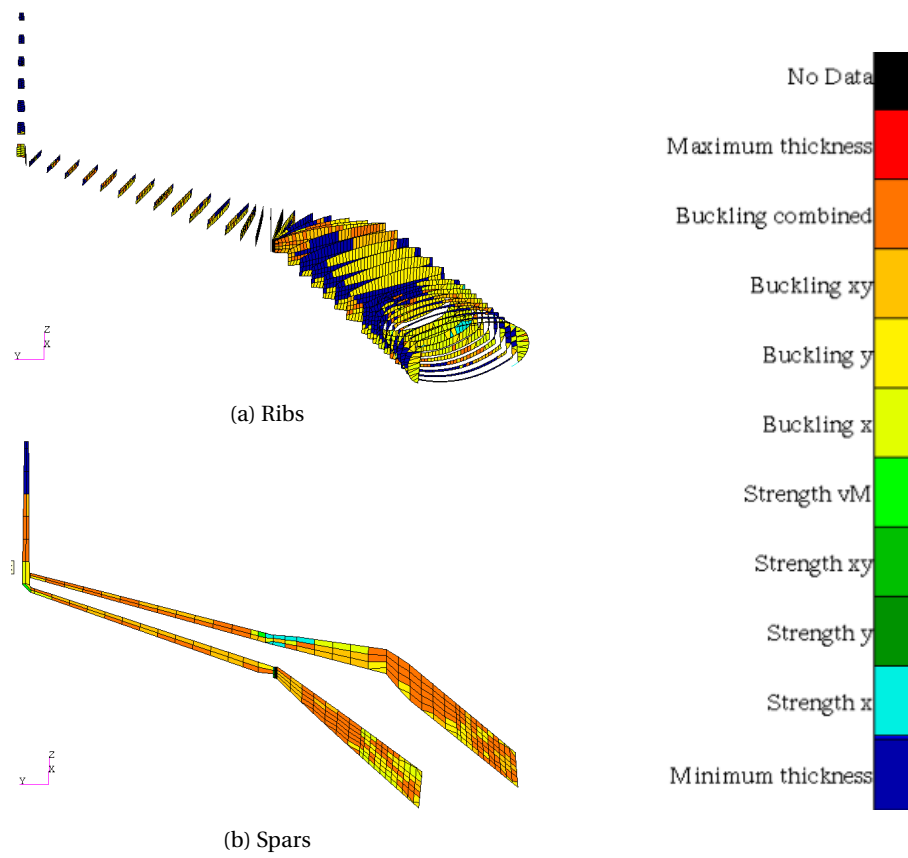


Figure E3: Critical Design Criteria

G

FULL REFERENCE AIRCRAFT RESULTS

G.1. THICKNESS

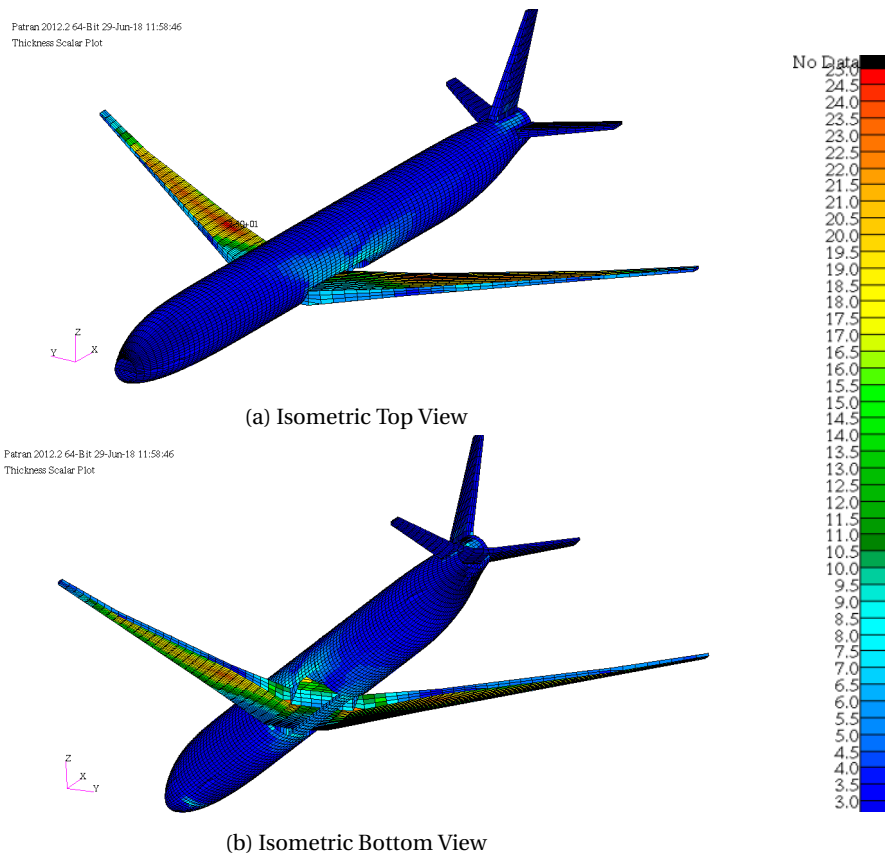


Figure G.1: Reference Aircraft Thickness

G.2. CRITICAL LOAD CASES

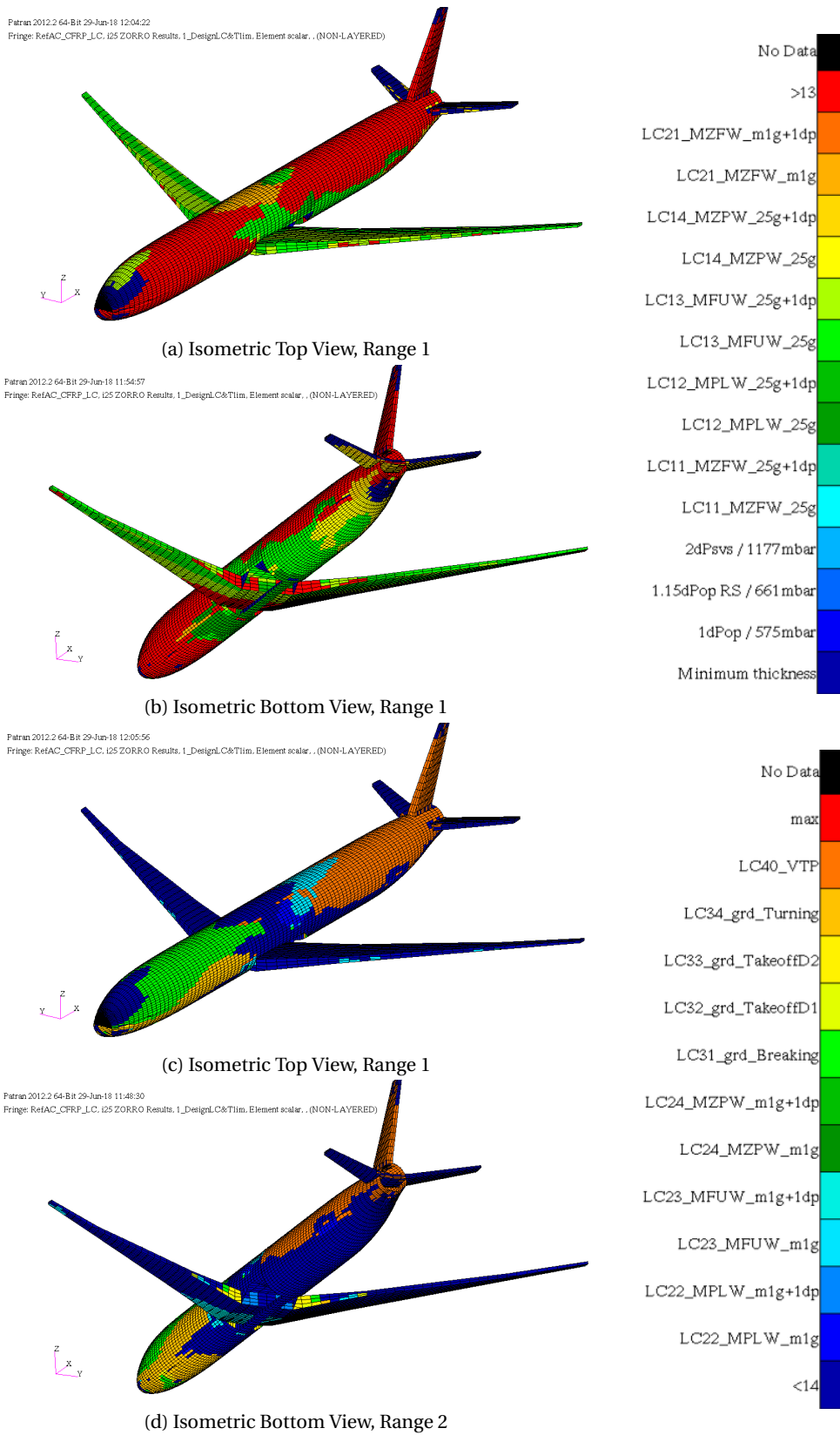


Figure G.2: Critical Load Conditions

G.3. CRITICAL DESIGN CRITERIA

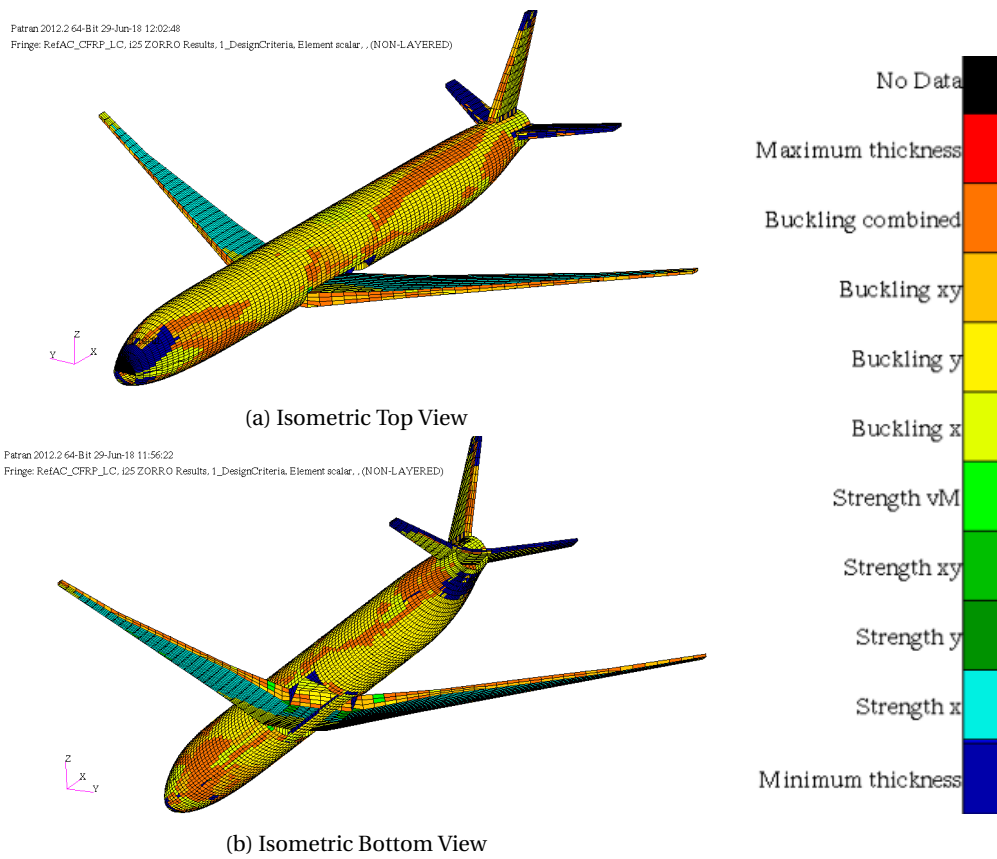


Figure G.3: Critical Design Criteria

BIBLIOGRAPHY

- [1] E. Faggiano, *Aerodynamic design optimization of a flying v aircraft*, (2016).
- [2] L. A. V. D. Schaft, *Design , Model Generation and Analysis of Flying V Structure Concept*, Master thesis, Technical University of Delft (2017).
- [3] M. Claeys, *Literature Study Report*, Tech. Rep. (Delft University of Technology, 2017).
- [4] D. P. Raymer, *Aircraft Design: A Conceptual Approach*, Vol. 3rd Edition (1999) p. 923.
- [5] *Patran 2012 User Guide*, MSC Software (2012).
- [6] K. Bender, *ODILILA Manual*, EIXWL, Future Projects, Airbus, 6th ed. (2018).
- [7] S. A. S. Airbus, *Aircraft Characteristics Airport and Maintenance Planning*, Tech. Rep. (Airbus Customer Services, Technical Data Support and Services, 2017).
- [8] <http://aviationweek.com/commercial-aviation/flying-a350-airbus-s-most-technologically-advanced->
(), [Online; 12/03/2018].
- [9] [http://www.airbus.com/aircraft/passenger-aircraft/a350xwb-family/a350-900.html#
details](http://www.airbus.com/aircraft/passenger-aircraft/a350xwb-family/a350-900.html#details) (), [Online; 12/03/2018].
- [10] <http://www.aerospaceweb.org/aircraft/jetliner/a350/> (), [Online; 12/03/2018].
- [11] https://en.wikipedia.org/wiki/Airbus_A350_XWB (), [Online; 12/03/2018].
- [12] E. P. Office, *ZorroM Userguide and Constraint Parameters*, Airbus, a ed. (2017).
- [13] *Esdu 200xy*, .
- [14] H. Schlichting and E. A. Truckenbrodt, *Aerodynamik des Flugzeuges: Erster Band* (2000) p. 480.
- [15] H. Schlichting and E. A. Truckenbrodt, *Aerodynamik des Flugzeuges: Zweiter Band* (2000) p. 514.